

Dissipative quantum state preparation and metastability in two-photon micromasers

Andreas Kouzelis,^{1,2} Katarzyna Macieszczak,^{3,1,2} Jiří Minář,^{4,5,1,2} and Igor Lesanovsky^{1,2}

¹*School of Physics and Astronomy, University of Nottingham, Nottingham, NG7 2RD, United Kingdom*

²*Centre for the Mathematics and Theoretical Physics of Quantum Non-Equilibrium Systems,*

School of Physics and Astronomy, University of Nottingham, Nottingham, NG7 2RD, United Kingdom

³*TCM Group, Cavendish Laboratory, University of Cambridge, Cambridge, CB3 0HE, United Kingdom*

⁴*Institute for Theoretical Physics, University of Amsterdam, Science Park 904, 1098 XH Amsterdam*

⁵*Department of Physics, Lancaster University, Lancaster, LA1 4YB, United Kingdom*

We study the preparation of coherent quantum states via a two-photon micromaser for applications in quantum metrology. While this setting can be in principle realized in a host of physical systems, we focus here on a situations where atoms interact with the electric field of a cavity through the Jaynes-Cummings Hamiltonian. We show that for achieving the desired two-photon micromaser dynamics the conventional approach of considering atoms with three relevant states and coupling them in two-photon resonance to the cavity field is not sufficient. Instead, additional levels are required in order to cancel emerging Starks shifts in leading order. Once this is accomplished the dynamics of the cavity is described by a discrete dissipative map that features a degenerate stationary state manifold of pure states. We derive the analytic form of these states, and show that they include Schrödinger cat states. In order to analyze the usefulness of these states for phase estimation protocols we analyze the quantum Fisher information in the transient as well as the stationarity regime and find that it exceeds the standard quantum limit. To account for realistic imperfections, we consider single-photon losses from the cavity and higher-order corrections in the far-detuned limit, which result in metastability of formerly stationary cavity states, and long-time dynamics with a unique mixed stationary state. Despite being mixed, this stationary state can still feature quantum Fisher information that exceeds the standard quantum limit. Our work delivers a comprehensive overview of the highly intricate dynamics of two-photon micromasers with particular focus on phase estimation. While the focus of the current work is on a physical realization of this setup with atoms coupled to a cavity, the results can be directly translated to optomechanical systems.

CONTENTS

I. Introduction	2	VI. Application in phase estimation	17
II. Two-photon micromaser with (5+1)-level atoms	3	A. QFI for micromaser in far-detuned limit	17
A. Atom-cavity interaction	3	B. QFI for micromaser with single-photon losses	19
B. Micromaser dynamics	4	VII. Experimental considerations	20
III. Two-photon micromaser	4	VIII. Conclusions	21
A. Effective two-photon atom-cavity interaction	4	References	21
B. Properties of two-photon micromaser dynamics	5	Appendix A: (5+1) micromaser	24
IV. Pure stationary states of two-photon micromaser	6	Appendix B: Adiabatic elimination for atom-cavity interaction	25
A. Pure stationary states	6	Appendix C: Pure stationary states of two-photon micromasers	30
B. Stationary decoherence free subspace	7	Appendix D: Hard walls and Pell equation	32
C. Schrödinger cat states in weak-coupling limit	8	Appendix E: Soft walls	33
D. Hard and soft walls	8	Appendix F: Review of metastability theory	40
V. Metastability in the cavity dynamics	11	Appendix G: Derivations of metastable dynamics	41
A. Metastability due to higher-order corrections in the far-detuned limit	11	Appendix H: Classical micromaser dynamics for thermal atoms	50
B. Metastability due to single-photon losses	13		
C. Metastability of hard walls	16		

Appendix I: Continuous versus discrete cavity dynamics 52

Appendix J: Identifying possible level scheme in Rydberg atoms 53

I. INTRODUCTION

There is currently an intense effort to engineer quantum states in a number of platforms ranging from atomic ensembles to nanomechanical, cavity and circuit QED systems. The impressive experimental progress is documented by the creation of Schrödinger cat states with more than 100 photons, together with the so-called compass states [1], in circuit QED [2], generation of squeezed coherent states in mechanical oscillators [3–6], and squeezed cat states using light at optical wavelengths [7–9], travelling (itinerant) squeezed coherent states in the microwave domain [10–12] and spin-squeezed states in atomic ensembles [13]. There are also experimental developments and theoretical proposals for interfacing different platforms in hybrid setups such as coupling mechanical oscillator with passing Rydberg atoms via electric charge [14] or with NV center via magnetic field [15].

Nowadays, the generation of quantum states goes beyond the well-established paradigm of squeezed coherent and cat states. A general paradigm of dissipative quantum state preparation was developed in [16, 17], and encompasses the so-called grid states [18–20], as well as squeezed and displaced superpositions of a finite number of phonons [21, 22]. The produced quantum states find applications to quantum information processing and quantum enhanced sensing [23–25], ranging from ultra sensitive force measurements in optomechanical systems [26, 27] to probes of macroscopic-scale decoherence [28, 29] or dark matter detection [30].

Among possible approaches to the robust quantum state engineering are those based on two-photon processes. In the seminal work on two-photon micromasers by Haroche and co-workers [31, 32] a stream of three-level atoms passed through a microwave cavity allowing for photon exchange between the cavity field and the atoms. For the energy gap between the ground and the excited (top) atom levels equal to double the frequency of the cavity and the middle level being far-detuned, the resulting dynamics corresponded to a simultaneous exchange of two photons between the atom and the cavity [31, 33–35]. Following this work the two-photon resonance is now exploited in stabilization of Schrödinger cat states [36], in ultrasensitive electromeasurements based on Rydberg atoms interacting with a microwave cavity [37], in two-photon lasing by a superconducting qubit [38], or in dynamical protection and reservoir engineering in circuit QED [39–41]. Despite the importance of the two-photon interactions in generation, manipulation and exploitation of quantum information, it has been shown that the two-

photon micromasers based on three-level systems feature only squeezed vacuum (squeezed single photon) or a Fock state as their stationary states [42].

In this work we argue that the limited set of two-photon micromasers stationary states is due to the Stark shifts present in the effective two-photon dynamics [31, 33–35]. We show that the Stark shifts can be removed by considering a scheme with $(5 + 1)$ -level atoms, where four single-photon transitions are driven by the cavity field and one transition is driven by a classical Rabi field (see Fig. 1). This leads to the atom-cavity interaction given by a two-photon Jaynes-Cummings Hamiltonian [43] without the spurious Stark shifts, and opens doors to the dissipative generation of novel pure quantum states.

For a pure state of incoming atoms, we derive the resulting pure stationary states, which depend both on the initial atomic state and the time-integral of the atom-cavity coupling strength, in contrast with the 3-level setup where the stationary state depend only on the atomic state [42, 44, 45]. In particular, we investigate the usefulness of the generated state in phase estimation by means of the quantum Fisher information (QFI) [46–48]. We find that a number of states yields the QFI exceeding not only the standard quantum limit, but also the performance of the squeezed coherent, cat and squeezed cat states generated by the micromaser in the weak-coupling limit. Some of the generated states with a high QFI display a delocalized Wigner function [49] and bear resemblance to the so-called grid states [18–20].

To account for cavity imperfections and finite detuning of the cavity fields from the atomic transitions, we consider single-photon losses from the cavity and higher-order corrections to the effective two-photon atom-cavity interaction. In the limit of a small loss rate and large detunings, we discuss the resulting metastability of the pure states and their long-time dynamics leading to a unique mixed stationary state of the cavity field [50]. In the weak-coupling regime, our results are consistent with the recent findings for the harmonic oscillator with two-photon driving and two-photon losses, which features Schrödinger cat states as pure stationary states [39, 51], but in the presence of single-photon losses, displays mixing dynamics and a unique stationary state [52–54]. Importantly, we find that, although the stationary states of the cavity are no longer pure, their QFI can still feature enhancement beyond the standard quantum limit.

The article is structured as follows. We first discuss the dynamics of micromaser with $(5 + 1)$ -level atoms in Sec. II and the effective two-photon dynamics in the far-detuned regime in Sec. III. In Sec. IV we investigate the resulting pure stationary states of the cavity field, while in Sec. V we include the effects of single-photon losses and higher-order corrections. Motivated by the application in quantum metrology, in Sec. VI we characterise the dissipatively generated states by the QFI. Finally, in Sec. VII we discuss possible experimental implementations, and conclude in Sec. VIII.

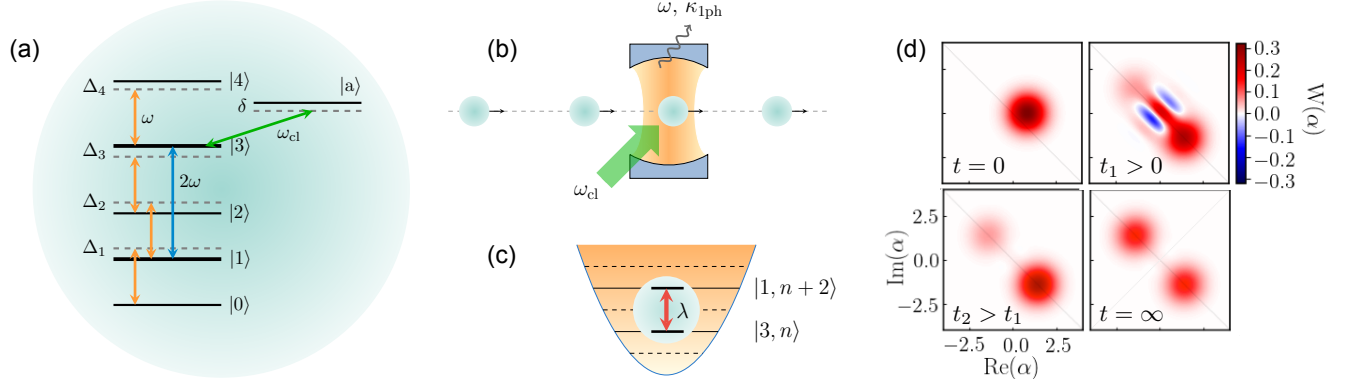


FIG. 1. **(a) Atomic level structure:** the transitions $|j-1\rangle \leftrightarrow |j\rangle$, $j = 1, \dots, 4$ are coupled to the cavity field with the strengths g_j and detunings Δ_j . The transition $|3\rangle \leftrightarrow |a\rangle$ is driven by a classical field with Rabi frequency G and detuning δ (see Sec. II A). **(b) Micromaser:** atoms are passing through a lossy cavity one at a time, interacting with a single-mode quantized cavity field of frequency ω (orange) and a classical Rabi field G of frequency ω_{cl} (green) (see Sec. II B). **(c) Effective dynamics:** at the two-photon resonance $\Delta_2 = -\Delta_3$, the (5+1)-level model reduces to an effective two-photon Jaynes-Cummings interaction with the coupling strength λ between the cavity field (depicted as a quantum harmonic oscillator) and the effective two-level atom with ground and excited states $|1\rangle$ and $|3\rangle$ (see Sec. III). **(d) Micromaser dynamics in weak-coupling regime:** the Wigner function (22) for the cavity state is shown. The initial coherent state $|\alpha\rangle$ with $\alpha = 0.6$ evolves first into a DFS spanned by the odd and even cat states (time t_1), which would be stationary if not for single-photon losses from the cavity that renders it metastable. After the first metastable regime, the macroscopic coherence dephases (time t_2), leading to metastable mixture of coherent states. This mixture then finally relaxes into a unique stationary state (time $t = \infty$) via mixing dynamics. In the second metastable regime ($t \geq t_2$), the system state features a single reflection symmetry, while the final parity-symmetric stationary state features two reflection symmetries (see Sec. III B). The parameters as in Fig. 6(b), see Sec. V B for discussion.

II. TWO-PHOTON MICROMASER WITH (5+1)-LEVEL ATOMS

In this section we introduce the (5+1)-level model of the atom-cavity interaction, which forms the basis of this work, and discuss the corresponding micromaser dynamics.

A. Atom-cavity interaction

We consider (5+1)-level atoms with the levels $|j\rangle$ and the energies E_j , $j = 0, 1, \dots, 4, a$, and the cavity field with the frequency ω , so that the free Hamiltonian

$$H'_0 = \omega \left(a^\dagger a + \frac{1}{2} \right) + \sum_{j=0, \dots, 4, a} E_j \sigma_{jj}, \quad (1)$$

where $\sigma_{ij} = |i\rangle\langle j|$, a and a^\dagger denote the cavity annihilation and creation operators, and we have set $\hbar = 1$.

The transitions $|j-1\rangle \leftrightarrow |j\rangle$ are coupled to the cavity field with the strengths g_j , $j = 1, \dots, 4$, and the transition $|3\rangle \leftrightarrow |a\rangle$ to the auxiliary level $|a\rangle$ is driven by a classical field of frequency ω_{cl} and Rabi frequency G [see Fig. 1(a) and [55]]. Therefore, the atom-cavity interaction

$$H'_{\text{int}}(t) = (a + a^\dagger) \sum_{j=1}^4 g_j \sigma_{j(j-1)} + (G e^{-i\omega_{cl}t} + G^* e^{i\omega_{cl}t}) \sigma_{a3} + \text{H.c.} \quad (2)$$

We assume that the detunings, Δ_j , $j = 1, \dots, 4$, and δ , defined as

$$(E_j - E_0) = j\omega + \sum_{i=1}^j \Delta_i, \quad j = 1, \dots, 4, \quad (3a)$$

$$(E_a - E_0) = 3\omega + \sum_{i=1}^3 \Delta_i + \omega_{cl} + \delta, \quad (3b)$$

are much smaller than the corresponding energy gaps, $|\Delta_j| \ll 2\omega$ for $j = 1, \dots, 4$, and $|\delta| \ll 2\omega_{cl}$, cf. Fig. 1(a), and perform the rotating wave approximation for (2) in the frame rotating with (1) (see Appendix A). The resulting Jaynes-Cummings Hamiltonian [56] is time-dependent in the initial frame, due to the dynamics of the classical field [cf. Eq. (2)]. We thus choose to work in the frame rotating with $\omega_{cl}\sigma_{aa} + \omega N$, where $N = a^\dagger a + \sum_{j=1}^4 j\sigma_{jj} + 3\sigma_{aa}$ is the total number of excitations. The resulting Jaynes-Cummings Hamiltonian reads

$$H_0 = \sum_{j=1}^4 \sigma_{jj} \sum_{i=1}^j \Delta_i + \sigma_{aa} \left(\delta + \sum_{j=1}^3 \Delta_j \right), \quad (4a)$$

$$H_{\text{int}} = a \sum_{j=1}^4 g_j \sigma_{j(j-1)} + G \sigma_{a3} + \text{H.c.}, \quad (4b)$$

up to a constant. Since the total number of excitations N is conserved by $H = H_0 + H_{\text{int}}$, the dynamics can in principle be solved exactly by diagonalising this Hamiltonian restricted to 6-dimensional eigenspaces of N .

B. Micromaser dynamics

The *micromaser* is a setup in which atoms pass through the cavity, one at a time, and interact with its field [see Fig. 1(b)]. In this work we make the following assumptions [57]:

1. Atoms are prepared *identically and independently* (in a product state) with respect to one another and the cavity.
2. The atomic beam is *monochromatic*, i.e., velocity of all atoms is the same.
3. The atom state is *invariant* under the dynamics in Eq. (4a), i.e., $e^{-itH_0} \rho_{\text{at}} e^{itH_0} = \rho_{\text{at}}$.

Assumption 1. guarantees that the dynamics is *Markovian*, while Assumptions 2. and 3. render it *time-homogenous* (see Appendix A for details).

Discrete dynamics. In the frame rotating with the free Hamiltonian, Eq. (1), the cavity state changes only when an atom is passing through. We have

$$\rho^{(k)} = \text{Tr}_{\text{at}} \left\{ U(\tau) \left[\rho_{\text{at}} \otimes \rho^{(k-1)} \right] U^\dagger(\tau) \right\}, \quad (5)$$

where $\rho^{(k)}$ denotes the cavity state after the passage of k atoms in state ρ_{at} and τ is time of the atom-cavity interaction

$$U(\tau) = \left\{ \mathcal{T} e^{-i \int_0^\tau dt [H_{\text{int}}(t) + H_0]} \right\}, \quad (6)$$

with the dependence of the interaction on t due to the coupling strengths $g_j(t)$, $j = 1, \dots, 4$, and $G(t)$ being determined by the atom position that changes in time [cf. Eqs. (4a) and (4b)] [58].

In this work we also assume *two-photon resonance*

$$\Delta_2 = -\Delta_3 = \Delta \quad (7)$$

[see Fig. 1(a)], which leads to degeneracy of $|1\rangle$ and $|3\rangle$ in H_0 . Therefore, we can consider atoms initially in a *pure state* ($|c_g|^2 + |c_e|^2 = 1$)

$$|\psi_{\text{at}}\rangle = c_g |1\rangle + c_e |3\rangle, \quad (8)$$

which is invariant as required by Assumption 3. The amplitudes c_e and c_g will allow us control the coherence of the generated cavity states.

For the state in Eq. (8) the dynamics in Eq. (5) can be expressed with the Kraus operators

$$M_j = \langle j | U(\tau) | \psi_{\text{at}} \rangle \quad (9)$$

as

$$\rho^{(k)} = \sum_{j=0, \dots, 4, \text{a}} M_j \rho^{(k-1)} M_j^\dagger \equiv \mathcal{M} \left[\rho^{(k-1)} \right], \quad (10)$$

where \mathcal{M} denotes the corresponding superoperator. We have $\sum_{j=0, \dots, 4, \text{a}} M_j^\dagger M_j = \mathbb{1}$, which guarantees the trace-preserving dynamics $\mathcal{M}^\dagger(\mathbb{1}) = \mathbb{1}$. The general case of the dynamics with a mixed atom state instead of the pure state in Eq. (8) is discussed in Appendices G and H.

Continuous dynamics. The *average* dynamics of the cavity, coarse-grained in time over intervals τ , is governed by the time-homogeneous master equation [59, 60]

$$\frac{d}{dt} \rho(t) = \nu \mathcal{M}[\rho(t)] - \nu \rho(t) \equiv \mathcal{L}[\rho(t)], \quad (11)$$

where we assumed that time at which atoms arrive to the cavity is exponentially distributed at the rate ν [31, 57, 61]. The dynamics is trace-preserving, $\mathcal{L}^\dagger(\mathbb{1}) = 0$, which follows from the properties of the Kraus operators. In this work, we will mostly consider the continuous dynamics (11). The comparison of the results in the main text to the case of discrete dynamics (10) can be found in Appendix I.

III. TWO-PHOTON MICROMASER

In this section we discuss the dynamics of the (5+1) micromaser in the far-detuned limit where an effective two-photon dynamics with tunable Stark shifts is obtained. We further focus on the case when the Stark shifts are cancelled. This condition will prove to be crucial for dissipative generation of novel pure quantum states of the cavity.

A. Effective two-photon atom-cavity interaction

In order to obtain *two-photon dynamics* of the atom and the cavity, we consider the levels $|0\rangle$, $|2\rangle$, $|4\rangle$ and $|a\rangle$ to be far detuned from the one-photon transitions, i.e., $|g_j/\Delta_j| \ll 1$, $j = 1, \dots, 4$ and $|G/\delta| \ll 1$. In this case H_{int} in Eq. (4b) can be treated as a perturbation of H_0 in Eq. (4a) by means of adiabatic elimination [62–64]. In Appendix B we show that up to the second order the dynamics couples only the levels $|1\rangle$ and $|3\rangle$ with the effective Hamiltonian

$$H_{\text{eff}} = -\frac{g_2 g_3}{\Delta} a^2 \sigma_{31} - \frac{g_2^* g_3^*}{\Delta} a^{\dagger 2} \sigma_{13} \quad (12)$$

$$+ \left[\frac{|g_1|^2}{\Delta_1} - a^\dagger a \left(\frac{|g_2|^2}{\Delta} - \frac{|g_1|^2}{\Delta_1} \right) \right] \sigma_{11}$$

$$- \left[\left(\frac{|G|^2}{\delta} + \frac{|g_3|^2}{\Delta} \right) + a^\dagger a \left(\frac{|g_4|^2}{\Delta_4} + \frac{|g_3|^2}{\Delta} \right) \right] \sigma_{33}.$$

In Eq. (12) we omitted the term $\Delta_1 (\sigma_{11} + \sigma_{33})$ (constant in the considered subspace of $|1\rangle$ and $|3\rangle$). As H_{eff} conserves the number of excitations $N_{\text{eff}} = a^\dagger a + \sigma_{11} + 3\sigma_{33}$, the corresponding atom-cavity dynamics can be solved exactly by diagonalising H_{eff} restricted to 2-dimensional N_{eff} eigenspaces (see Appendix C).

The second and third lines in Eq. (12) correspond to the Stark shifts, which crucially influence the dynamics of cavity coherences in the Fock basis (cf. [34, 65–67]). In particular, the Stark shift are cancelled when

$$\frac{|g_1|^2}{\Delta_1} = \frac{|g_2|^2}{\Delta} \quad (13a)$$

$$\frac{|g_4|^2}{\Delta_4} = -\frac{|g_3|^2}{\Delta} \quad (13b)$$

$$\frac{|G|^2}{\delta} = -\frac{|g_3|^2 + |g_2|^2}{\Delta}, \quad (13c)$$

in which case the Hamiltonian (12) reduces to the two-photon Jaynes-Cummings Hamiltonian [43]

$$H_{\text{eff}} = \lambda a^2 \sigma_{31} + \lambda^* a^{\dagger 2} \sigma_{13}, \quad (14)$$

where $\lambda = -g_2 g_3 / \Delta$ is the effective two-photon coupling strength [see Fig. 1(c)] and we omitted $\frac{|g_2|^2}{\Delta} (\sigma_{11} + \sigma_{33})$ (constant in the considered subspace of $|1\rangle$ and $|3\rangle$).

In this work we focus on the micromaser dynamics generated by Eq. (14). Such an effective atom-cavity interaction is not possible to be obtained in 3-level scheme [34, 35, 42, 44, 68], which corresponds to $|\Delta_1|, |\Delta_4|, |\delta| \rightarrow \infty$ (or equivalently $g_1 = g_4 = G = 0$) in (12) and

$$H_{\text{eff}}^{3\text{-level}} = -\frac{g_2 g_3}{\Delta} a^2 \sigma_{31} - \frac{g_2^* g_3^*}{\Delta} a^{\dagger 2} \sigma_{13} \quad (15)$$

$$- \frac{|g_2|^2}{\Delta} a^\dagger a \sigma_{11} - \frac{|g_3|^2}{\Delta} (a^\dagger a + 1) \sigma_{33}.$$

Indeed, (5+1)-level scheme in Fig. 1 is a *minimal* model to cancel the Stark shifts [cf. Eq. (13) and see Appendix B].

The choice of the effective dynamics as in Eq. (14) is motivated by the dissipative generation of a plethora of distinct pure quantum states (see Sec. IV). In Appendix C we show that only in this case the adiabatic two-photon dynamics between the cavity and the atoms generates stationary states of the cavity which are pure and dependent on both the atom state and the atom-cavity coupling. For any other setup, including the 3-level scheme with Eq. (15), pure stationary states, if generated, always correspond to the squeezed vacuum state and squeezed single-photon state, which are independent from the atom state. This observation also means that our study together with the earlier work [42, 44, 68] provides a *complete* analysis of dissipative generation of quantum states in two-photon micromasers based on single-photon Jaynes-Cummings interaction [56].

B. Properties of two-photon micromaser dynamics

We now discuss features of micromaser dynamics with the effective two-photon Hamiltonian in Eq. (14).

Dynamics. The atom in a pure superposition in Eq. (8) determines the micromaser dynamics via the Kraus operators [cf. Eq. (9)]

$$M_g = \langle 1 | e^{-i \int_0^\tau dt H_{\text{eff}}(t)} | \psi_{\text{at}} \rangle$$

$$= c_g \cos \left(\phi \sqrt{a^{\dagger 2} a^2} \right) - i c_e a^{\dagger 2} \frac{\sin \left(\phi \sqrt{a^2 a^{\dagger 2}} \right)}{\sqrt{a^2 a^{\dagger 2}}}, \quad (16a)$$

$$M_e = \langle 3 | e^{-i \int_0^\tau dt H_{\text{eff}}(t)} | \psi_{\text{at}} \rangle$$

$$= -i c_g a^2 \frac{\sin \left(\phi \sqrt{a^{\dagger 2} a^2} \right)}{\sqrt{a^{\dagger 2} a^2}} + c_e \cos \left(\phi \sqrt{a^2 a^{\dagger 2}} \right), \quad (16b)$$

where $H_{\text{eff}}(t)$ is the effective atom-cavity interaction in Eq. (14) and $\phi = \int_0^\tau dt \lambda(t)$ is the integrated coupling strength [we assume $\lambda(t)$ is real] [69]. There are only two Kraus operators, as the effective dynamics couples only $|1\rangle$ and $|3\rangle$ levels, which can be viewed as the ground state and the excited state of the effective two-level atom interacting with the cavity. The discrete dynamics of the cavity is given by [cf. Eq. (10)]

$$\rho^{(k)} = \sum_{j=g,e} M_j \rho^{(k-1)} M_j^\dagger \equiv \mathcal{M}_0 [\rho^{(k-1)}], \quad (17)$$

while the corresponding master equation is [cf. Eq. (11)]

$$\frac{d}{dt} \rho(t) = \nu \mathcal{M}_0 [\rho(t)] - \nu \rho(t) \equiv \mathcal{L}_0 [\rho(t)]. \quad (18)$$

The subscript 0 in Eqs. (17) and (18) indicates the far-detuned limit in which two-photon dynamics is achieved. We will consider the effect of the higher-order corrections in this limit, as well as single photon losses later in Sec. V. Here we further discuss the symmetry properties of the dynamics.

Conservation of photon-number parity. The micromaser dynamics generated by (16) features only two-photon transitions, so that the parity

$$P = (-1)^{a^\dagger a} \quad (19)$$

commutes with the Kraus operators,

$$[M_{g,e}, P] = 0. \quad (20)$$

Therefore, the parity is conserved during the evolution,

$$\frac{d}{dt} \text{Tr} [P \rho(t)] = \text{Tr} \{ P \mathcal{L}_0 [\rho(t)] \} = \text{Tr} \left[\mathcal{L}_0^\dagger(P) \rho(t) \right] = 0, \quad (21)$$

as we have $\mathcal{M}_0^\dagger(P) = P$ and thus $\mathcal{L}_0^\dagger(P) = 0$. In particular, a cavity state initially supported in the even (odd) subspace, remains there at all times. This is manifested by the conservation of the projection on the odd and even subspace, $\mathbf{1}_\pm = (\mathbf{1} \pm P)/2$. Therefore, parity conservation implies the existence of an even and an odd

stationary states. We will show in the next Sec. IV these states can be pure.

Real-valued dynamics. Let the relative phase in the initial atomic state (8) be φ , i.e., $c_g/c_e = e^{i\varphi}|c_g/c_e|$. The Kraus operators (16) then become real upon the transformation $a \mapsto e^{-i(\varphi/2-\pi/4)}a$ of the photon number basis. Therefore, for an initial state of the cavity with real-valued coefficients in the transformed basis, it remains real at all times. We conclude that the odd and even stationary states are real-valued in this basis.

Symmetries of Wigner function. Finally, the parity conservation and real-valued dynamics imply, for the odd and even stationary states, two *reflection symmetries* of the Wigner function [49, 70]

$$W(\alpha) = \frac{2}{\pi} \text{Tr} [\rho D(\alpha) P D(-\alpha)], \quad (22)$$

where $D(\alpha) = \exp(\alpha a^\dagger - \alpha^* a)$ is the displacement operator [see Figs. 2(a) and 3]. First, for an even or odd ρ , we have $P\rho P = \rho$, while $P^2 = \mathbb{1}$ and $PD(\alpha)P = D(-\alpha)$, and thus $W(\alpha) = \frac{2}{\pi} \text{Tr} \{\rho [PD(\alpha)P] P [PD(-\alpha)P]\} = W(-\alpha)$, which is the *inversion symmetry*. Second, for a real-valued cavity state in the transformed basis $a \mapsto e^{-i(\varphi/2-\pi/4)}a$, we have $W(\alpha) = W^*(\alpha) = \frac{2}{\pi} \text{Tr} [\rho^* D(\alpha^*) P D(-\alpha^*)] = W(\alpha^*)$, which is a *reflection symmetry* with respect to the real axis [cf. the system state for $t \geq t_2$ in Fig. 1(d)]. Therefore, together with the inversion symmetry, we also obtain a *reflection symmetry* with respect to the imaginary axis.

IV. PURE STATIONARY STATES OF TWO-PHOTON MICROMASER

We show that the two-photon micromaser introduced in Sec. III features pure stationary states of the odd and the even parity. The coherences between the states are also stationary, thus forming a decoherence free subspace [71–73]. In particular, in the weak-coupling limit, the stationary states become odd and even Schrödinger cat states [74, 75]. We also discuss the possibility of obtaining trapping states [42], i.e., states with a fixed photon number. This in turn provides an insight into emergent slow timescales during the approach to pure stationary states.

A. Pure stationary states

The stationary states of the cavity satisfy $\frac{d}{dt}\rho_{ss} = \mathcal{L}_0(\rho_{ss}) = 0$, which is equivalent to $\mathcal{M}_0(\rho_{ss}) = \rho_{ss}$. When the stationary state is pure, i.e., $\rho_{ss} = |\Psi_{ss}\rangle\langle\Psi_{ss}|$, it is necessarily an eigenstate of all operators in \mathcal{L}_0 [16, 17], or equivalently, an eigenstate of all Kraus operators in

\mathcal{M}_0 ,

$$M_g|\Psi_{ss}\rangle = \alpha|\Psi_{ss}\rangle, \quad (23a)$$

$$M_e|\Psi_{ss}\rangle = \beta|\Psi_{ss}\rangle. \quad (23b)$$

This follows directly from the fact that, in order to maintain its purity, the cavity state must be uncorrelated from the outgoing atom state, $U_{\text{eff}}(\tau)(|\psi_{\text{at}}\rangle \otimes |\Psi_{ss}\rangle) = (\alpha|1\rangle + \beta|3\rangle) \otimes |\Psi_{ss}\rangle$ [cf. Eq. (16)] and we have $|\alpha|^2 + |\beta|^2 = 1$ from the state normalisation.

Recurrence relation. For the pure stationary state $|\Psi_{ss}\rangle = \sum_{n=0}^{\infty} c_n |n\rangle$, Eq. (23) corresponds to

$$\alpha c_{n+2} = c_g \cos_n(\phi) c_{n+2} - i c_e \sin_n(\phi) c_n, \quad (24a)$$

$$\beta c_n = -i c_g \sin_n(\phi) c_{n+2} + c_e \cos_n(\phi) c_n, \quad (24b)$$

where we defined $\cos_n(\phi) = \cos[\phi\sqrt{(n+1)(n+2)}]$ and $\sin_n(\phi) = \sin[\phi\sqrt{(n+1)(n+2)}]$. The solutions exist when the determinant of Eq. (24), $\alpha\beta + c_e c_g - \cos_n(\phi)(\alpha c_e + \beta c_g)$ is 0, and, thus,

$$\alpha = \pm c_g, \quad \beta = \mp c_e, \quad (25)$$

leading to recurrence relation for coefficients of the stationary states,

$$c_{n+2} = \mp i \frac{c_e}{c_g} \frac{\sin_n(\phi)}{1 \mp \cos_n(\phi)} c_n = \mp i \frac{c_e}{c_g} \left[\cot_n\left(\frac{\phi}{2}\right) \right]^\pm c_n. \quad (26)$$

We note that the odd and even stationary states are determined independently by Eq. (26), which a consequence of the parity conserving dynamics (cf. Sec. III B). Here we assumed that $c_g \neq 0$ and $1 \mp \cos_n(\phi) \neq 0$. We revisit these assumptions in Sec. IV D.

Boundary conditions. Since $a^2|0\rangle = 0 = a^2|1\rangle$, from Eqs. (16) and (23) we also obtain the boundary conditions

$$\alpha c_0 = c_g c_0, \quad \alpha c_1 = c_g c_1, \quad (27)$$

which determine the outgoing atom state as

$$\alpha = c_g \quad \text{and} \quad \beta = -c_e, \quad (28)$$

independently of ϕ [42, 44]. Therefore, the recurrence relation (26) leads to the existence of odd and even pure stationary states,

$$|\Psi_+\rangle = c_0|0\rangle + c_0 \sum_{n=1}^{\infty} \left(-i \frac{c_e}{c_g}\right)^n \prod_{k=0}^{n-1} \cot_{2k}\left(\frac{\phi}{2}\right) |2n\rangle, \quad (29a)$$

$$|\Psi_-\rangle = c_1|1\rangle + c_1 \sum_{n=1}^{\infty} \left(-i \frac{c_e}{c_g}\right)^n \prod_{k=0}^{n-1} \cot_{2k+1}\left(\frac{\phi}{2}\right) |2n+1\rangle, \quad (29b)$$

where c_0 and c_1 are determined, up to a phase, by the state normalisation. In contrast to the case of the 3-level

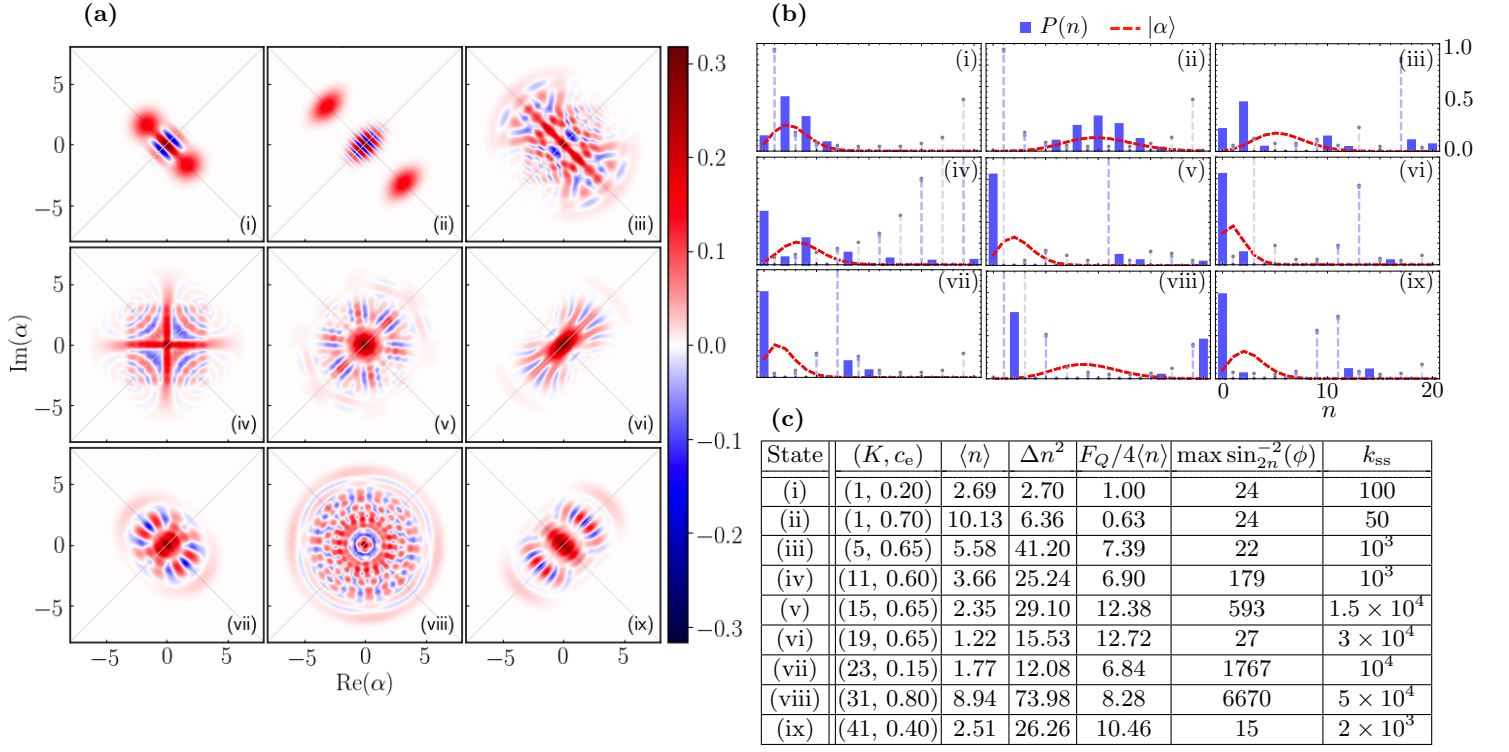


FIG. 2. **Pure stationary states of cavity dynamics:** (a) Wigner function [Eq. (22)] for even cavity stationary states corresponding to the parameters in (c) [and indicated in Fig. 9(d)]. The two reflection symmetries (along diagonal grey lines) are due to the stationary states being parity-symmetric and real-valued (after adding the phase $\pi/4$) (see Sec. III B). (b) The photon-number distribution of the states (blue bars, only even photon numbers) is compared to that of the coherent states with the same average photon-number $\langle n \rangle$ (red dashed lines). Blue dashed lines show $\cot_{2n}^2(\phi)/10$, which diverges as $4/\sin_{2n}^2(\phi)$ [grey dashed lines] for soft walls concurring with the boundary condition for stationary states (see Sec. IV D). (c) Properties of stationary states (i-ix): the parameters (K, c_e) [which determine ϕ by Eq. (41), where the hard wall is at $m = 20$; for ϕ see also the last panel in Fig. 9, while $c_g = \sqrt{1 - c_e^2}$], the mean photon-number $\langle n \rangle$, the variance Δn^2 , the enhancement (81) in phase estimation, the maximal rate related to even soft wall $\max_{0 \leq 2n \leq m} 1/\sin_{2n}^2(\phi)$, and the estimated number of atoms k_{ss} for which the stationary states are reached, as characterized by the fidelity $F[\rho_{ss}; \rho(k)] = \text{Tr} \sqrt{\sqrt{\rho_{ss}} \rho(k) \sqrt{\rho_{ss}}} \geq 0.99$, for the cavity initially in the vacuum state $|0\rangle$.

micromaser [42, 44], here the stationary states are dependent not only on the incoming atom state, (8), but also on the integrated coupling ϕ , which allows for dissipative generation of plethora of distinct stationary states. In Fig. 2 we show a few examples of the even stationary states of Eq. (29). We discuss their properties in the context for applications for quantum metrology in Sec. VI.

B. Stationary decoherence free subspace

Since the eigenvalues α and β of the Kraus operators M_g and M_e [cf. Eqs. (23) and (25)], are the same for the odd and the even pure stationary states, the even-odd coherences, $|\Psi_+\rangle\langle\Psi_-|$ and $|\Psi_-\rangle\langle\Psi_+|$ are also stationary, i.e.,

$$\mathcal{L}_0(|\Psi_+\rangle\langle\Psi_-|) = \nu(\alpha_+\alpha_-^* + \beta_+\beta_-^* - 1)|\Psi_+\rangle\langle\Psi_-| = 0. \quad (30)$$

Therefore, any superposition of $|\Psi_+\rangle$ and $|\Psi_-\rangle$ is stationary, and thus they form a decoherence-free subspace (DFS) of a qubit [71–73].

The existence of the DFS can be made apparent, by choosing the shifted Kraus operators

$$\widetilde{M}_g = M_g - c_g \mathbb{1}, \quad (31a)$$

$$\widetilde{M}_e = M_e + c_e \mathbb{1}, \quad (31b)$$

as jump operators in the master equation (18), in which case,

$$\frac{d}{dt}\rho(t) = \frac{\nu}{2} \sum_{j=g,e} \left[2\widetilde{M}_j \rho(t) \widetilde{M}_j^\dagger - \widetilde{M}_j^\dagger \widetilde{M}_j \rho(t) - \rho(t) \widetilde{M}_j^\dagger \widetilde{M}_j \right], \quad (32)$$

where we used the fact that $c_g^* M_g - c_g M_g^\dagger - c_e^* M_e + c_e M_e^\dagger = 0$ [cf. Eq. (16)]. Therefore, the pure stationary states $|\Psi_+\rangle$ and $|\Psi_-\rangle$ are *dark*, i.e., $\widetilde{M}_{g,e}|\Psi_\pm\rangle = 0$, and thus their coherences are also stationary.

In general, the asymptotic state of the cavity is

$$\begin{aligned} \lim_{t \rightarrow \infty} e^{t\mathcal{L}_0} \rho &\equiv \Pi_0(\rho) \\ &= |\Psi_+\rangle\langle\Psi_+| \text{Tr}(\mathbb{1} + \rho) + |\Psi_-\rangle\langle\Psi_-| \text{Tr}(\mathbb{1} - \rho) \\ &\quad + |\Psi_+\rangle\langle\Psi_-| \text{Tr}(L_+ - \rho) + |\Psi_-\rangle\langle\Psi_+| \text{Tr}(L_- + \rho), \end{aligned} \quad (33)$$

where the superoperator Π_0 projects the initial cavity state ρ on the stationary DFS, and $\mathbb{1}_+$ and $\mathbb{1}_-$, and $L_{+-} = L_{-+}^\dagger$, are conserved operators supported in the even and odd subspace, and in the odd-even coherences, respectively, with $\text{Tr}(L_{+-}|\Psi_+\rangle\langle\Psi_-|) = 1$. The disjoint support of the conserved quantities reflects the strong parity symmetry, (20), which implies that the master operator \mathcal{L}_0 is block-diagonal with respect to: the odd subspace, the even subspace, the even-odd coherences and the odd-even coherences, so that the corresponding parts of a density matrix evolve independently [39, 76, 77]. Although in general L_{+-} , L_{-+} are not known analytically, they can be obtained numerically via

$$L_{+-} = \lim_{t \rightarrow \infty} e^{t\mathcal{L}_0^\dagger} (|\Psi_-\rangle\langle\Psi_+|), \quad (34)$$

where the choice of the initial operator in the space of odd-even coherences as $|\Psi_-\rangle\langle\Psi_+|$, ensures the normalisation of L_{+-} .

C. Schrödinger cat states in weak-coupling limit

We show that in the limit of the weak coupling, Schrödinger cat states are recovered as stationary states of the cavity and its dynamics corresponds to two-photon drive and two-photon losses [39, 52–54, 78, 79] [see Fig. 1(d) and state (i) in Fig. 2].

Steady states. In the limit of the weak coupling, $|\phi| \ll 1$, the recurrence relation (26) with the boundary condition (28) can be approximated as

$$\frac{c_{n+2}}{c_n} = -i \frac{c_e}{c_g} \frac{2}{\phi \sqrt{(n+1)(n+2)}} + \mathcal{O} \left[\frac{c_e}{c_g} \phi \sqrt{(n+1)(n+2)} \right], \quad (35)$$

defining the stationary states as the odd and even Schrödinger cat states [74, 75] [see state (i) in Fig. 2]

$$|\Psi_\pm\rangle = \frac{|\alpha\rangle \pm |-\alpha\rangle}{\sqrt{2 \pm 2e^{-2|\alpha|^2}}}, \quad \alpha = e^{-i\frac{\pi}{4}} \sqrt{\frac{2c_e}{c_g \phi}}, \quad (36)$$

with the coherent state $|\alpha\rangle \equiv e^{-|\alpha|^2/2} \sum_{n=0}^{\infty} \alpha^n / \sqrt{n!} |n\rangle$. For validity of the approximation (35) we require that the neglected terms are small,

$$\begin{aligned} \sum_{n=0}^{\infty} |c_n|^2 \left| \frac{c_e}{c_g} \right|^2 |\phi^2 (n+1)(n+2)| &= \left| \frac{c_e}{c_g} \right|^2 \phi^2 \langle a^2 a^{\dagger 2} \rangle_{\Psi_\pm} \\ &= 4 \left| \frac{c_e}{c_g} \right|^4 + 8\phi \left| \frac{c_e}{c_g} \right|^3 \tanh |\alpha|^2 + 2\phi^2 \left| \frac{c_e}{c_g} \right|^2 \ll 1. \end{aligned}$$

Therefore, the conditions for obtaining Schrödinger cat states as stationary states are

$$|c_e| \ll 1 \quad \text{and} \quad |\phi| \ll 1. \quad (37)$$

Dynamics. The Kraus operators in Eq. (31) can be expanded in ϕ up to the linear terms as

$$\widetilde{M}_g \approx -ic_e \phi a^{\dagger 2} \approx 0, \quad (38a)$$

$$\widetilde{M}_e \approx 2c_e \mathbb{1} - ic_g \phi a^2, \quad (38b)$$

where in the first line we further neglected the second-order terms with respect to both ϕ and c_e [which is small as imposed by the weak-coupling limit of Eq. (37)]. Therefore, from Eq. (32) we arrive at the cavity dynamics

$$\begin{aligned} \frac{d}{dt} \rho &= -i[g_{2\text{ph}}^* a^2 + g_{2\text{ph}} a^{\dagger 2}, \rho] \\ &\quad + \kappa_{2\text{ph}} a^2 \rho a^{\dagger 2} - \frac{\kappa_{2\text{ph}}}{2} (a^{2\dagger} a^2 \rho + \rho a^{2\dagger} a^2) \end{aligned} \quad (39)$$

with

$$g_{2\text{ph}} = \nu c_g^* c_e \phi \quad \text{and} \quad \kappa_{2\text{ph}} = \nu |c_g|^2 \phi^2, \quad (40)$$

which are of the second order [cf. Eq. (37)]. Equation (40) describes an extensively studied model of two-photon drive and two-photon losses [39, 52–54, 78, 79]. In particular, the conserved quantities L_{+-} and L_{-+} in Eq. (34) are known exactly [39] and thus so are the asymptotic states in Eq. (33). In Appendix G we show that the two-photon cavity dynamics in Eq. (40) is robust to non-monochromaticity of the atom beam, but it is modified by two-photon injections when the atom state is mixed rather than pure [cf. Eq. (8)].

D. Hard and soft walls

Here we investigate the case of the atom-cavity coupling strength such that the cavity dynamics is no longer connected. We characterise the corresponding conditions for the coupling strength, and discuss the purity of the resulting stationary states. Among others, this situation allows to prepare the cavity in a fixed photon number state, so called trapping states [42]. We also discuss the approximate case in which slow timescales arise in the relaxation to the stationary states.

Hard walls. The terms of the Kraus operators in Eq. (16) that connect the cavity states $|m\rangle$ and $|m+2\rangle$ are proportional to $\sin_m(\phi)$. Therefore, when the integrated interaction strength ϕ gives $\sin_m(\phi) = 0$ for some m , that is

$$\phi = \frac{K\pi}{\sqrt{(m+1)(m+2)}} \quad \text{with} \quad K = \pm 1, \pm 2, \dots, \quad (41)$$

the Kraus operators become *block-diagonal* in the Fock space, with the dynamics on the left (photon numbers $n \leq m$) and on the right ($n > m$) being independent. As the initial cavity state supported below m and of

	$\cos_{m_1}(\phi) = 1$	$\cos_{m_1}(\phi) = -1$
m_1 even	m_{2n} odd, m_{2n+1} even $\cos_{m_n}(\phi) = 1$	m_{2n} odd, m_{2n+1} even $\cos_{m_n}(\phi) = (-1)^n$
m_1 odd	m_n odd $\cos_{m_n}(\phi) = 1$	m_n odd $\cos_{m_n}(\phi) = (-1)^n$

TABLE I. **Parity of hard walls** located at m_n from Eq. (43) [cf. Eq. (41)]. The green shaded case is the only situation leading to pure states between the hard walls [cf. Eqs. (45) and (46) and see Fig. 3].

the same parity as m , remains supported below m at all times, we refer to this case as a *hard wall* at m .

The cavity dynamics features either no hard walls, or infinitely many, as we now show. This is due to the fact that, for a given coupling strength ϕ , and the parameters m_1 and K_1 of the first wall, Eq. (41) for m_n and K_n or another wall, corresponds to the *Pell equation*, [80, 81]

$$x^2 - Dy^2 = 1, \quad (42)$$

where the arguments $x = 2m_n + 3$ and $y = 2K_n/K_1$ and the parameter $D = (m_1 + 1)(m_1 + 2)$ (see also Appendix D). As D is not a square of an integer, the hyperbolic equation (42) is known to feature infinitely many integer solutions, determined by a recurrence relation [82]. This translates into the *recurrence relation* for the hard walls,

$$m_n = m_{n-1}(2m_1 + 3) + 3(m_1 + 1) \quad (43a)$$

$$+ 2(m_1 + 1)(m_1 + 2) K_{n-1}/K_1,$$

$$K_n = K_{n-1}(2m_1 + 3) + K_1(2m_{n-1} + 3). \quad (43b)$$

where K_{n-1}/K_1 is necessarily an integer (cf. Appendix D). From Eq. (43) we have that for the first hard wall at even m_1 , the parity of the n th wall, m_n oscillates with period 2, while for odd m_1 , all walls are found at m_n are odd [see Tab. I]. Similarly, for even K_1 , K_n is always even and thus $\cos_{m_n}(\phi) = (-1)^{K_n} = 1$, while for odd K_1 , the K_n parity oscillates with period 2, and so does $\cos_{m_n}(\phi)$ [cf. Tab. I]. Finally, solving Eq. (43), the position m_n of hard walls *grows exponentially* with n ,

$$m_n = \frac{(2m_1 + 3 + 2\sqrt{D})^n + (2m_1 + 3 - 2\sqrt{D})^n}{4} - 3. \quad (44)$$

Trapping states [42]. A hard wall in the dynamics can be used to obtain a pure Fock state of a fixed photon number, as follows. Consider the cavity being pumped by the excited atoms ($|c_e| = 1$, $c_g = 0$). In the absence of hard walls, there is no stationary state and the energy of the cavity increases without a bound. In contrast, for a first hard wall at m_1 , when the initial cavity state is of the same parity as m_1 and supported below m_1 , the asymptotic state is the pure trapping state $|\Psi_{ss}\rangle = |m_1\rangle$, while generally an initial state evolves then into a mixed state

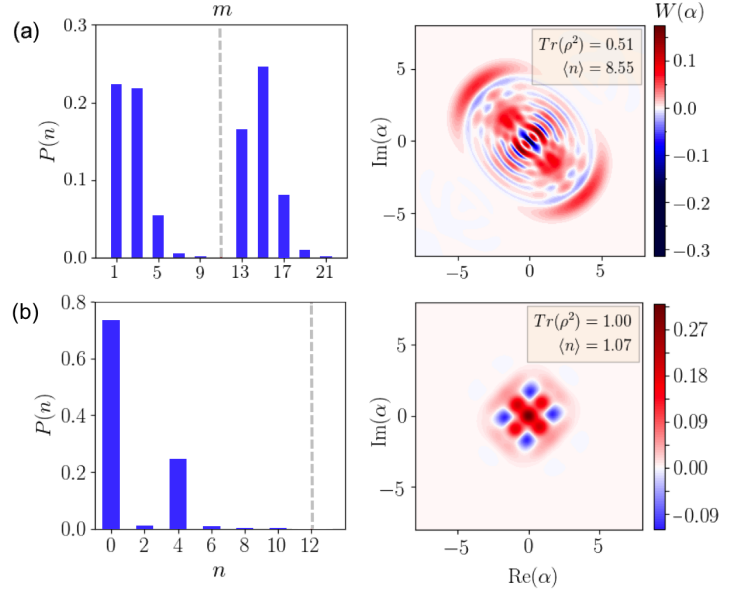


FIG. 3. **Steady states in the presence of hard walls.** The photon-number distribution $P(n)$ and the Wigner function [Eq. (22)] for: **(a)** the equal mixture of the odd pure stationary states obtained from the initial superposition of odd Fock states $(|1\rangle + |15\rangle)/\sqrt{2}$ for $c_e = 0.3$ and the odd hard wall (dashed red) at $m = 11$ with $K = 1$ ($\phi \approx 0.252$) **(b)** the approximately pure stationary state obtained from the initial vacuum state $|0\rangle$ for $c_e = 0.4$ and the even hard wall (dashed gray) at $m = 12$ with $K = 8$ ($\phi \approx 0.593$).

supported on all trapping states $|m_n\rangle$ [for the first wall at m_1 odd, and thus all walls odd, the asymptotic state is also supported on the even pure state, Eq. (24)] [see Eq. (16)]. The asymptotic distribution, $\langle m_n | \rho_{ss} | m_n \rangle$, is given by the initial supports between subsequent walls of the same parity. It is also possible for coherences between the trapping states $|m_n\rangle$ to be stationary. This requires $\cos_{m_n}(\phi) = (-1)^{K_n}$ to be of the same sign [cf. Eq. (30)]. Therefore, from Eq. (43) all the coherences are stationary for K_1 even. For K_1 odd and m_1 even, only the coherences between the trapping states of the same parity are stationary, while for both K_1 and m_1 odd, all trapping states are of odd parity, with coherences between every second trapping state are stationary [cf. Tab. I].

Pure stationary states between hard walls. When atoms are prepared in the superposition (8), a hard wall at m implies *boundary conditions* for the pure stationary states. Namely, for $\sin_m(\phi) = 0$ and $\cos_m(\phi) = (-1)^K$, Eq. (24) gives

$$\beta c_m = (-1)^K c_e c_m, \quad (45)$$

for the coefficient c_m of the pure stationary state before the wall, and

$$\alpha c_{m+2} = (-1)^K c_g c_{m+2}, \quad (46)$$

for the coefficient c_{m+2} of the pure stationary state after the wall. For a pure stationary state to exist between subsequent walls at m_n and $m_{n'}$ of the same

parity, the corresponding boundary conditions after m_n and before $m_{n'}$ must be simultaneously fulfilled, i.e., $\cos_{m_n}(\phi) = -\cos_{m_{n'}}(\phi)$, which requires $(K_{n'} - K_n)$ being odd [see Eq. (41)]. In particular, for the state before the first wall at m_1 , Eq. (45) together with Eq. (27), requires $\cos_{m_1}(\phi) = -1$, i.e., odd K_1 . In general, from Eq. (43) we can conclude that, the stationary states between the walls are pure only when both m_1 and K_1 are odd, i.e., there are only odd hard walls [see Tab. I]. Otherwise, the stationary states must be mixed (except for the stationary state before the first wall which is also pure for even m_1 and odd K_1). They can, however, be approximately pure if the support of the state vanishes at one of their boundaries [cf. Eqs. (45) and (46), and see Fig. 3(b) [83]].

Note that the boundary conditions in Eqs. (45) and (46) impose the eigenvalue of the Kraus operators, (25), to be of opposite sign for the states before and after the wall. Therefore, when many pure stationary states exist [odd hard walls for m_1 and K_1 odd from Eq. (43)], the coherences only between the stationary states with the same boundary condition are stationary [every second stationary state], while the other decay with the eigenvalue of \mathcal{L}_0 equal -2ν [cf. Eq. (30)]. This result can be understood as the hard wall imprinting with every passing atom the opposite phases on the two stationary states before and after the wall, so that on average the coherence undergoes *dephasing* [84] [see Fig. 3(a)]. Furthermore, no coherences between pure stationary states and mixed stationary states are stationary [85].

Soft walls. We now discuss a more general case when the terms of the Kraus operators in Eq. (16) that connect the cavity states $|m\rangle$ and $|m+2\rangle$ instead of equal 0 are close to 0, i.e. $\sin_m(\phi) \approx 0$. We refer to this situation as a *soft wall* at m .

We now show there exist infinitely many arbitrary small soft walls, provided that the integrated coupling strength ϕ/π is irrational, or $\phi/\pi = p/q$ is rational with the even irreducible numerator p [for a hard wall where ϕ is given by Eq. (41), ϕ/π is irrational, but with a rational square]. From the Taylor series

$$\phi\sqrt{(n+1)(n+2)} = \phi\left(n + \frac{3}{2}\right) + \mathcal{O}\left(\frac{\phi}{n}\right), \quad (47)$$

so that for large n we have $\sin_n(\phi) \approx \sin[\phi(n+3/2)]$, i.e., it corresponds to n rotations of a unit circle by ϕ with the initial phase $3\phi/2$. It is known that for an irrational ϕ/π , the orbits of the rotation (values of $e^{i\phi n}$ for all n) are dense in the circle, so they pass by any point on the circle within an arbitrary proximity, and, from *Poincaré recurrence theorem*, this takes place infinitely many times. As these properties of the rotation are not changed by the initial phase, the cavity dynamics features infinitely many soft walls for both parities [cf. the case ϕ_3 (grey diamonds) in Fig. 4 and [86]]. In contrast, for a rational $\phi/\pi = p/q$, the orbits of the rotation are periodic with the period q for even p , and $2q$

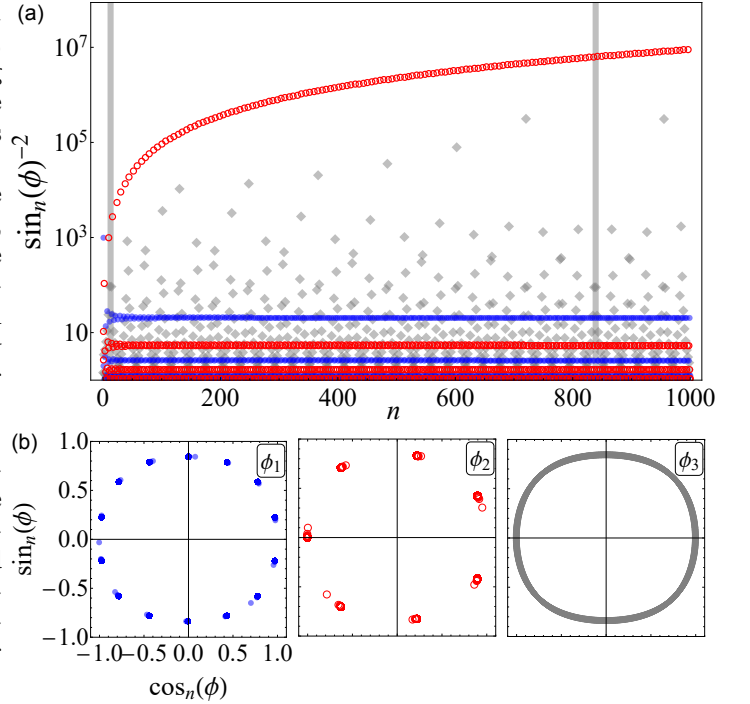


FIG. 4. **Soft walls.** (a) The function $\sin_n^{-2}(\phi)$ for: rational $\phi_1/\pi = 5/7$ (blue dots), $\phi_2/\pi = 6/7$ (red circles), and irrational $\phi_3/\pi = 7/\sqrt{210}$ (grey diamonds), with the hard walls (grey lines) at $m_1 = 13$ and $m_2 = 839$. For ϕ_1 the walls remain finite, in contrast to ϕ_2 , where $\sin_n^{-2}(\phi)$ diverges as n^{-2} [cf. Eq. (47)] and ϕ_3 , where soft walls appear due to recurrence of the irrational rotation. (b) The orbits for both ϕ_1 and ϕ_2 are approx. periodic (with period 14 and 7), while for ϕ_3 the orbit is dense.

for odd p . Therefore, from (47), the orbits of $\sin_m(\phi)$ become approximately periodic for large n , but with a shift in phase $3\phi/2$ [see the cases of ϕ_1 (blue dots) and ϕ_2 (red circles) in Fig. 4(b)]. Nevertheless, soft walls appear when the shifted periodic orbit features $\sin[\phi(m+3/2)] = 0 = \sin(k\pi)$. This requires $(2m+3)p = 2kq$, i.e., p to be even. Thus, the period q of the soft wall recurring is odd, so that the soft walls appear at m of both parities. Moreover, $\cos_m(\phi) \approx \cos[\phi(m+3/2)] = (-1)^{p/2}$ and $\sin_m^{-2}(\phi) \approx (8m+12)^2/\phi^2$ [cf. the case ϕ_2 (red circles) in Fig. 4].

Dynamics with soft walls [$\sin_m(\phi) \approx 0$] can be considered as a local perturbation of the dynamics where the soft walls are replaced by hard walls [$\sin_m(\phi) = 0$] [see Eq. (E5) in Appendix E]. This auxiliary dynamics features stationary states supported between the hard walls, but when the walls are soft, those states are no longer stationary, but become *metastable* [50, 87]. At long times the metastable states undergo effective dynamics at rates proportional to the perturbation size, i.e., $\nu \sin_m^2(\phi)$. Furthermore, as the perturbation is local, the effective dynamics only connects states across a single wall or introduces coherences between states separated by two walls, while the dynamics rates are propor-

tional to the state amplitude directly next to the wall (see Appendix E 2.). If the amplitude is small, the timescales of the dynamics are further extended [compare last two columns in Fig. 2(c)]. Finally, note that from Eq. (29) the resulting stationary state must be pure. It is, however, approximately composed only from the metastable states supported between the walls, which can be pure or mixed [depending on the boundary conditions in Eqs. (45) and (46)]. Therefore, the stationary state is approximately supported only on the pure metastable states, and those states must obey the same boundary conditions as in Eq. (27) (to guarantee that coherences between them are also long-lived) [in Fig. 2(b) those are the states after a blue and before a grey soft wall]. Thus, the photon number distribution in the stationary state is generally *multimodal*, where the modes correspond to the pure states with the same boundary conditions. These modes are distinct as they are separated at least by two walls [cf. Eqs. (45) and (46), and see Fig. 2(b) and Appendix E].

Importance of soft and hard walls for cavity dynamics. We have shown that, depending on the integrated coupling strength ϕ , the dynamics can feature infinitely many hard (or soft) walls, in which case the Kraus operators are (almost) block-diagonal leading to multiple stationary (or metastable) states supported between the walls. Hard walls can be used to prepare the cavity in a trapping state with a fixed photon number (a Fock state) corresponding to the position of the hard wall. Hard walls also motivate a natural truncation point for the cavity space in the simulations of the cavity dynamics, which we exploit in Figs. 2-11. On the other hand, the appearance of soft walls indicates multiple slow timescales in the cavity dynamics, and thus in general implies that long experimental timescales are needed to achieve the pure stationary states in Eq. (29) [see last two columns in Fig. 2(c) and Fig. 9]. However, soft walls introduce strong variations in the structure of the pure stationary states of the micromaser [cf. Eq. (29) and see Appendix E] and can be beneficial for quantum metrology applications (see Sec. VI).

V. METASTABILITY IN THE CAVITY DYNAMICS

In Sections III and IV we considered the cavity dynamics in the far-detuned limit, where the cavity interacted with the atoms via the two-photon Jaynes-Cummings Hamiltonian. The parity of photon number in the cavity was conserved, leading to existence of even and odd stationary states. These states were in general pure, and coherences between them were stationary as well.

Now we address the issue of how the dynamics and the stationary states of the cavity are modified beyond the two-photon approximation of Secs. III and IV. First, in Sec. V A we discuss the effect of finite detuning in-

roducing higher-order corrections to two-photon Jaynes-Cummings Hamiltonian. Second, in Sec. V B we investigate the effect of single-photon losses from the cavity. Finally, in Sec. V C we discuss the effect on the dynamics in the presence of hard walls. We assume that the above perturbation to the cavity dynamics are weak, and this separation in parameter scales, leads to a clear separation of timescales in the dynamics, known as *metastability* [50]. For the reader's convenience we provide a short review of metastability theory for open quantum systems in Appendix F.

A. Metastability due to higher-order corrections in the far-detuned limit

The two-photon micromaser investigated in Secs. III and IV, relies on the assumption of the far-detuned limit, i.e., $g_j/\Delta_j, G/\delta \ll 1$, $j = 0, \dots, 4$ [cf. Fig. 1]. Now we discuss how the micromaser dynamics is changed by the higher-order corrections to the atom-cavity interaction.

Breaking of parity conservation. Recall that beyond the far-detuned limit, (14), the atom-cavity interaction, (4b), couples all atom levels. This corresponds to six, rather than only two, Kraus operators [cf. Eqs. (9) and (16)]

$$M_j = \langle j|U(\tau)|\psi_{\text{at}}\rangle, \quad j = 0, \dots, 4, a, \quad (48)$$

where $U(\tau)$, describes the atom-cavity interaction during time τ when the atom, initially in $|\psi_{\text{at}}\rangle$, passes through the cavity. These Kraus operators either *conserve or swap the cavity parity* P [cf. Eq. (19)] depending on j ,

$$\begin{aligned} M_j P &= \langle j|U(\tau)P|\psi_{\text{at}}\rangle = -\langle j|U(\tau)(-1)^N|\psi_{\text{at}}\rangle = \\ &= -\langle j|(-1)^N U(\tau)|\psi_{\text{at}}\rangle = (-1)^{j+1} P M_j, \end{aligned} \quad (49)$$

where we used the fact that the dynamics conserves the total number of excitations $N = a^\dagger a + \sum_{j=1}^4 j \sigma_{jj} + 3\sigma_{aa}$, i.e., $[U(\tau), N] = 0$, while $(-1)^N |j\rangle = (-1)^j P |j\rangle$ and thus $(-1)^N |\psi_{\text{at}}\rangle = -P |\psi_{\text{at}}\rangle$ for the initial atom state as in Eq. (8). For $j = 0, 2, 4$ the Kraus operator swaps the parity, $M_j P + P M_j = 0$, while for $j = 1, 3, a$, the Kraus operator conserves the parity, $M_j P - P M_j = 0$. Therefore, beyond the far-detuned limit, although the cavity dynamics in Eqs. (10) and (11), does no longer conserve the parity, (21), it still features *weak parity symmetry* [76, 77],

$$[\mathcal{P}, \mathcal{L}] = 0 = [\mathcal{P}, \mathcal{M}], \quad (50)$$

where the parity superoperator $\mathcal{P}(\rho) = P\rho P$ (cf. Sec. IIIB). From the weak parity symmetry, it follows that \mathcal{L} is block-diagonal in the eigenspaces of \mathcal{P} , i.e., odd-even and even-odd coherences evolve independently from the mixtures of even and odd states. In particular, if \mathcal{L} features a unique stationary state, it must be a mixture of odd and even states without coherences between them.

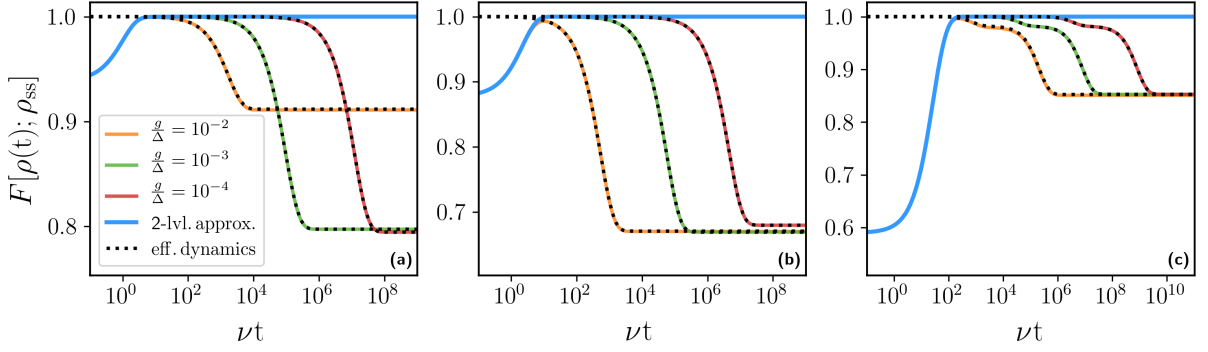


FIG. 5. **Dynamics of (5+1)-level micromaser versus effective 2-photon micromaser.** The fidelities $F[\rho_{ss}; \rho(t)] = \text{Tr} \sqrt{\sqrt{\rho_{ss}} \rho(t) \sqrt{\rho_{ss}}}$ of the stationary state ρ_{ss} in the two-photon micromaser with respect to its evolving state $\rho(t)$ (blue solid line), Eq. (18), and to the evolving state $\rho(t)$ of (5+1)-micromaser, Eq. (11), for increasing values of detuning (orange, green, red solid lines), while keeping the integrated coupling ϕ constant. Excellent agreement is observed during the metastable regime, whose length increases with the square of the detuning and coupling strength ratio, and is followed by the long-time dynamics well-approximated by the effective dynamics in the DFS (black dotted lines), Eq. (51). These results are observed for different atom states, coupling strengths, and initial cavity states: **(a)** $c_e = 0.3$, $\phi = 1.0$, $|\psi_{\text{in}}\rangle = |0\rangle$ (the vacuum), **(b)** $c_e = 0.2$, $\phi = 0.3$, $|\psi_{\text{in}}\rangle = |1\rangle$ (the single-photon state), **(c)** $c_e = 0.1$, $\phi = 0.1$, $|\psi_{\text{in}}\rangle = |\alpha\rangle$, $\alpha = 1$ (a coherent state). The coupling strengths and the detunings in the (5+1)-level model are chosen uniformly as $g_1 = g_2 = g_3 = g_4 = g$ and $\Delta_1 = \Delta_2 = -\Delta_3 = -\Delta_4 = \Delta$, together with $G = 2g$ and $\delta = 2\Delta$, and thus satisfy Eq. (13).

Higher-order corrections to cavity dynamics. The approximation of far-detuned regime yields two-photon interaction of the cavity with only two atomic levels $|1\rangle$ and $|3\rangle$, Eq. (14), and thus two parity-conserving Kraus operators M_1 and M_3 [denoted as M_g and M_e in Eq. (16)]. Beyond this approximation the remaining Kraus operators, M_0, M_2, M_4, M_a , also contribute to the cavity dynamics, and enter as the first-order corrections in $|g_j/\Delta_j|, |G/\delta| \ll 1$, $j = 1, \dots, 4$, while M_1 and M_3 are altered only in the second-order (a consequence of the parity conservation). The expressions are given and derived in Appendix B.

Metastability and perturbation theory. In Fig. 5 we compare the dynamics of the (5+1) micromaser, Eq. (11), with the two-photon dynamics, Eq. (18), obtained in the far-detuned limit. We observe that the (5+1) micromaser features the *initial relaxation* to the DFS of even and odd pure stationary states of the two-photon dynamics [Eq. (29)]. This is followed by the regime of apparent stationarity, i.e., the *metastable regime*, before the *final relaxation* towards the true stationary state at much longer times. Furthermore, the metastable regime becomes more pronounced with the increasing detuning, as the far-detuned limit is approached, but the asymptotic stationary state remains manifestly different from

the metastable one. This indicates that higher-order corrections to the atom-cavity dynamics affect the micromaser dynamics in a perturbative way, and, due to parity breaking, lift the degeneracy of the (formerly) stationary states. We therefore adapt it as the working assumption, which will enable us to analytically derive and investigate the long-time dynamics of the micromaser. We note, however, that the numerical simulations in this work are performed for *truncated* cavity space, which is infinite (see also Sec. IV D). Although for finitely dimensional systems the perturbative approach we utilize here is known to be convergent [88], the cavity is a infinitely dimensional system and its unperturbed dynamics in principle features infinitely many-timescales. Therefore, in principle a formal analysis as in Ref. [54] should be performed.

The DFS of pure stationary states of the cavity (see Sec. IV B) correspond to the eigenmodes with eigenvalue 0 of the master dynamics \mathcal{L}_0 in Eq. (18). To investigate the full dynamics \mathcal{L} of the cavity in Eq. (11) we consider it as the perturbation of \mathcal{L}_0 . In this case, the higher-order corrections in the far-detuned limit of the cavity and atom interactions, lift the degeneracy of zero-eigenmodes, thus introducing their long-time dynamics (see Appendix G for derivation)

$$\frac{d}{dt} \rho(t) = \nu \begin{bmatrix} -\langle X \rangle_+ & \langle X \rangle_- & 0 & 0 \\ \langle X \rangle_+ & -\langle X \rangle_- & 0 & 0 \\ 0 & 0 & -i\Omega - \frac{1}{2}(\langle X \rangle_+ + \langle X \rangle_-) & \eta \sqrt{\langle X \rangle_+ \langle X \rangle_-} \\ 0 & 0 & \eta^* \sqrt{\langle X \rangle_+ \langle X \rangle_-} & i\Omega - \frac{1}{2}(\langle X \rangle_+ + \langle X \rangle_-) \end{bmatrix} \rho(t), \quad (51)$$

where $\rho(t)$ belongs to the DFS spanned by $|\Psi_+\rangle$ and $|\Psi_-\rangle$ (we assumed there is a unique stationary state of even and odd parity, i.e. there are no hard walls of \mathcal{L}_0). The long-time dynamics is expressed in the DFS basis $|\Psi_+\rangle\langle\Psi_+|$, $|\Psi_-\rangle\langle\Psi_-|$, $|\Psi_+\rangle\langle\Psi_-|$, $|\Psi_-\rangle\langle\Psi_+|$. The non-trivial long-time dynamics of the pure states of the cavity means that they are no longer stationary, but instead become *metastable*, and at long times relax to a *unique stationary state* approximated by the stationary state of Eq. (51) (cf. Fig. 5)

$$\rho_{ss} \approx \frac{\langle X \rangle_-}{\langle X \rangle_- + \langle X \rangle_+} |\Psi_+\rangle\langle\Psi_+| + \frac{\langle X \rangle_+}{\langle X \rangle_- + \langle X \rangle_+} |\Psi_-\rangle\langle\Psi_-|. \quad (52)$$

The *block-diagonal* structure of the effective dynamics generator in Eq. (51), with the coher-

ences $|\Psi_+\rangle\langle\Psi_-|$, $|\Psi_-\rangle\langle\Psi_+|$, evolving independently from $|\Psi_+\rangle\langle\Psi_+|$, $|\Psi_-\rangle\langle\Psi_-|$, reflects the weak parity symmetry of dynamics, Eq. (50), which further manifests in diagonal structure of the stationary state in Eq. (52). The dynamics features the Hamiltonian part [89, 90] from the second-order corrections in the parity-conserving Kraus operators M_1 and M_3 , with the frequency

$$\Omega \equiv \text{Im}\langle c_g(M_1 - M_g)^\dagger - c_e(M_3 - M_e)^\dagger \rangle_+ - \text{Im}\langle c_g(M_1 - M_g)^\dagger - c_e(M_3 - M_e)^\dagger \rangle_-, \quad (53)$$

and the dissipative counterpart [91] induced by the (first-order) corrections in the parity swapping operators, where

$$X \equiv M_0^\dagger M_0 + M_2^\dagger M_2 + M_4^\dagger M_4, \quad (54)$$

so that $\langle X \rangle_\pm$ is positive and of the second-order,

$$\begin{aligned} \langle X \rangle_\pm = & 2|c_g|^2 \frac{|g_2|^2}{\Delta \Delta_1} \left\langle (n+1) - (n+1) \cos \left[\tau \Delta_1 + \tau \frac{|g_2|^2}{\Delta} (n+2) \right] \right\rangle_\pm + 2|c_g|^2 \frac{|g_2|^2}{\Delta^2} \left\langle n - n \cos \left[\tau \Delta + \tau \frac{|g_2|^2 + |g_3|^2}{\Delta} (n-1) \right] \right\rangle_\pm \\ & + 2|c_e|^2 \frac{|g_3|^2}{\Delta^2} \left\langle (n+1) + (n+1) \cos \left[\tau \Delta + \tau \frac{|g_2|^2 + |g_3|^2}{\Delta} (n+1) \right] \right\rangle_\pm - 2|c_e|^2 \frac{|g_3|^2}{\Delta \Delta_4} \left\langle n + n \cos \left[\tau \left(\Delta_4 - \frac{|g_2|^2}{\Delta} - \frac{|g_3|^2}{\Delta} n \right) \right] \right\rangle_\pm \\ & + 2 \left\langle -i \frac{g_2^* g_3}{\Delta^2} (a^\dagger)^2 \sin \left[\tau \Delta + \tau (n+1) \frac{|g_2|^2 + |g_3|^2}{\Delta} \right] + i \frac{g_2 g_3^*}{\Delta^2} \sin \left[\tau \Delta + \tau (n+1) \frac{|g_2|^2 + |g_3|^2}{\Delta} \right] a^2 \right\rangle_\pm, \end{aligned} \quad (55)$$

with $\langle \cdot \rangle_\pm = \langle \Psi_\pm | \cdot | \Psi_\pm \rangle$ and $n = a^\dagger a$. We note that the parity-conserving M_a , does not contribute to the second-order dynamics [cf. Eqs. (54) and (56)], as the pure stationary states are eigenstates of M_a in the first order (see Appendix G). Furthermore, the dynamics of coherences depends on

$$\eta = \frac{\text{Tr} \left(L_{+-} \sum_{j=0,2,4} M_j |\Psi_-\rangle\langle\Psi_+| M_j^\dagger \right)}{\sqrt{\langle X \rangle_+ \langle X \rangle_-}}, \quad (56)$$

where L_{+-} is a conserved quantity in the far-detuned limit corresponding to the coherence $|\Psi_+\rangle\langle\Psi_-|$ [see Eq. (34) in Sec. IV B]. From the complete-positivity of the perturbative long-time dynamics [50], we have $|\eta| \leq 1$. Although L_{+-} , and thus also η , generally are not known analytically, η can be obtained numerically without diagonalising \mathcal{L}_0 (see Appendix G).

In Fig. 5 we compare the dynamics of the cavity in (5+1) model (solid lines), Eq. (11), to the effective long-time dynamics within the DFS (dotted lines), Eq. (51), and observe a very good agreement in the relaxation towards the stationary state, Eq. (52), taking place after the metastable regime. Note that the effective dynamics depends via Ω and $\langle X \rangle_\pm$ both on the second order of the corrections to the far-detuned limit, $|g_j/\Delta_j|, |G/\delta| \ll 1$, $j = 1, \dots, 4$, as well as the interaction time τ . Thus, the structure of the final stationary state can be changed without altering the initial relax-

ation towards the metastable DFS, which depends only on the integrated coupling ϕ [see Fig. 5(a)]. Furthermore, Eq. (51) determines the final relaxation timescales towards the unique stationary state. The timescales are inversely proportional to the second order of the corrections to the far-detuned limit [cf. Eqs. (53), (54) and (56)], and thus the free parameters $g_2, g_3, \Delta, \Delta_1/\Delta > 0, \Delta_4/\Delta < 0$ and $\delta/\Delta < 0$ in Eq. (13) can be further optimised in order to extend the length of metastability regime (while keeping ϕ constant).

Finally, we note that relaxing of the conditions of Eq. (13) which we have chosen to obtain the two-photon Jaynes-Cummings Hamiltonian of atom cavity-interaction [Eq. (14)] will lead to a perturbation of the two-photon Hamiltonian [cf. Eq. (12)] and thus corrections to parity-conserving Kraus operators M_g and M_e . Therefore, analogously to Eq. (53), in the lowest order of corrections to Eq. (13) only a unitary dynamics will be induced in DFS (see Appendix G). We can conclude that the design is stable, which is necessary for any experimental implementation of (5+1)-model (see also Sec. VII).

B. Metastability due to single-photon losses

We now discuss a realistic setup in which the cavity undergoes *single-photon losses* [57], typically due to im-

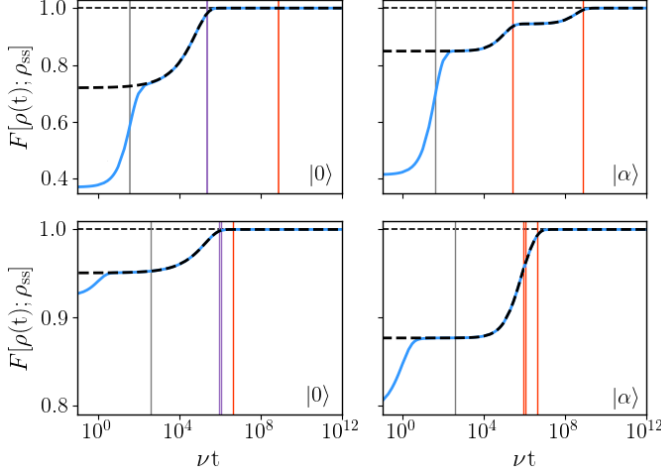


FIG. 6. Dynamics of micromaser with single-photon losses. The fidelity [cf. Fig. 5] between the cavity state $\rho(t)$ and the stationary state (62) is compared for the dynamics of two-photon micromaser with single-photon losses (blue solid line), (58), and the effective dynamics in the DFS (black dashed line), (60). The effective dynamics approximates well the long-time dynamics of the cavity for the initial states $|0\rangle$ (a,c) and $|\alpha\rangle$, $\alpha = 0.6$ (b,d), both in the weak-coupling limit [$c_e = 0.1$, $\phi = 0.1$ in (a,b)], where additional metastable regime (second plateau) is observed (b), and at the finite coupling [$c_e = 0.2$, $\phi = 1.0$ in (c,d)]. The loss rate was chosen as $\kappa/\nu = 10^{-6}$, and the vertical lines indicate the timescales of the dynamics determined by the eigenvalues of Eq. (58), $(-\text{Re}\lambda_k)^{-1}$ for $k = 5, 4, 2$ (black, purple, red) which are ordered in decreasing real value [see also Eqs. (63) and (64) and cf. Appendix F].

$$\frac{d}{dt}\rho(t) = \kappa \begin{bmatrix} -\langle n \rangle_+ & \langle n \rangle_- & 0 & 0 \\ \langle n \rangle_+ & -\langle n \rangle_- & 0 & 0 \\ 0 & 0 & -\frac{1}{2}(\langle n \rangle_+ + \langle n \rangle_-) & \eta_{\text{loss}}\sqrt{\langle n \rangle_+ \langle n \rangle_-} \\ 0 & 0 & \eta_{\text{loss}}\sqrt{\langle n \rangle_+ \langle n \rangle_-} & -\frac{1}{2}(\langle n \rangle_+ + \langle n \rangle_-) \end{bmatrix} \rho(t), \quad (60)$$

where we expressed the dynamics in the basis $\{|\Psi_+\rangle\langle\Psi_+|, |\Psi_-\rangle\langle\Psi_-|, |\Psi_+\rangle\langle\Psi_-|, |\Psi_-\rangle\langle\Psi_+|\}$, and denoted the average loss rate as $\kappa\langle n \rangle_{\pm} = \kappa\langle\Psi_{\pm}|a^{\dagger}a|\Psi_{\pm}\rangle$. The dynamics is *block-diagonal* due to the weak parity symmetry, Eq. (59), so that the densities and the coherences evolve independently. The dynamics of coherences further depends on the real coefficient

$$\eta_{\text{loss}} = \frac{\text{Tr}(L_{+-} a |\Psi_-\rangle\langle\Psi_+| a^{\dagger})}{\sqrt{\langle n \rangle_+ \langle n \rangle_-}}, \quad |\eta_{\text{loss}}| \leq 1, \quad (61)$$

in analogy to Eq. (56), that can be determined numerically without diagonalizing \mathcal{L}_0 [see Eq. (34) and Appendix G]. In particular, in the weak-coupling regime where the DFS corresponds to Schrödinger-cat states we

perfect mirrors

$$\mathcal{L}_{1\text{ph}}[\rho(t)] = \kappa a \rho(t) a^{\dagger} - \frac{\kappa}{2} [a^{\dagger} a \rho(t) + \rho(t) a^{\dagger} a], \quad (57)$$

where κ is the single-photon loss rate. Provided that losses of photons can be assumed to take place when no atom is found within the cavity, i.e., the atom passage time τ is such that $\kappa\tau \ll 1$, the single-photon losses can be considered independent of the atom-cavity dynamics [31, 57], so that the cavity state evolves as

$$\frac{d}{dt}\rho(t) = (\mathcal{L}_0 + \mathcal{L}_{1\text{ph}})[\rho(t)]. \quad (58)$$

In Eq. (58) we assumed the far-detuned limit of Eq. (18).

Similarly as in the case of higher-order corrections in the far-detuned limit, the single-photon loss swaps the parity $aP + Pa = 0$ [Eq. (19)], thus leading to the weak parity symmetry of the dynamics [cf. Eq. (50)]

$$[\mathcal{P}, \mathcal{L}_{1\text{ph}}] = 0. \quad (59)$$

Metastability. In Fig. 6 we consider the cavity dynamics in the presence of small losses (blue solid lines), Eq. (58) with $\kappa \ll \nu$, and observe a plateau in the relaxation towards the unique stationary state of the dynamics. This manifests a *metastable regime* in the dynamics when cavity states appear stationary for different initial conditions, although the true stationary state has not been achieved [see also Fig 1(d)].

If the losses are treated as a perturbation of the cavity dynamics \mathcal{L}_0 , the formerly stationary states in the DFS of $|\Psi_+\rangle$ and $|\Psi_-\rangle$, Eq. (29), undergo the following dynamics [cf. Eq. (51) and see Appendix G for derivation]

have $\eta_{\text{loss}} = 1$, as the photon loss does not perturb the states outside the DFS (see Sec. IV C and [39]).

In Fig. 6 the effective dynamics of Eq. (60) (black dashed line) indeed approximates well the long-time dynamics of the cavity. This confirms that the initial relaxation of the cavity state takes the system into the DFS spanned by $|\Psi_+\rangle$ and $|\Psi_-\rangle$ [cf. Eq. (33)]. The DFS then remains metastable until timescales inversely proportional to the average loss rates. Then, the final relaxation takes place into a *unique stationary state*, well approximated by the stationary state of Eq. (60),

$$\rho_{\text{ss}} \approx \frac{\langle n \rangle_-}{\langle n \rangle_- + \langle n \rangle_+} |\Psi_+\rangle\langle\Psi_+| + \frac{\langle n \rangle_+}{\langle n \rangle_- + \langle n \rangle_+} |\Psi_-\rangle\langle\Psi_-|, \quad (62)$$

cf. [52, 53]. The stationary state does not feature odd-even coherences because of the weak parity symmetry in Eq. (59) (see Fig. 7). Finally, we note that the rates of the effective dynamics are proportional to the average photon number, so that, as expected, the states with more photons are more sensitive to losses. In particular, in the stationary state (62) the state with the lower average photon number has larger weight.

An analogous result to Eq. (60) can be obtained for a cavity in a thermal environment. In this case photons are lost from the cavity at the rate $\kappa(n_{\text{th}} + 1)$, but they are also be injected to the cavity [which process is described as by replacing a by a^\dagger in Eq. (57)] at the rate κn_{th} , and n_{th} is a average photon number in the environment.

Emergent classical metastability in weak coupling limit. For small interactions, $|\phi| \ll 1$, where the stationary states of the lossless cavity are approximated by Schrödinger-cat states the dynamics in Fig. 6(b) features two plateaus corresponding to *two metastability regimes* [see also Fig. 1(d) and Sec. IV C].

The timescales of the long-time dynamics are determined by the eigenvalues of Eq. (60) (see also Appendix F). The stationary state in Eq. (62) necessarily corresponds to the eigenvalue $\lambda_1 = 0$, while

$$\lambda_2 = -\frac{\kappa}{2} \left(\langle n \rangle_+ + \langle n \rangle_- - 2|\eta_{\text{loss}}| \sqrt{\langle n \rangle_+ \langle n \rangle_-} \right) \quad (63a)$$

$$\lambda_3 = -\frac{\kappa}{2} \left(\langle n \rangle_+ + \langle n \rangle_- + 2|\eta_{\text{loss}}| \sqrt{\langle n \rangle_+ \langle n \rangle_-} \right) \quad (63b)$$

$$\lambda_4 = -\kappa (\langle n \rangle_+ + \langle n \rangle_-), \quad (63c)$$

ordered in decreasing real part.

In the weak-coupling limit, $\eta_{\text{loss}} = 1$ in Eq. (61), so that $\lambda_{2,3} = -\kappa (\sqrt{\langle n \rangle_+} \mp \sqrt{\langle n \rangle_-})^2/2$. Therefore, when the average photon numbers in the even and odd Schrödinger-cat states are similar [$\langle n \rangle_+ = |\alpha|^2 \tanh(|\alpha|^2)$, $\langle n \rangle_- = |\alpha|^2 \coth(|\alpha|^2)$ with $|\alpha|^2 = 2|c_e/c_g\phi| \gg 1$; cf. Eq. (37)], a *separation in the spectrum* of the long time-dynamics emerges

$$-\lambda_2 \approx \frac{\kappa}{4} \frac{(\langle n \rangle_+ - \langle n \rangle_-)^2}{\langle n \rangle_+ + \langle n \rangle_-} \ll -\lambda_3 \approx \kappa (\langle n \rangle_+ + \langle n \rangle_-) = \lambda_4, \quad (64)$$

see Fig. 6(a,b). This separation directly leads to metastability regime for times $(-\lambda_3)^{-1} \ll t \ll (-\lambda_2)^{-1}$ when the faster eigenmodes of the long-time dynamics corresponding to λ_3 and λ_4 have decayed, while the decay of the slow mode corresponding to λ_2 is negligible [see Fig. 7 and Appendix F]. In this case only the stationary state and the slow eigenmode contribute to the cavity state [50, 87] (see also [92])

$$\rho(t) \approx \rho_{\text{ss}} + c(|\Psi_-\rangle\langle\Psi_+| + |\Psi_+\rangle\langle\Psi_-|), \quad (65)$$

where $c = \text{Re}[\langle\Psi_+|\rho_{\text{in}}|\Psi_-\rangle]$ and ρ_{in} is the initial cavity state projected on the DFS, Eq. (33). Therefore, the second metastable regime is observed only for initial states with feature odd-even coherences [cf. Figs. 6(a)

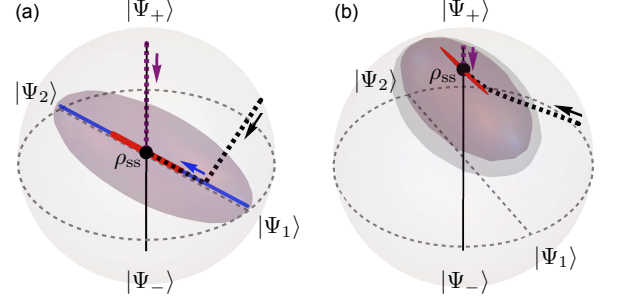


FIG. 7. Effective long-time dynamics due to single-photon losses. The DFS of the odd and even states (29) (the Bloch sphere in light grey) is shown under the effective dynamics in Eq. (60), for times $t = (-\lambda_4)^{-1}$, $(-\lambda_3)^{-1}$ and $(-\lambda_2)^{-1}$ (grey, purple, red) [see Eq. (63) and vertical lines in Fig. 6]. Due to the weak parity symmetry, the stationary state (black dot), Eq. (62), is found on the vertical axis (black line) representing mixtures of even and odd states, while when the initial state is odd or even, its dynamics remains confined to the vertical axis at all times (cf. purple dashed trajectory). As the effective dynamics is also real, the coherence eigenmodes correspond to the axis between the states in Eq. (67) (dashed grey) and its perpendicular on the equator. The trajectories for two initial states are also shown: $|\Psi_+\rangle$ (dashed purple) and $\cos(\pi/6)|\Psi_+\rangle + e^{i\pi/4}\sin(\pi/6)|\Psi_-\rangle$ (dashed black). In (a) due to separation of the characteristic timescales of the dynamics as given by Eq. (64), classical metastable manifold emerges [blue; the image of DFS under the dynamics of at $t = (-\lambda_2)^{-1}/100$], well approximated by mixtures of the states $|\Psi_1\rangle$ and $|\Psi_2\rangle$ in Eq. (67) (dashed grey axis). Here an initial state first relaxes onto the manifold (black arrow along black dashed trajectory), and only at later times relaxes towards the stationary state (blue arrow) [see also Fig. 6(b)]. Parameters: (a) as in Fig. 6(a,b) leading to $\eta_{\text{loss}} \approx 1.00$, $\langle n \rangle_+ \approx 1.92$ and $\langle n \rangle_- \approx 2.07$; (b) as in Fig. 6(c,d) leading to $\eta_{\text{loss}} \approx 0.99$, $\langle n \rangle_+ \approx 0.11$ and $\langle n \rangle_- \approx 1.01$.

and 6(b)]. Furthermore, during the metastable regime the cavity state can be also be regarded as a *classical mixture* [87] with the probability $p = 1/2 + c$,

$$\rho(t) \approx p|\Psi_1\rangle\langle\Psi_1| + (1-p)|\Psi_2\rangle\langle\Psi_2| \quad (66)$$

of the *coherent states* [cf. Fig. 1(d)]

$$|\Psi_{1,2}\rangle = \frac{1}{\sqrt{2}}(|\Psi_+\rangle \pm |\Psi_-\rangle) \approx |\pm\alpha\rangle, \quad (67)$$

see Fig 7. Eq. (66) follows from the fact that in the weak-coupling limit $\rho_{\text{ss}} \approx (|\Psi_+\rangle\langle\Psi_+| + |\Psi_-\rangle\langle\Psi_-|)/2$ [see Eq. (62)]. Note that the classical metastability can also take place beyond weak coupling limit if both $|\eta_{\text{loss}}| \approx 1$ and $\langle n \rangle_+ \approx \langle n \rangle_-$.

The origin of the classical metastability can be understood by representing Eq. (60) in terms of the master equation within the DFS [59, 60],

$$\frac{d}{dt}\rho(t) = \gamma J\rho(t)J^\dagger - \frac{\gamma}{2} [J^\dagger J\rho(t) + \rho(t)J^\dagger J], \quad (68)$$

where the dissipation rate is given by the average photon loss

$$\gamma = \kappa \frac{\langle n \rangle_+ + \langle n \rangle_-}{2}. \quad (69)$$

The jump operator J describes the effect of a single photon loss on the DFS by *flipping the parity* [cf. [52, 54]]

$$J = \frac{1}{N} \left[\left(\langle n \rangle_+ + \sqrt{\langle n \rangle_+ \langle n \rangle_-} \right) |\Psi_+\rangle\langle\Psi_-| + \left(\langle n \rangle_- + \sqrt{\langle n \rangle_+ \langle n \rangle_-} \right) |\Psi_-\rangle\langle\Psi_+| \right], \quad (70)$$

with the normalization factor $N = \sqrt{\langle n \rangle_+ + \langle n \rangle_-} (\sqrt{\langle n \rangle_+} + \sqrt{\langle n \rangle_-})$. In Eq. (68) we assumed $\eta_{\text{loss}} = 1$. In particular, when the average photon number in the even and odd states is similar, $\langle n \rangle_+ \approx \langle n \rangle_-$, the jump operator in Eq. (70) can be approximated as the spin flip,

$$J \approx \frac{1}{\sqrt{2}} (|\Psi_+\rangle\langle\Psi_-| + |\Psi_-\rangle\langle\Psi_+|) \quad (71)$$

$$= \frac{1}{\sqrt{2}} (|\Psi_1\rangle\langle\Psi_1| - |\Psi_2\rangle\langle\Psi_2|),$$

which exactly leads to *dephasing* of coherences between the states in Eq. (67) [see Figs. 1(d) and 7] and takes place at the rate γ in Eq. (69). The states $|\Psi_1\rangle$ and $|\Psi_2\rangle$ themselves are left invariant by the dephasing, and thus we conclude that the states in Eq. (66) are metastable.

Dynamics of lossy cavity beyond the far-detuned limit. In this section we have considered single-photon losses from the cavity in the far-detuned limit [see Eq. (58)]. As we discussed earlier in Sec. V A, the higher-order corrections in the far-detuned limit also modify the cavity dynamics [see Eq. (51)]. These corrections can be incorporated in the analysis of dynamics with single-photon losses. In the lowest order of corrections, the long-time dynamics of the cavity is described by the sum of the contributions, i.e., the sum of Eqs. (51) and (60). The resulting dynamics features weak parity symmetry and has the unique stationary state,

$$\rho_{\text{ss}} \approx p_+ |\Psi_+\rangle\langle\Psi_+| + (1 - p_+) |\Psi_-\rangle\langle\Psi_-|, \quad (72)$$

$$p_+ = \frac{\kappa \langle n \rangle_- + \nu \langle X \rangle_-}{\kappa (\langle n \rangle_- + \langle n \rangle_+) + \nu (\langle X \rangle_- + \langle X \rangle_+)}.$$

In Appendices G2.b. and G2.c. we also discuss the long-time-dynamics of the cavity for the case of a mixed rather than pure atom state [cf. Eq. (8)] and for a non-monochromatic atom beam. Both those perturbations conserve the parity (20) and thus, in the lowest order, simply lead to the *dephasing* of odd-even coherences in the DFS.

C. Metastability of hard walls

We now discuss the effective dynamics due to higher-order corrections in the far-detuned limit and single-photon losses [cf. Eqs. (51) and (60)] in the case when

the unperturbed dynamics features hard walls and, thus, multiple stationary states of the same parity (see Sec. IV D). In particular we show that there exist no trapping states in the presence of higher-order corrections in the far-detuned limit or single-photon losses.

No hard walls beyond far-detuned limit. A hard wall at m refers to the case of the zero probability of connecting states $|m\rangle$ and $|m+2\rangle$ [cf. Eqs. (16) and (41)]. As the wall affects only the states of the same parity [the subsequent walls are exponentially separated, see Eq. (44)], any perturbations in the dynamics that swap the parity allow for circumventing hard walls and lead to a unique stationary state [see Fig. 8].

For the first wall being even, there exist infinitely many even and odd stationary states between hard walls, which we denote ρ_k^+ and ρ_k^- , $k = 0, 1, \dots$ [cf. Tab I]. Due to single-photon losses or higher-order corrections these states become metastable and at long times undergo transitions: from ρ_k^+ to ρ_{k-1}^- or to ρ_k^- at the respective rates $\gamma_{k,k-1}^+$ and $\gamma_{k,k}^+$, and from ρ_k^- to ρ_k^+ or to ρ_{k+1}^+ at the respective rates $\gamma_{k,k}^-$ and $\gamma_{k,k+1}^-$, where

$$\gamma_{k,k'}^\pm = \kappa \langle n \rangle_{k,k'}^\pm + \nu \langle X \rangle_{k,k'}^\pm, \quad (73)$$

and $\langle n \rangle_{k,k'}^\pm = \text{Tr}(\mathbb{1}_{k'}^\mp a \rho_k^\pm a^\dagger)$ and $\langle X \rangle_{k,k'}^\pm = \sum_{j=0,2,4} \text{Tr}(\mathbb{1}_{k'}^\mp M_j \rho_k^\pm M_j^\dagger)$, while $\mathbb{1}_k^\pm$ is the projection on the support of ρ_k^\pm [cf. Eqs. (51) and (60)]. The rates in Eq. (73) simply depend on the overlap of the perturbed state, i.e., the state after a photon loss, with the support of a state of the opposite parity. Note that the *ladder structure* of the transitions obeys detailed balance [see Fig. 8(a)]. Thus, the stationary state is approximated as

$$\rho_{\text{ss}} \approx \sum_{k=0}^{\infty} p_k^+ \rho_k^+ + \sum_{k=0}^{\infty} p_k^- \rho_k^-, \quad (74)$$

which is determined by the rates, in the recurrence relation

$$\frac{p_k^+}{p_{k-1}^+} = \frac{\gamma_{k-1,k}^-}{\gamma_{k,k-1}^+}, \quad \frac{p_k^-}{p_k^+} = \frac{\gamma_{k,k}^+}{\gamma_{k,k}^-}, \quad (75)$$

cf. Eq. (72).

When the first hard wall is odd, there are no hard walls of even parity. As the effective dynamics features only the transitions between the states of opposite parity, we only have transitions from $|\Psi_+\rangle\langle\Psi_+|$ into ρ_k^- , and from ρ_k^- to $|\Psi_+\rangle\langle\Psi_+|$, for $j = 0, 1, \dots$, with the respective rates γ_k^+ and γ_k^- ,

$$\gamma_k^\pm = \kappa \langle n \rangle_k^\pm + \nu \langle X \rangle_k^\pm, \quad (76)$$

where $\langle n \rangle_k^- = \text{Tr}(n \rho_k^-)$ and $\langle X \rangle_k^- = \text{Tr}(X \rho_k^-)$, while $\langle n \rangle_k^+ = \text{Tr}(\mathbb{1}_k^- a |\Psi_+\rangle\langle\Psi_+| a^\dagger)$ and $\langle X \rangle_k^+ = \sum_{j=0,2,4} \text{Tr}(\mathbb{1}_k^- M_j |\Psi_+\rangle\langle\Psi_+| M_j^\dagger)$ with the projection $\mathbb{1}_k^-$

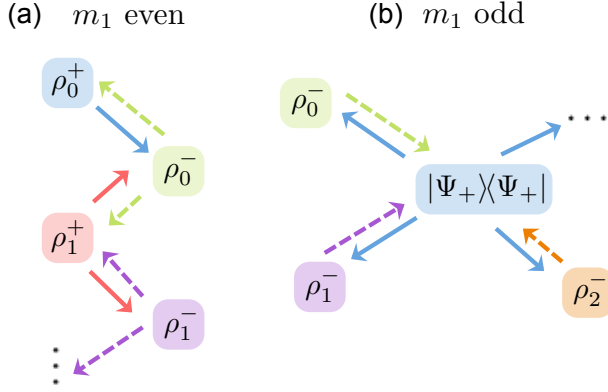


FIG. 8. **Dynamics of lossy cavity with hard walls.** (b) A first wall at even m_1 leads to hard walls of both parities [cf. Tab. I] and multiple even and odd stationary states. Single-photon losses induce local transitions between states of opposite parity: from ρ_k^+ only to ρ_{k-1}^- and ρ_k^- (solid arrows), and from ρ_k^- only to ρ_k^+ or ρ_{k+1}^+ (dashed arrows). This ladder structure of the dynamics implies a detailed balance. (b) A first wall at odd m_1 leads to only odd hard walls and multiple odd stationary states. Single photon losses induce transitions between from the unique even state $|\Psi_+\rangle\langle\Psi_+|$ to odd states ρ_k^- , $k = 0, 1, \dots$ (solid arrows) and from the odd states to the even state (dashed arrows) [cf. Tab. I]. This star structure again leads to detailed balance.

on the support of ρ_k^- . Note that the *star structure* also obeys detailed balance [see Fig. 8(b)]. Thus, the stationary state is approximated by

$$\rho_{ss} \approx p_+ |\Psi_+\rangle\langle\Psi_+| + \sum_{k=0}^{\infty} p_k^- \rho_k^-, \quad \text{with} \quad \frac{p_k^-}{p_+} = \frac{\gamma_k^+}{\gamma_k^-}. \quad (77)$$

See Appendix G for the derivation of Eqs. (73-77) and the corresponding dynamics of coherences.

No trapping states beyond far-detuned limit. In particular, for the cavity being pumped by the excited atoms, $|c_e| = 1$, the long-time dynamics due to losses or corrections to far-detuned limit, Eqs. (73), features only the transitions that increase the photon number: ρ_k^+ is transformed into ρ_k^- , while ρ_k^- is transformed into ρ_{k+1}^+ , at the respective rates $\kappa \text{Tr}(n \rho_k^\pm) + \nu \text{Tr}(X \rho_k^\pm)$. Thus, there exists no trapping state beyond the far-detuned limit.

VI. APPLICATION IN PHASE ESTIMATION

In Sections III and IV we discussed the dynamics of two-photon micromaser with atom-cavity interactions described by Jaynes-Cummings Hamiltonian, Eq. (14). This dynamics lead to pure stationary state of the cavity dependent on both the initial atom state and the integrated coupling strength, Eq. (29). Below we investigate the usefulness of the generated states for applications in phase estimation setups. We find that weak coupling does not yield a quantum enhancement in estimation precision, but strong coupling creates states which lead to an

enhanced sensitivity. Although experimental imperfections, such as single-photon losses, lead to mixed states, we find that they can still enable enhancement in phase estimation.

Quantum Fisher information (QFI). We consider a phase φ which is to be estimated as unitarily encoded in a cavity state ρ by the photon number operator $n = a^\dagger a$,

$$\rho_\varphi = e^{-i\varphi n} \rho e^{i\varphi n}. \quad (78)$$

This corresponds to the situation when, after dissipatively preparing the cavity in the state ρ by atom passages, the phase is subsequently encoded in the cavity state, e.g., by changing the cavity frequency by $\delta\omega$ to induce the phase $\varphi = \delta\omega t$ over time t [24]. The errors in the unbiased estimation of φ are then bounded, $\Delta^2\varphi \geq F_Q(\rho)^{-1}$, by the inverse of the quantum Fisher information [46, 47, 93, 94],

$$F_Q(\rho) = 2 \sum_{j,j'} \frac{(p_j - p_{j'})^2}{p_j + p_{j'}} |\langle E_j | n | E_{j'} \rangle|^2, \quad (79)$$

where Eq. (79) is expressed in the orthonormal eigenbasis of the state $\rho = \sum_j p_j |E_j\rangle\langle E_j|$. In particular, for pure states, $\rho = |\Psi\rangle\langle\Psi|$, the QFI is simply proportional to the photon number variance,

$$F_Q(|\Psi\rangle) = 4 (\langle\Psi|n^2|\Psi\rangle - \langle\Psi|n|\Psi\rangle^2). \quad (80)$$

For example, for the coherent state $|\alpha\rangle$, the photon distribution is Poissonian, and thus $F_Q(|\alpha\rangle) = 4\langle n \rangle = 4|\alpha|^2$, which is referred to as *standard quantum limit*. Therefore, the phase estimation with ρ features the *quantum enhancement* over the classical strategy using the same amount of resources, i.e., the coherent state with the same average photon number, whenever [95–97]

$$\frac{F_Q(\rho)}{4\langle n \rangle} > 1. \quad (81)$$

Considering this figure of merit is motivated by experimental limitations on the allowed energy, $\hbar\omega\langle n \rangle$, of the probe photon field. In such a case, further increase in the phase estimation precision can be achieved only by non-classical distribution of the field, e.g., squeezing.

A. QFI for micromaser in far-detuned limit

In Fig. 9 we consider the QFI for an evolving cavity state and for the asymptotic stationary state. The QFI varies significantly across the parameter space of the atom state and integrated coupling strength. Importantly, multiple distinct stationary states achieve *high enhancement over the classical limit*.

High QFI and Wigner function. The QFI, (79), which quantifies how sensitive is a state ρ to phase rotations, is directly related to the Wigner function, Eq. (22). The

QFI equals the speed of change in the overlap between the Wigner functions for ρ and ρ_φ [Eq. (78)] [25]. Furthermore, the Wigner function for ρ_φ is simply the Wigner function for ρ but rotated by φ . Therefore, for the states (iii-ix) with high values of the QFI the sign of the Wigner function highly oscillates [see Fig. 2(a)], thus ensuring a high QFI.

Enhancement in precision due to soft walls. The enhancement above the classical limit, Eq. (81), is facilitated by the presence of soft walls in the dynamics.

The stationary states, Eq. (29), are dependent on the initial atom state and the integrated coupling strength, but the atom parameters alone imply the exponential decay in the photon number distribution for $|c_e| \leq 1/\sqrt{2}$. The integrated coupling can instead facilitate a sharp revival in the occupation probability via a soft wall; for the wall at m , $\sin_m(\phi) \approx 0$ with $\cos_m(\phi) \approx 1$, we have $c_{m+2}/c_m \approx -i2\sin_m^{-1}(\phi) c_e/c_g$ (see Appendix E for further discussion). The revivals correspond directly to *multi-modal photon number distribution* [see Fig. 2(b)]. Since the considered stationary states are pure, their QFI is simply proportional to the photon number variance (80) and features the *square* of distance between modes averages

$$F_Q(|\Psi\rangle) = \sum_k p_k F_Q(|\Psi_k\rangle) + 4 \sum_k \sum_{k' > k} p_k p_{k'} (\langle n \rangle_k - \langle n \rangle_{k'})^2, \quad (82)$$

where $|\Psi\rangle = \sum_k \sqrt{p_k} |\Psi_k\rangle$ and $|\Psi_k\rangle$ represents the orthonormal k th mode. Thus, the QFI features quadratic rather than linear scaling with the average, which may lead to the precision enhancement, Eq. (81). Multiple soft walls in close proximity can also lead to a unimodal distribution, but with a spread significantly wider than for the corresponding coherent states [see state (iv) in Fig. 2(b)]. The same mechanism is present for the stationary states of both parities [cf. Fig. 10].

The presence of soft-walls introduces, however, long timescales of reaching pure stationary states, with cavity states being mixed at earlier times (purple shading in Fig. 9), even when the initial parity is fixed [see Sec. IV D and Fig. 2(c)]. The mixedness of the cavity state in general lowers the estimation precision, which is captured by convexity of the QFI. Nevertheless, in Fig. 9 we observe that the local maxima in the enhancement (iii-ix) are already present after passage of 100 atoms, and their value increases with time as the corresponding pure stationary states are approached (cf. the scale bars).

The revivals in photon probability distribution are highly sensitive to the coupling ϕ value, with their derivative proportional to m and $\sin_m^{-1}(\phi)$. Therefore, the structure of the cavity states varies significantly with ϕ , allowing for preparations of distinct states (see Fig. 2) and is the reason for strong variations of the QFI in Fig. 9 [98].

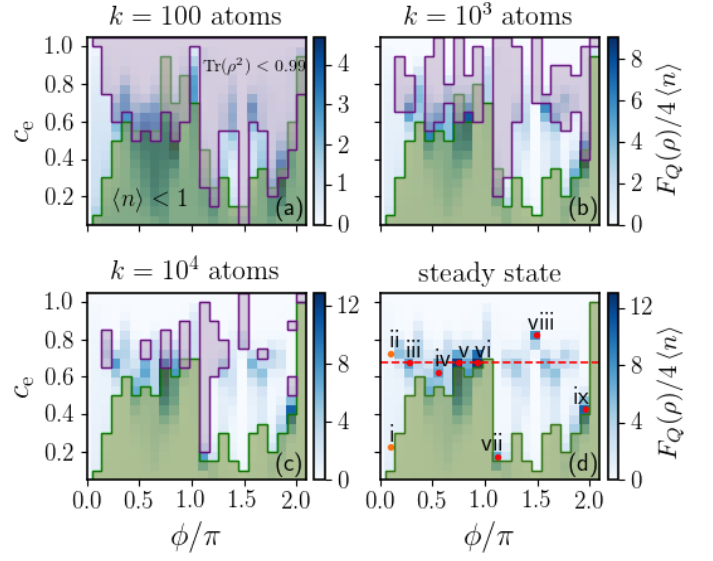


FIG. 9. Phase estimation with dissipatively generated cavity states. The four panels show the ratio of the QFI to the performance of the corresponding coherent state, $F_Q(\rho)/4\langle n \rangle$ for the cavity initially in the vacuum $|0\rangle$ after the passage of $k = 100, 10^3, 10^4$ atoms and for the stationary state [Eq. (29)]. The enhancement is shown as a function of the atom state [Eq. (8)] and integrated coupling ϕ . We sample the ϕ -axis for $\phi_{20,K}$, Eq. (41), with odd $K = 1, 3, \dots, 43$, which gives the hard wall at $m = 20$ and allows convergence to stationary state also for $c_e > 1/\sqrt{2}$ (note that a larger m would generally allow higher $\langle n \rangle$ and could also enable a higher enhancement in precision). The purple-shading shows regions with reduced purity $\text{Tr}(\rho^2) < 0.99$, whereas the green shading excludes low average photon number, $\langle n \rangle < 1$. The red dots in the steady-state panel mark the stationary states (i-ix) analysed in Fig. 2. The states (iii-ix) correspond to the states at the local maxima of the precision enhancement, while (i,ii) correspond to the standard and squeezed Schrödinger cat states. A complex phase of c_e does not change the results, but the stationary states are not periodic in ϕ , and thus here we show only a part of the parameter space.

Absence of enhancement in weak coupling limit. In the weak-coupling limit, the cat and squeezed-cat states are generated, examples of which are marked as states (i,ii) in Figs. 2 and 9. These states, although non-classical, do not feature the enhancement in the phase estimation precision. The parity-symmetry allows for a superposition of the coherent states with the opposite phase, $\pm\alpha$, but with the same average photon number, $|\alpha|^2$. Therefore, the photon number distribution remains unimodal with the spread of the coherent state [cf. Fig. 2(b)]. We note, however, that the enhancement proportional to $|\alpha|^2$ can be achieved via the linear operation of displacing the cat state in Eq. (36) by $\pm\alpha$, which would give a bimodal photon distribution with the modes centred at 0 and $|\alpha|^2$.

Coherence in DFS and QFI. In a general, an initial cavity state evolves into a mixed state inside the stationary DFS, but this cannot significantly reduce the enhance-

ment present in the pure stationary states of fixed parity.

From the conservation of the parity by the phase generator, $[n, P] = 0$, we have that $\langle \Psi_+ | n | \Psi_- \rangle = 0$. This simplifies the QFI for any state within the DFS,

$$\rho = p |\Psi_+\rangle\langle\Psi_+| + (1-p) |\Psi_-\rangle\langle\Psi_-| + c |\Psi_+\rangle\langle\Psi_-| + c^* |\Psi_-\rangle\langle\Psi_+|, \quad (83)$$

where $|c|^2 \leq p(1-p)$, to [99]

$$F_Q(\rho) = p F_Q(|\Psi_+\rangle) + (1-p) F_Q(|\Psi_-\rangle) + 4|c|^2 (\langle n \rangle_+ - \langle n \rangle_-)^2. \quad (84)$$

Therefore, the QFI increases with coherence $|c|$. It is maximal for the pure state $\sqrt{p}|\Psi_+\rangle + \sqrt{1-p}|\Psi_-\rangle$ [here $c = \sqrt{p(1-p)}$], and minimal for the mixed state $p|\Psi_+\rangle\langle\Psi_+| + (1-p)|\Psi_-\rangle\langle\Psi_-|$ [100]. Moreover, the precision enhancement, Eq. (81), behaves as the QFI, since for all c the average photon number remains constant, $\langle n \rangle = p \langle n \rangle_+ + (1-p) \langle n \rangle_-$.

If the average photon number is similar in the odd and even states, the lack of coherence does not significantly affect the precision. More generally, if the odd and even stationary states feature the enhancement, $F_Q(|\Psi_\pm\rangle)/4\langle n \rangle_\pm \geq 1$, this is the case for any ρ , as

$$\frac{F_Q(\rho)}{4\langle n \rangle} = \bar{p} \frac{F_Q(|\Psi_+\rangle)}{4\langle n \rangle_+} + (1-\bar{p}) \frac{F_Q(|\Psi_-\rangle)}{4\langle n \rangle_-} + |c|^2 \frac{(\langle n \rangle_+ - \langle n \rangle_-)^2}{\langle n \rangle}, \quad (85)$$

where

$$0 \leq \bar{p} = \frac{p \langle n \rangle_+}{p \langle n \rangle_+ + (1-p) \langle n \rangle_-} \leq 1. \quad (86)$$

Furthermore, even if only the even (or the odd) stationary state features the enhancement, the precision of a mixed state in Eq. (83) still beats the standard quantum limit provided the probability p of the even [(1-p) of the odd] stationary state is sufficiently large [cf. Eq. (85) and see [101]].

Cavity coherence from atom coherence. The high QFI in Fig. 9 relies on the existence of pure coherent even and odd stationary states of the cavity. This crucial coherence of the stationary states of fixed parity is created by the passage of pure coherent states of atoms, Eq. (8), which establish a phase reference for the cavity phase, Eq. (29). Indeed, whenever the atom state is mixed, but diagonal, the even and odd stationary states of the cavity are not diagonal in the photon number basis, and thus feature non-zero QFI (see Appendix G). For diagonal states of atoms, however, the phase reference is absent, and the resulting cavity state is diagonal in photon number basis (with the QFI equal 0), as the cavity achieves equilibrium with the effective atom temperature given by the relative population of the two atomic levels (see Appendix H).

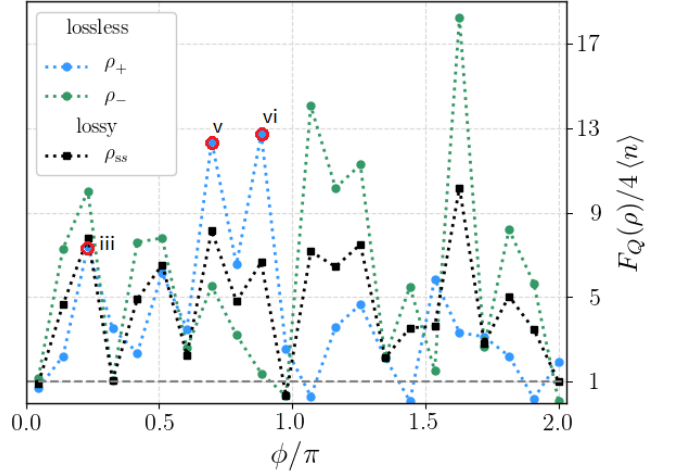


FIG. 10. **Effect of single-photon losses on phase estimation precision.** (a) The enhancement (81) in the phase estimation is shown as a function of the integrated coupling ϕ [$c_e = 0.65$ corresponding to dashed red line in Fig. 9]. The enhancement in the stationary state of lossy dynamics (black) [Eq. (87)] is shown against the enhancement in the even (blue) and odd (green) states that are stationary for lossless cavity. For the majority of parameter space we observe the enhancement in phase estimation, i.e. $F_Q(\rho)/4\langle n \rangle > 1$ (values above the horizontal dashed grey line). Here the lossy stationary state is given by perturbative Eq. (62). (b) Average photon number in even and odd stationary states. We observe the correlation of high photon number to when the QFI of a lossy stationary state differs from Eq. (87) in (a), as it determines the size of the correction from the single-photon losses (together with the relaxation timescales in the lossless case [cf. Fig. 9]).

B. QFI for micromaser with single-photon losses

In Sec. V A and Sec. V B we have shown that due to the finite detunings or the presence of single-photon losses, the pure stationary states $|\Psi_+\rangle$ and $|\Psi_-\rangle$ of two-photon micromaser, Eq. (29), are rendered metastable, and the cavity dynamics leads instead to a unique stationary state approximated by their classical mixture [see Eqs. (52), (62) and (72)]. Below we argue that in this limit the introduced mixedness does not significantly reduce the enhancement in the phase estimation precision. Therefore, the dissipatively generated cavity states can still be used quantum enhanced phase estimation.

The stationary state of a lossy cavity, Eq. (62), is approximated by a mixture of the even and odd states, $\rho_{ss} \approx \rho$ with $p = \langle n \rangle_- / (\langle n \rangle_+ + \langle n \rangle_-)$. In this case [cf. Eq. (84)]

$$\frac{F_Q(\rho)}{4\langle n \rangle} = \frac{1}{2} \left[\frac{F_Q(|\Psi_+\rangle)}{4\langle n \rangle_+} + \frac{F_Q(|\Psi_-\rangle)}{4\langle n \rangle_-} \right], \quad (87)$$

so that the enhancement higher than 2 present in the even or the odd state implies $\frac{F_Q(\rho)}{4\langle n \rangle} > 1$ [cf. Fig. 10]. Note that we assume losses to take place only during the

generation of the cavity state, but not during the phase encoding [cf. Eq. (78)].

It is important to comment here on corrections to Eq. (62) and thus to Eq. (87). In derivation of the effective dynamics induced by single-photon losses, Eq. (62), we assumed that the losses act as a perturbation of the cavity dynamics, i.e., timescales of lossy dynamics are much longer than the timescale τ of the relaxation into the pure stationary states (29). In this case, the corrections to the stationary state in Eq. (62) are proportional to $\kappa\tau$ [50, 88]. Note that this perturbative approximation is *limited by two factors*.

First, the influence of the single-photon losses is proportional to the average-photon number [cf. Eq. (62)] as losses affects each photon independently. Therefore, states with higher photon number are more fragile to losses. This is also the reason, why losses present during the phase encoding (i.e., for *fixed* strength of noise, κt for $\varphi = \delta\omega t$), lead to the enhancement in phase estimation limited to a constant $[(e^{\kappa t} - 1)]$ above the standard scaling [102–104].

Second, the soft walls which facilitate multimodal distribution and thus the enhancement in precision, imply long relaxation time τ . The relaxation timescales due to soft walls are however not directly related to the average photon number (cf. Sec. IV D).

Beyond the perturbative approximation, i.e., when losses take place at earlier timescales than τ , they instead lead to the mixing dynamics of the pure states between the walls, analogously as discussed for hard walls in Sec. V C. This dynamics results in the stationary state without any coherences across the walls, $\rho_{ss} \approx \sum_k p_k^{ss} |\Psi_k\rangle\langle\Psi_k|$ where $|\Psi_k\rangle$ denotes a mode between the subsequent walls. Thus, the QFI does not feature the quadratic scaling [cf. Eq. (82)] and becomes

$$F_Q(\rho_{ss}) \approx \sum_k p_k^{ss} F_Q(|\Psi_k\rangle). \quad (88)$$

Therefore, the precision enhancement is generally lost [see Fig. 10].

Therefore, for the precision enhancement to be maintained in the presence of losses, it is crucial to remain within the perturbative approximation. For this it is necessary that $\kappa\tau$ decreases inversely with the average photon number of the even and odd stationary states of the lossless cavity. Importantly, this requirement can be achieved by increasing the rate ν of atom passages, since $\tau \propto \nu^{-1}$ [cf. Eq. (11)].

Similarly, the higher-order corrections in the far-detuned limit discussed in Sec. V A will lead to the mixed stationary state approximated by Eq. (52), and thus Eq. (85) [with $c = 0$]. Here, however, the corrections cannot be minimised by increasing the rate ν , but only by increasing atom detunings [see Fig. 1(a)]. In Appendix G 2.c. we also discuss the influence of a non-monochromatic atom beam on the precision enhancement.

VII. EXPERIMENTAL CONSIDERATIONS

We now review possible platforms to implement the Hamiltonian (14).

Rydberg atoms. Atoms excited to their higher principal quantum number states, so called Rydberg atoms, interacting with a microwave cavity are the setup where two-photon micromasers were originally developed [31, 32]. In order to realize the (5+1)-level setup studied in this work with Rydberg atoms, the challenge is to identify five Rydberg levels coupled by the same cavity field, see Fig. 1(a), fulfilling the conditions in Eq. (13) to cancel the dynamical and static Stark shifts.

To provide a concrete example, we have performed a systematic search using the ARC package [105, 106] (see also [107, 108] for related software development), see Appendix J for details of the procedure. As the number of possibilities grows rapidly with the number of basis states, we have limited our search to 30 basis states close to the levels realizing two-photon micromaser in Ref. [32], namely the ladder configuration a ladder configuration $39S_{\frac{1}{2}} \leftrightarrow 39P_{\frac{3}{2}} \leftrightarrow 40S_{\frac{1}{2}}$. Trying to match the conditions (13a,13b) [here we assume that the condition (13c) can be satisfied by tuning the Rabi frequency G and the detuning δ of the external laser], we have identified the set of transitions $37S_{\frac{1}{2}} \leftrightarrow 37P_{\frac{3}{2}} \leftrightarrow 38S_{\frac{1}{2}} \leftrightarrow 38P_{\frac{3}{2}} \leftrightarrow 39S_{\frac{1}{2}}$ with $(f_a, f_b) \approx (0.95, 1.02)$, $\omega \approx 500$ GHz, $|\Delta_j| \approx 21$ GHz, $g_j \approx 0.3$ MHz and $|\lambda| \approx 5$ Hz. Here, the coefficients $f_{a,b}$ are defined as $|g_1|^2/\Delta_1 = f_a|g_2|^2/\Delta_2$, $|g_4|^2/\Delta_4 = -f_b|g_3|^2/\Delta_3$, so that the conditions (13) are reached for $f_a = f_b = 1$.

Before commenting on this result, let us first have a look at the achievable coupling strength ϕ . Considering the speed v of atoms passing through a cavity of mode waist w and interaction time $\tau = w/v$ and taking $w \approx 2$ mm and $v \approx 100$ ms⁻¹ [36], we get $\phi = \lambda\tau = \lambda w/v \approx 10^{-4} \ll 1$. This precludes large values of $\phi \sim 1$ [109]. This should be contrasted with the values of the two-photon Rabi frequency $\Omega \approx 10$ kHz from [32], which allows for $\phi \sim O(1)$. It should be also compared to the values of single photon loss rate $\kappa \approx 100$ Hz [36].

Clearly, the limitation of the (limited) search we have performed is the small two-photon Rabi frequency λ . Further improvements in the search strategy include considering larger set of basis states, including larger l , which would accommodate also σ^\pm polarizations and, in particular, the level manipulations with external electric field \mathcal{E} through the DC Stark effect, which would allow for tuning the detunings Δ_j , see Appendix J for further discussion.

Circuit QED. While circuit QED represents ideal platform to realize Hamiltonians with strong higher order photon processes [39–41, 110], the implementation of the

Hamiltonian (14) is not straightforward. Here, an interesting possibility is a scheme studied in Ref. [111], which realized a system with a tunable coupling between a transmon qubit and a microwave resonator. The corresponding Hamiltonian is an effective single-photon Jaynes-Cummings model, $H = \lambda(t)\tilde{a}^\dagger\tilde{\sigma}_- + \lambda(t)^*\tilde{a}\tilde{\sigma}_+$, where $\tilde{a}, \tilde{\sigma}$ are the effective photonic and atomic operators dressed by the anharmonic Jaynes-Cummings Hamiltonian of the qubit-cavity system. Based on this result, it is an interesting question whether the two-photon Jaynes-Cummings Hamiltonian Eq. (14) can be achieved by appropriate modification of the scheme of Ref. [111].

VIII. CONCLUSIONS

We have proposed a novel scheme to realize two-photon micromasers. Exploiting a (5+1)-level structure of atoms passing through a cavity, we have shown that the atom parameters can be tuned to achieve an effective two-photon interaction Hamiltonian without the Stark shifts, unlike in the three-level micromasers. We have found this allows for dissipative generation of pure states with high quantum Fisher information in phase estimation. Furthermore, we have found that the pure odd and even parity stationary states span a decoherence free subspace, corresponding to a qubit. Thus, in addition to phase estimation, the discussed scheme could be exploited in quantum information processing [cf. [39]], as a quantum memory or as a quantum processor with unitary operations implemented by perturbing the micromaser dynamics [89, 90, 112].

To account for realistic imperfections, we have consid-

ered effects of higher-order corrections in the far-detuned limit, and single-photon losses from the cavity. For small enough imperfections, there exists a pronounced metastable regime with metastable states corresponding to the formerly stationary states. After the metastable regime, the relaxation to a unique stationary state takes place. Importantly, even after the metastable regime, the generated stationary states, although mixed, can still feature a significant enhancement in phase estimation precision.

Future research directions include identifying experimental schemes to implement (5+1)-level model and constructing feedback schemes to counteract the mixing dynamics of metastable states due to single-photon losses.

ACKNOWLEDGMENTS

We would like to thank A. Armour, C. Davis-Tilley, M. Marcuzzi, M. Guta and J. Home for informative and useful discussions. J.M. would like to thank R. J. C. Spreeuw and H.B. van Linden van den Heuvell for useful discussion on Rydberg atoms. The research leading to these results has received funding from the European Research Council under the European Unions Seventh Framework Programme (FP/2007-2013) [ERC Grant Agreement No. 335266 (ESCQUMA)] and from the European Unions H2020 research and innovation programme [Grant Agreement No. 800942 (ErBeStA)]. Funding was also received from the EPSRC [Grants No. EP/M014266/1 and No. EP/P026133/1]. I.L. gratefully acknowledges funding through the Royal Society Wolfson Research Merit Award. K.M. was supported through the Henslow Research Fellowship.

-
- [1] W. H. Zurek, *Nature* **412**, 712 (2001).
 - [2] B. Vlastakis, G. Kirchmair, Z. Leghtas, S. E. Nigg, L. Frunzio, S. M. Girvin, M. Mirrahimi, M. H. Devoret, and R. J. Schoelkopf, *Science* **342**, 607 (2013).
 - [3] E. E. Wollman, C. Lei, A. Weinstein, J. Suh, A. Kronwald, F. Marquardt, A. Clerk, and K. Schwab, *Science* **349**, 952 (2015).
 - [4] M. Rashid, T. Tufarelli, J. Bateman, J. Vovrosh, D. Hempston, M. S. Kim, and H. Ulbricht, *Phys. Rev. Lett.* **117**, 273601 (2016).
 - [5] J. M. Pirkkalainen, E. Damskägg, M. Brandt, F. Massel, and M. A. Sillanpää, *Phys. Rev. Lett.* **115**, 243601 (2015).
 - [6] F. Lecocq, J. B. Clark, R. W. Simmonds, J. Aumentado, and J. D. Teufel, *Phys. Rev. X* **5**, 041037 (2015).
 - [7] A. Ourjoumtsev, H. Jeong, R. Tualle-Brouiri, and P. Grangier, *Nature* **448**, 784 (2007).
 - [8] J. Etesse, M. Bouillard, B. Kanseri, and R. Tualle-Brouiri, *Phys. Rev. Lett.* **114**, 193602 (2015).
 - [9] K. Huang, H. Le Jeannic, J. Ruaudel, V. B. Verma, M. D. Shaw, F. Marsili, S. W. Nam, E. Wu, H. Zeng, Y.-C. Jeong, R. Filip, O. Morin, and J. Laurat, *Phys. Rev. Lett.* **115**, 023602 (2015).
 - [10] E. Flurin, N. Roch, F. Mallet, M. H. Devoret, and B. Huard, *Phys. Rev. Lett.* **109**, 183901 (2012).
 - [11] F. Mallet, M. A. Castellanos-Beltran, H. S. Ku, S. Glancy, E. Knill, K. D. Irwin, G. C. Hilton, L. R. Vale, and K. W. Lehnert, *Phys. Rev. Lett.* **106**, 220502 (2011).
 - [12] Y. Nakamura and T. Yamamoto, *IEEE Photonics Journal* **5**, 0701406 (2013).
 - [13] L. Pezzè, A. Smerzi, M. K. Oberthaler, R. Schmied, and P. Treutlein, *Rev. Mod. Phys.* **90**, 035005 (2018).
 - [14] R. Stevenson, J. Minář, S. Hofferberth, and I. Lesanovsky, *Phys. Rev. A* **94**, 043813 (2016).
 - [15] K. V. Kepesidis, M.-A. Lemonde, A. Norambuena, J. R. Maze, and P. Rabl, *Phys. Rev. B* **94**, 214115 (2016).
 - [16] S. Diehl, A. Micheli, A. Kantian, B. Kraus, H. P. Büchler, and P. Zoller, *Nat. Phys.* **4**, 878 (2008).
 - [17] B. Kraus, H. P. Büchler, S. Diehl, A. Kantian, A. Micheli, and P. Zoller, *Phys. Rev. A* **78**, 042307 (2008).
 - [18] D. Gottesman, A. Kitaev, and J. Preskill, *Phys. Rev. A* **64**, 012310 (2001).

- [19] K. Duivenvoorden, B. M. Terhal, and D. Weigand, Phys. Rev. A **95**, 012305 (2017).
- [20] B. M. Terhal and D. Weigand, Phys. Rev. A **93**, 012315 (2016).
- [21] M. Brunelli, O. Houhou, D. W. Moore, A. Nunnenkamp, M. Paternostro, and A. Ferraro, arXiv preprint arXiv:1804.00014 (2018).
- [22] M. Brunelli and O. Houhou, arXiv preprint arXiv:1809.05266 (2018).
- [23] W. J. Munro, K. Nemoto, G. J. Milburn, and S. L. Braunstein, Phys. Rev. A **66**, 023819 (2002).
- [24] A. Gilchrist, K. Nemoto, W. J. Munro, T. Ralph, S. Glancy, S. L. Braunstein, and G. Milburn, Journal of Optics B: Quantum and Semiclassical Optics **6**, S828 (2004).
- [25] P. A. Knott, T. J. Proctor, A. J. Hayes, J. P. Cooling, and J. A. Dunningham, Phys. Rev. A **93**, 033859 (2016).
- [26] G. Anetsberger, O. Arcizet, Q. P. Unterreithmeier, R. Rivière, A. Schliesser, E. M. Weig, J. P. Kotthaus, and T. J. Kippenberg, Nature Physics **5**, 909 (2009).
- [27] E. Gavartin, P. Verlot, and T. J. Kippenberg, Nature nanotechnology **7**, 509 (2012).
- [28] S. Bose, K. Jacobs, and P. L. Knight, Phys. Rev. A **59**, 3204 (1999).
- [29] M. Arndt and K. Hornberger, Nature Physics **10**, 271 (2014).
- [30] J. Bateman, I. McHardy, A. Merle, T. R. Morris, and H. Ulbricht, Scientific reports **5** (2015).
- [31] L. Davidovich, J. M. Raimond, M. Brune, and S. Haroche, Phys. Rev. A **36**, 3771 (1987).
- [32] M. Brune, J. M. Raimond, P. Goy, L. Davidovich, and S. Haroche, Phys. Rev. Lett. **59**, 1899 (1987).
- [33] M. Brune, J. M. Raimond, and S. Haroche, Phys. Rev. A **35**, 154 (1987).
- [34] I. Ashraf, J. Gea-Banacloche, and M. S. Zubairy, Phys. Rev. A **42**, 6704 (1990).
- [35] A. H. Toor, S.-Y. Zhu, and M. S. Zubairy, Phys. Rev. A **53**, 3529 (1996).
- [36] A. Sarlette, J. M. Raimond, M. Brune, and P. Rouchon, Phys. Rev. Lett. **107**, 010402 (2011).
- [37] A. Facon, E.-K. Dietsche, D. Grosso, S. Haroche, J.-M. Raimond, M. Brune, and S. Gleyzes, Nature **535**, 262 (2016).
- [38] P. Neilinger, M. Reháček, M. Grajcar, G. Oelsner, U. Hübner, and E. Il'ichev, Phys. Rev. B **91**, 104516 (2015).
- [39] M. Mirrahimi, Z. Leghtas, V. V. Albert, S. Touzard, R. J. Schoelkopf, L. Jiang, and M. H. Devoret, New Journal of Physics **16**, 045014 (2014).
- [40] A. Roy, Z. Leghtas, A. D. Stone, M. Devoret, and M. Mirrahimi, Phys. Rev. A **91**, 013810 (2015).
- [41] Z. Leghtas, S. Touzard, I. M. Pop, A. Kou, B. Vlastakis, A. Petrenko, K. M. Sliwa, A. Narla, S. Shankar, M. J. Hatridge, *et al.*, Science **347**, 853 (2015).
- [42] M. Orszag, L. Roa, and R. Ramírez, Phys. Rev. A **48**, 4648 (1993).
- [43] C. C. Gerry, Phys. Rev. A **37**, 2683 (1988).
- [44] M. Orszag, R. Ramírez, J. C. Retamal, and L. Roa, Phys. Rev. A **45**, 6717 (1992).
- [45] L. Roa, Phys. Rev. A **50**, R1995 (1994).
- [46] C. Helstrom, Phys. Lett. A **25**, 101 (1967).
- [47] C. Helstrom, IEEE Trans. Inform. Theory **14**, 234 (1968).
- [48] S. L. Braunstein and C. M. Caves, Phys. Rev. Lett. **72**, 3439 (1994).
- [49] K. E. Cahill and R. J. Glauber, Phys. Rev. **177**, 1882 (1969).
- [50] K. Macieszczak, M. Guță, I. Lesanovsky, and J. P. Garrahan, Phys. Rev. Lett. **116**, 240404 (2016).
- [51] Azouit, Rémi, Sarlette, Alain, and Rouchon, Pierre, ESAIM: COCV **22**, 1353 (2016).
- [52] F. Minganti, N. Bartolo, J. Lolli, W. Casteels, and C. Ciuti, Scientific reports **6** (2016).
- [53] N. Bartolo, F. Minganti, W. Casteels, and C. Ciuti, Phys. Rev. A **94**, 033841 (2016).
- [54] R. Azouit, A. Sarlette, and P. Rouchon, in *2015 IEEE 54th Annual Conference on Decision and Control (CDC)* (IEEE, 2015) pp. 6447–6453.
- [55] Alternatively, the auxiliary level $|a\rangle$ can be coupled to the level $|1\rangle$, instead of $|3\rangle$, in order to compensate for the Stark shifts in the effective Hamiltonian. The coupling of three-level atom to a classical Rabi field was considered in [113].
- [56] E. T. Jaynes and F. W. Cummings, Proceedings of the IEEE **51**, 89 (1963).
- [57] B.-G. Englert, arXiv preprint quant-ph/0203052 (2002).
- [58] The atom-cavity interaction (4b) in Eq. (6) takes place in the different frame to Eq. (5), but the frames differ by $-H_0$ to which ρ_{at} is invariant (Assumption 3) (see Appendix A for derivation).
- [59] G. Lindblad, Comm. Math. Phys **48**, 119 (1976).
- [60] V. Gorini, A. Kossakowski, and E. C. G. Sudarshan, Journal of Mathematical Physics **17**, 821 (1976).
- [61] E. S. Guerra, A. Z. Khoury, L. Davidovich, and N. Zagury, Phys. Rev. A **44**, 7785 (1991).
- [62] C. C. Tannoudji, J. Dupont-Roc, and G. Grynberg, eds., *Atom-Photon Interactions* (John Wiley & Sons, 1998).
- [63] M. Alexanian and S. K. Bose, Phys. Rev. A **52**, 2218 (1995).
- [64] A. B. Klimov, L. L. Sánchez-Soto, A. Navarro, and E. C. Yustas, Journal of Modern Optics **49**, 2211 (2002).
- [65] A. H. Toor and M. S. Zubairy, Phys. Rev. A **45**, 4951 (1992).
- [66] A. W. Boone and S. Swain, Quantum Optics: Journal of the European Optical Society Part B **1**, 27 (1989).
- [67] H. T. Dung and N. D. Huyen, Phys. Rev. A **49**, 473 (1994).
- [68] M. Alexanian, S. Bose, and L. Chow, Journal of Luminescence **76**, 677 (1998).
- [69] If the coupling $\lambda(t)$ is complex, otherwise its phase adds to the relative phase between the atom state amplitudes c_g and c_e .
- [70] A. Royer, Phys. Rev. A **15**, 449 (1977).
- [71] P. Zanardi and M. Rasetti, Phys. Rev. Lett. **79**, 3306 (1997).
- [72] P. Zanardi, Phys. Rev. A **56**, 4445 (1997).
- [73] D. A. Lidar, I. L. Chuang, and K. B. Whaley, Phys. Rev. Lett. **81**, 2594 (1998).
- [74] V. Dodonov, I. Malkin, and V. Man'ko, Physica **72**, 597 (1974).
- [75] C. C. Gerry, Journal of Modern Optics **40**, 1053 (1993).
- [76] B. Buca and T. Prosen, New Journal of Physics **14**, 073007 (2012).
- [77] V. V. Albert and L. Jiang, Physical Review A **89**, 022118 (2014).
- [78] E. E. Hach III and C. C. Gerry, Phys. Rev. A **49**, 490

- (1994).
- [79] L. Gilles, B. M. Garraway, and P. L. Knight, Phys. Rev. A **49**, 2785 (1994).
- [80] E. J. Barbeau, *Pell's Equation* (Springer, 2003).
- [81] H. W. Lenstra, "Solving the pell equation," (2008).
- [82] G. N. Copley, The American Mathematical Monthly **66**, 288 (1959).
- [83] This corresponds to the presence of a soft wall with $\cos_{m'}(\phi) = -1$ between the hard walls (see Appendix E).
- [84] The coherence can be maintained using a feedback mechanism of counting the total number of atoms passing through the cavity, and then applying a phase flip, if necessary, to the final state (cf. [52]).
- [85] Coherence to a pure stationary state $|\Psi\rangle$ would be of the form $|\Psi\rangle\langle\Phi|$, where $|\Phi\rangle$ is within the disjoint support of a mixed stationary state ρ . Since $|\Psi\rangle$ can be considered a dark state [cf. Eq. (31)], any coherence decays with the corresponding effective Hamiltonian, unless it is a coherence to another dark state, i.e., pure state with the same boundary conditions as $|\Psi\rangle$. $|\Phi\rangle$ however corresponds to the mixed boundary conditions, since ρ is mixed.
- [86] If we are interested in the soft walls of the odd or even parity only, i.e., $\sin_{2n}(\phi)$ or $\sin_{2n+1}(\phi)$, they correspond to n rotations by 2ϕ with the initial phase shift $3\phi/2$ or $5\phi/2$, respectively. Thus, as for the irrational ϕ/π , $2\phi/\pi$ is also irrational, there exist infinitely many soft walls for both parities.
- [87] D. C. Rose, K. Macieszczak, I. Lesanovsky, and J. P. Garrahan, Phys. Rev. E **94**, 052132 (2016).
- [88] T. Kato, *Perturbation Theory for Linear Operators* (Springer, 1995).
- [89] P. Zanardi and L. Campos Venuti, Phys. Rev. Lett. **113**, 240406 (2014).
- [90] P. Zanardi and L. Campos Venuti, Phys. Rev. A **91**, 052324 (2015).
- [91] P. Zanardi, J. Marshall, and L. Campos Venuti, Phys. Rev. A **93**, 022312 (2016).
- [92] F. Minganti, A. Biella, N. Bartolo, and C. Ciuti, Phys. Rev. A **98**, 042118 (2018).
- [93] C. W. Helstrom, Information and Control **13**, 156 (1968).
- [94] S. L. Braunstein and C. M. Caves, Phys. Rev. Lett. **72**, 3439 (1994).
- [95] V. Giovannetti, S. Lloyd, and L. Maccone, Science **306**, 1330 (2004).
- [96] V. Giovannetti, S. Lloyd, and L. Maccone, Phys. Rev. Lett. **96**, 010401 (2006).
- [97] V. Giovannetti, S. Lloyd, and L. Maccone, Nat. Photon. **5**, 222 (2011).
- [98] We note that in general steady states can vary very strongly with ϕ . In particular, the support of the stationary state is limited by hard walls which exist at a given m only for values of ϕ given by Eq. (41). Nevertheless, when ϕ is varied, a given hard wall becomes a soft wall and the stationary state becomes metastable, so that it can be dissipatively generated in the corresponding metastable regime [cf. Sec. IV D].
- [99] Let $\rho = p_1|E_1\rangle\langle E_1| + p_2|E_2\rangle\langle E_2|$, with $|E_1\rangle = c_+|\Psi_+\rangle + c_-|\Psi_-\rangle$ and $|E_2\rangle = c_-^*|\Psi_+\rangle - c_+^*|\Psi_-\rangle$. From (79), we have $F_Q(\rho) = 4(p_1 - p_2)^2|\langle E_1|n|E_2\rangle|^2 + 4p_1[\text{Var}(n, |E_1\rangle)] - |\langle E_1|n|E_2\rangle|^2 + 4p_2[\text{Var}(n, |E_2\rangle)] - |\langle E_1|n|E_2\rangle|^2$, where $\text{Var}(n, |E_{1,2}\rangle)$ denotes the variance of n in $|E_{1,2}\rangle$ [cf. Eq. (80)]. Furthermore, $\text{Var}(n, |E_1\rangle) = |c_+|^2\text{Var}(n, |\Psi_+\rangle) + |c_-|^2\text{Var}(n, |\Psi_-\rangle) + |c_+c_-|^2(\langle n \rangle_+ - \langle n \rangle_-)^2$ [cf. Eq. (82)], while from the parity conservation by n , $|\langle E_1|n|E_2\rangle|^2 = |c_+c_-|^2(\langle n \rangle_+ - \langle n \rangle_-)^2$. Identifying $p = p_1|c_+|^2 + p_2|c_-|^2$ and $c = (p_1 - p_2)c_+c_-^*$ in (83), we arrive at (84).
- [100] In general the maximal QFI is achieved for: $p = 0$ when $F_Q(|\Psi_+\rangle) \geq F_Q(|\Psi_-\rangle) + 4(\langle n \rangle_+ - \langle n \rangle_-)^2$, $p = 1$ when $F_Q(|\Psi_-\rangle) \geq F_Q(|\Psi_+\rangle) + 4(\langle n \rangle_+ - \langle n \rangle_-)^2$ and $p = 1/2 + [F_Q(|\Psi_+\rangle) - F_Q(|\Psi_-\rangle)]/[8(\langle n \rangle_+ - \langle n \rangle_-)^2]$ otherwise. The minimal QFI is $\min[F_Q(|\Psi_+\rangle), F_Q(|\Psi_-\rangle)]$.
- [101] The minimal enhancement in the DFS is $\min[F_Q(|\Psi_+\rangle)/\langle n \rangle_+, F_Q(|\Psi_-\rangle)/\langle n \rangle_-]$.
- [102] J. Kołodzyński and R. Demkowicz-Dobrzański, Phys. Rev. A **82**, 053804 (2010).
- [103] B. M. Escher, R. L. de Matos Filho, and L. Davidovich, Nat. Phys. **7**, 406411 (2011).
- [104] M. G. Rafał Demkowicz-Dobrzański, Jan Kolodnyński, Nat. Comm. **3** (2012), 10.1038/ncomms2067.
- [105] N. Šibalić, J. D. Pritchard, C. S. Adams, and K. J. Weatherill, "Arc package," <https://arc-alkali-rydberg-calculator.readthedocs.io/en/latest/>.
- [106] N. Šibalić, J. D. Pritchard, C. S. Adams, and K. J. Weatherill, Computer Physics Communications **220**, 319 (2017).
- [107] S. Weber, C. Tresp, H. Menke, A. Urvoy, O. Firstenberg, H. P. Büchler, and S. Hofferberth, "Pairinteractions package," <https://pairinteraction.github.io/pairinteraction/sphinx/html/index.html>.
- [108] S. Weber, C. Tresp, H. Menke, A. Urvoy, O. Firstenberg, H. P. Büchler, and S. Hofferberth, J. Phys. B **50**, 133001 (2017).
- [109] We have used $w \approx 2$ mm as compared with $w \approx 10$ mm used in [36] to make it compatible with the mode volume $V = 70$ mm³ taken from [32].
- [110] P. Campagne-Ibarcq, E. Zalusky-Geller, A. Narla, S. Shankar, P. Reinhold, L. Burkhardt, C. Axline, W. Pfaff, L. Frunzio, R. J. Schoelkopf, and M. H. Devoret, Phys. Rev. Lett. **120**, 200501 (2018).
- [111] S. Zeytinoglu, M. Pechal, S. Berger, A. A. Abdumalikov, A. Wallraff, and S. Filipp, Phys. Rev. A **91**, 043846 (2015).
- [112] A. Beige, D. Braun, B. Tregenna, and P. L. Knight, Phys. Rev. Lett. **85**, 1762 (2000).
- [113] A. Y. Kazakov, J. Opt. B: Quantum and Semiclassical Optics **3**, 97 (2001).
- [114] M. O. Scully and M. S. Zubairy, eds., *Quantum Optics* (Cambridge University Press, Cambridge, UK, 2001).
- [115] S_k is only determined up to an anti-symmetric operator commuting with H_0 [cf. Eq. (B2)]. This freedom, therefore, corresponds only to unitary transformations in degenerate eigenbasis of H_0 , so that H_{diag} in (B1) remains diagonal up to this degeneracy. Here we assume this transformation to be identity.
- [116] P. Zanardi and L. Campos Venuti, Phys. Rev. Lett. **113**, 240406 (2014).
- [117] P. Zanardi and L. Campos Venuti, Phys. Rev. A **91**, 052324 (2015).
- [118] V. V. Albert, B. Bradlyn, M. Fraas, and L. Jiang, Phys. Rev. X **6**, 041031 (2016).
- [119] R. Azouit, A. Sarlette, and P. Rouchon, in *2016 IEEE 55th Conference on Decision and Control (CDC)* (2016) pp. 4559–4565.

- [120] The eigenvalues of \mathcal{M} can be found within a unit circle in the complex plane, which implies that the eigenvalues of \mathcal{L} are found within the circle of radius ν centred at $-\nu$.
- [121] The chosen upper bounds in the conditions for rotating wave approximation and far detuned limit can be of course made more stringent. We have chosen $1/10$ which is the first order satisfying the (order of magnitude) relation $1/10 \ll 1$. It turns out that for the set of basis states used, the number of post-selected levels reduces to 16 (0) if we set the bound to $1/20$ ($1/30$) instead. The latter case resulting in an empty set thus requires to enlarge the set of the basis states.
- [122] T. F. Gallagher, ed., *Rydberg atoms* (Cambridge University Press, Cambridge, 1994).
- [123] W. Li, I. Mourachko, M. W. Noel, and T. F. Gallagher, Phys. Rev. A **67**, 052502 (2003).
- [124] M. Saffman, T. G. Walker, and K. Mølmer, Rev. Mod. Phys. **82**, 2313 (2010).
- [125] J. D. Pritchard, *Cooperative Optical Non-linearity in a blockaded Rydberg ensemble*, Ph.D. thesis, Durham University (2012).
- [126] W. Van Wijngaarden, Journal of Quantitative Spectroscopy and Radiative Transfer **57**, 275 (1997).
- [127] M. S. O'Sullivan and B. P. Stoicheff, Phys. Rev. A **33**, 1640 (1986).

APPENDIX A: (5+1) MICROMASER

1. Hamiltonian transformations

Here we present the details of the transformations leading from Eq. (2) to Eq. (4). In the frame rotating with the free Hamiltonian H'_0 , Eq. (1), the interaction Hamiltonian (2) becomes

$$e^{itH'_0} H'_{\text{int}} e^{-itH'_0} = (a + e^{i2\omega t} a^\dagger) \sum_{j=1}^4 g_j e^{i\Delta_j t} \sigma_{j(j-1)} + (G + G^* e^{i2\omega_{\text{cl}} t}) e^{i\delta t} \sigma_{a3} + \text{H.c.} \quad (\text{A1})$$

Since $|\Delta_j|, |\delta| \ll \omega, \omega_{\text{cl}}$ are assumed, we can perform the rotating-wave approximation by neglecting the counter-rotating terms in (A1) (see, e.g., [114, ch. 5.2.2]). This leads to the atom-cavity interaction described by multi-level Jaynes-Cummings Hamiltonian [56]

$$H''_{\text{int}}(t) = a \sum_{j=1}^4 g_j e^{i\Delta_j t} \sigma_{j(j-1)} + G e^{i\delta t} \sigma_{a3} + \text{H.c.} \quad (\text{A2})$$

while in the initial frame we have

$$H_{\text{JC}}(t) = e^{-itH'_0} H''_{\text{int}}(t) e^{itH'_0} = a \sum_{j=1}^4 g_j \sigma_{j(j-1)} + G e^{-i\omega_{\text{cl}} t} \sigma_{a3} + \text{H.c.} \quad (\text{A3})$$

It is important to note that the new dynamics, $H'_0 + H_{\text{JC}}(t)$, conserves the number of excitations $N = n + \sum_{j=1}^4 j \sigma_{jj} + 3\sigma_{aa}$, where $n = a^\dagger a$ is the cavity photon number operator, i.e., $[N, H'_0 + H_{\text{JC}}(t)] = 0$. Moreover, it is possible and relevant, as we show in Sec. II B, to remove time-dependence from the dynamics (A3), by considering the frame rotating with $(\omega N + \omega_{\text{cl}} \sigma_{aa})$, which leads to the dynamics governed by Eq. (4).

2. Micromaser dynamics

Here we explain how the assumptions of Sec. II B lead to Markovian time-homogeneous dynamics of the cavity.

Assumption 1. Atoms are prepared *identically and in a product state* with respect to one another and the cavity.

We consider the joint initial state of the cavity and the atoms as $\rho^{(0)} \otimes (\rho_{\text{at}} \otimes \cdots \otimes \rho_{\text{at}} \otimes \cdots)$. In this case, in the frame rotating with the free Hamiltonian (1), the state $\rho^{(k)}$ of the cavity after the interaction with k atoms, depends only on its state $\rho^{(k-1)}$ before the interaction with k th atom,

$$\rho^{(k)} = \text{Tr}_{\text{at}} \left\{ U(t_k, \tau_k) \left[\rho_{\text{at}} \otimes \rho^{(k-1)} \right] U^\dagger(t_k, \tau_k) \right\}, \quad (\text{A4})$$

where t_k and τ_k denote the arrival time of k -th atom and the duration of its interaction with the cavity field respectively, while $U(t, \tau) = \mathcal{T} \exp \left\{ -i \int_t^{t+\tau} dt' H''_{\text{int}}(t') \right\}$ is the time-ordered evolution operator for the interaction (A2).

Assumption 2. The atomic beam is *monochromatic*, i.e., velocity of all atoms is the same.

In this case, the interaction time with the cavity is the same for all atoms, $\tau_k \equiv \tau$. A comment is that the atomic state ρ_{at} is typically not initialised for all atoms at $t = 0$ as written formally in *Assumption 1.* In practice they are prepared on their way to the cavity by passing through a laser resonant with the transition $|1\rangle \leftrightarrow |3\rangle$, which for atoms with the same velocity leads to the identical state (as the laser phase is constant in the frame rotating with H'_0). For discussion of changes in micromaser dynamics due to non-monochromatic atomic beam (see Appendix G).

Assumption 3. The atom state is *invariant* under the dynamics (4a), $e^{-itH_0}\rho_{\text{at}}e^{itH_0} = \rho_{\text{at}}$.

With *Assumption 2.* the cavity dynamics (A4) depends on time only via the time-dependent interaction Hamiltonian (A2). The interaction Hamiltonian is, however, time-independent in the frame of $(\omega N + \omega_{\text{cl}}\sigma_{\text{aa}})$ [cf. Eq. (4b)] which differs from the frame of H'_0 by the Hamiltonian $-H_0$ [Eq. (4a)]

$$U(t, \tau) = e^{-itH_0} \left\{ \mathcal{T} e^{-i \int_0^\tau dt' [H_{\text{int}}(t') + H_0]} \right\} e^{i(t+\tau)H_0}. \quad (\text{A5})$$

Since H_0 acts only on the atom state, for the invariant atom state $e^{i(t+\tau)H_0}\rho_{\text{at}}e^{-i(t+\tau)H_0} = \rho_{\text{at}}$ the cavity dynamics simplifies to (A4)

$$\rho^{(k)} = \text{Tr}_{\text{at}} \left\{ e^{-itH_0} U(\tau) \left[\rho_{\text{at}} \otimes \rho^{(k-1)} \right] U^\dagger(\tau) e^{itH_0} \right\} = \text{Tr}_{\text{at}} \left\{ U(\tau) \left[\rho_{\text{at}} \otimes \rho^{(k-1)} \right] U^\dagger(\tau) \right\}, \quad (\text{A6})$$

where we introduced $U(\tau)$ as in Eq. (6), and the last equality is due to the trace over the k th atom.

Exponential arrival times to the cavity. In the micromaser setup, it is assumed that at most one atom is found in the cavity at a time [see Fig. 1(b)]. A possible approach used to obtain this is for the levels $|j\rangle$, $j = 0, 1, \dots, 4, c$ in Fig. 1(a) to be a subset of highly excited levels (e.g., Rydberg levels) in a multi-level atom [57, 61]. The initial state of the atoms is then prepared by passing a stream of atoms, initially in a low-energy state, through the excitation region where the states $|j\rangle$, $j = 0, 1, \dots, 4, c$, can be excited. If the probability of excitation from the low-energy state is small, due to the law of rare events, the number of atoms that arrive to the cavity prepared in the relevant states $|j\rangle$, $j = 0, 1, \dots, 4, c$, up to times t is approximated by a Poisson distribution with the average νt , while the waiting time between the arrival of the consecutive excited atoms is given by the exponential distribution with the rate ν . Furthermore, this approach allows for coarse-graining the discrete dynamics in Eq. (10) to the continuous dynamics governed by the master equation in Eq. (11).

APPENDIX B: ADIABATIC ELIMINATION FOR ATOM-CAVITY INTERACTION

Here we consider adiabatic elimination [63, 64] for atom-cavity dynamics described by $H_0 + H_{\text{int}}$ of (4a) and (4b) at the resonance (7), which is necessary to ensure a *time-homogeneous* dynamics of the cavity field for the incoming atoms in the superposition (8). Here we derive the effective two-photon Hamiltonian of Eqs. (12) and (14), which arise in the second-order of couplings g_1 , g_2 , g_3 , g_4 and G [see Fig. 1(a)]. In Appendix B we derive the higher order-correction to the two-photon dynamics and the corresponding corrections to the Kraus operators (16), which introduce metastability and mixing long-time dynamics, as discussed in Sec. V A.

1. Effective Hamiltonian

We now derive the effective Hamiltonians of Eqs. (12) and (14).

Adiabatic elimination can be viewed as formally diagonalising $H = H_0 + H_{\text{int}}$, (4a) and (4b), by perturbation theory with respect to H_{int} . The Hamiltonian H is diagonalised by a unitary transformation e^S , where the anti-Hermitian operator S is assumed to be expanded in the coupling strength, $S = S_1 + S_2 + \dots$. Therefore,

$$\begin{aligned} H_{\text{diag}} &= e^S (H_0 + H_{\text{int}}) e^{-S} = H_0 + H_{\text{int}} + [S, H_0 + H_{\text{int}}] + \frac{1}{2!} [S, [S, H_0 + H_{\text{int}}]] + \dots \\ &= H_0 + (H_{\text{int}} + [S_1, H_0]) + \left([S_2, H_0] + [S_1, H_{\text{int}}] + \frac{1}{2!} [S_1, [S_1, H_0]] \right) + \dots, \end{aligned} \quad (\text{B1})$$

where we ordered the second line of (B1) in increasing power of the interaction strength. Note that H_{diag} is assumed diagonal up to initial degeneracy in H_0 of the atomic levels $|1\rangle$ and $|3\rangle$, which is due to the resonance (7). Therefore, from (B1), S is perturbatively determined [115] as [cf. [64]]

$$-[S_1, H_0] = H_{\text{int}}, \quad -[S_2, H_0] = \left([S_1, H_{\text{int}}] + \frac{1}{2!} [S_1, [S_1, H_0]] \right)', \quad \dots \quad (\text{B2})$$

where $(X)'$ denotes the off-diagonal elements of X in the eigenbasis of H_0 . The first condition simplifies Eq. (B1) to only even-number corrections,

$$H_{\text{diag}} = H_0 + \left([S_2, H_0] + \frac{1}{2} [S_1, H_{\text{int}}] \right) + \dots, \quad (\text{B3})$$

which is a consequence of the assumed two-photon resonance in H_0 and single-photon interactions in H_{int} . Substituting (B2) to (B3), we obtain

$$H_{\text{diag}} = H_0 + \begin{bmatrix} -a^\dagger a \frac{|g_1|^2}{\Delta_1} & 0 & 0 & 0 & 0 & 0 \\ 0 & a a^\dagger \frac{|g_1|^2}{\Delta_1} - a^\dagger a \frac{g_2^2}{\Delta_2} & 0 & a^{\dagger 2} \frac{g_2^* g_3^* (\Delta_2 - \Delta_3)}{2\Delta_2 \Delta_3} & 0 & 0 \\ 0 & 0 & a a^\dagger \frac{|g_2|^2}{\Delta_2} - a^\dagger a \frac{|g_3|^2}{\Delta_3} & 0 & 0 & 0 \\ 0 & a^2 \frac{g_2 g_3 (\Delta_2 - \Delta_3)}{2\Delta_2 \Delta_3} & 0 & a a^\dagger \frac{|g_3|^2}{\Delta_3} - a^\dagger a \frac{|g_4|^2}{\Delta_4} - \frac{|G|^2}{\delta} & 0 & 0 \\ 0 & 0 & 0 & 0 & a a^\dagger \frac{|g_4|^2}{\Delta_4} & 0 \\ 0 & 0 & 0 & 0 & 0 & \frac{|G|^2}{\delta} \end{bmatrix} + \dots \quad (\text{B4})$$

for the operators

$$S_1 = \begin{bmatrix} 0 & -a^\dagger \frac{g_1^*}{\Delta_1} & 0 & 0 & 0 & 0 \\ a \frac{g_1}{\Delta_1} & 0 & -a^\dagger \frac{g_2^*}{\Delta_2} & 0 & 0 & 0 \\ 0 & a \frac{g_2}{\Delta_2} & 0 & -a^\dagger \frac{g_3^*}{\Delta_3} & 0 & 0 \\ 0 & 0 & a \frac{g_3}{\Delta_3} & 0 & -a^\dagger \frac{g_4^*}{\Delta_4} & -\frac{G^*}{\delta} \\ 0 & 0 & 0 & a \frac{g_4}{\Delta_4} & 0 & 0 \\ 0 & 0 & 0 & \frac{G}{\delta} & 0 & 0 \end{bmatrix}, \quad (\text{B5})$$

$$S_2 = \begin{bmatrix} 0 & 0 & 0 & -a^{\dagger 2} \frac{g_1^* g_2^* (\Delta_1 - \Delta_2)}{2\Delta_1 \Delta_2 (\Delta_1 + \Delta_2)} & 0 & 0 & 0 \\ 0 & 0 & 0 & 0 & 0 & 0 & 0 \\ a^2 \frac{g_1 g_2 (\Delta_1 - \Delta_2)}{2\Delta_1 \Delta_2 (\Delta_1 + \Delta_2)} & 0 & 0 & 0 & 0 & -a^{\dagger 2} \frac{g_3^* g_4^* (\Delta_3 - \Delta_4)}{2\Delta_3 \Delta_4 (\Delta_3 + \Delta_4)} & -a^\dagger \frac{g_3^* G^* (\Delta_3 - \delta)}{2\Delta_3 \delta (\delta + \Delta_3)} \\ 0 & 0 & 0 & 0 & 0 & 0 & 0 \\ 0 & 0 & a^2 \frac{g_3 g_4 (\Delta_3 - \Delta_4)}{2\Delta_3 \Delta_4 (\Delta_3 + \Delta_4)} & 0 & 0 & 0 & -a \frac{g_4 G^* (\Delta_4 + \delta)}{2\Delta_4 \delta (-\Delta_4 + \delta)} \\ 0 & 0 & a \frac{g_3 G (\Delta_3 - \delta)}{2\Delta_3 \delta (\delta + \Delta_3)} & 0 & a^\dagger \frac{g_4^* G (\Delta_4 + \delta)}{2\delta \Delta_4 (-\Delta_4 + \delta)} & 0 & 0 \end{bmatrix}. \quad (\text{B6})$$

It should be emphasised that atom-cavity interaction, Eq. (B4), takes place in the diagonalising basis [cf. Eq. (B1)] given by $e^S(|j\rangle \otimes |n\rangle) = |j\rangle \otimes |n\rangle + S_1(|j\rangle \otimes |n\rangle) + \dots$, where the atom levels are labelled by $j = 0, \dots, 4, a$, while $n = 0, 1, 2, \dots$ denotes a photon number in the cavity. In the far-detuned limit of $|g_j/\Delta_j| \ll 1$ for $j = 1, \dots, 4, a$ and $|G/\delta| \ll 1$, the lowest-order corrections, the diagonalising basis corresponds to the original atomic levels $|0\rangle, \dots, |4\rangle$ and $|a\rangle$, in tensor product with the photon number basis of the cavity states. In particular, in Sec. III A, H_{diag} restricted to the levels $|1\rangle$ and $|3\rangle$ is considered [cf. Eqs. (4a) and (4b)]. Below we consider corrections to the dynamics beyond this approximation.

Convergence of perturbation theory. Due to conservation of the number of excitations, $N = a^\dagger a + \sum_{j=1}^4 j \sigma_{jj} + 3\sigma_{aa}$, although the cavity space dimension is infinite, the perturbation theory above is effectively performed on (at most) 6-dimensional subspaces spanned by $|0\rangle \otimes |n\rangle$, $|1\rangle \otimes |n-1\rangle$, $|2\rangle \otimes |n-2\rangle$, $|3\rangle \otimes |n-3\rangle$, $|4\rangle \otimes |n-4\rangle$ and $|a\rangle \otimes |n-3\rangle$, for $n = 0, 1, \dots$ denoting the photon number in the cavity. For given N , the effective perturbation size can be approximated as $\|H_{\text{int}}\| \|(H_0 - \Delta_1)^+\| = \mathcal{O}[\max(N \max_j |g_j|, G) / \min(|\Delta_1|, |\Delta_2|, |\Delta_4|, \delta)]$, where $(H_0 - \Delta_1)^+$ denotes the pseudo-inverse [88, 91, 116, 117]. This defines the far-detuned limit for a given N . When the dynamics in the two-level approximation (16) features well-defined stationary states and the initial cavity state is bounded, i.e., it has a finite support below n_{in} , we expect the stationary state to be achieved at a finite-relaxation time τ_{relax} exploring

effectively a finite cavity space, cf., e.g., [54]. If the perturbation size is small for $N \gg \nu\tau_{\text{relax}}$, for full atom-cavity dynamics given by $H_0 + H_{\text{int}}$ there exists a metastable regime where 2-level approximation holds and a metastable state is given by the former stationary state. At longer times the effective dynamics resulting from the higher-order correction takes place and leads to a unique stationary state (see also Sec. V A). In the next section we consider these higher-order corrections to dynamics.

2. Higher-order corrections to cavity dynamics

The cavity dynamics generated by the effective Hamiltonian (B4) corresponds to the adiabatic elimination (B1) carried out to the lowest non-trivial order in the perturbation $g_j/\Delta_j, G/\delta$. We now discuss how this effective dynamics, which is parity preserving, is modified by higher-order corrections. The analysis below is for a general setup of Fig. 1(a), with two photon resonance in Eq. (7) leading to the effective Hamiltonian in Eq. (12). Therefore, the results apply both to 3-level model [31, 33–35, 42, 44, 68] and (5+1) model, where the Stark shifts can be removed in the far-detuned limit [cf. Eq. (14)]. We analyse the latter case in Sec. III, and discuss the influence of the higher-order corrections in Sec. V A.

Kraus operators. The Kraus operators, which describe the change in the cavity state due to passage of a single atom, are given by [cf. Eq. (48)]

$$M_j = \langle j|U(\tau)|\psi_{\text{at}}\rangle = \langle j|e^{-S}U_{\text{diag}}(\tau)e^S|\psi_{\text{at}}\rangle \quad j = 0, \dots, 4, \text{a}, \quad (\text{B7})$$

where $U(\tau) = e^{-i\tau[H_{\text{int}}+H_0]}$, $U_{\text{diag}}(\tau) = e^{-i\tau H_{\text{diag}}}$, and $|\psi_{\text{at}}\rangle$ is the pure state of the atom entering the cavity. We have assumed for simplicity that the field-atom coupling strength is constant, $H_{\text{int}}(t) = H_{\text{int}}$. Considering $|\psi_{\text{at}}\rangle$ to be given by (8), i.e., a superposition between $|1\rangle$ and $|3\rangle$, the Kraus operators (derived below) M_0, M_2, M_4 swap the parity, while the Kraus operators M_1, M_3 and M_a , conserve the parity [cf. Eq. (49)].

Time-independent corrections. We consider the expansion of (B7) with respect to $S = S_1 + S_2 + \dots$, where j in S_j denotes the power of the coupling strength g, G (the time-dependent perturbative corrections in $U_{\text{diag}}(\tau)$ will be discussed later). We have

$$M_j = \langle j|U_{\text{diag}}(\tau)|\psi_{\text{at}}\rangle + (-\langle j|S_1U_{\text{diag}}(\tau)|\psi_{\text{at}}\rangle + \langle j|U_{\text{diag}}(\tau)S_1|\psi_{\text{at}}\rangle) \\ + \left[-\langle j|S_1U_{\text{diag}}(\tau)S_1|\psi_{\text{at}}\rangle + \langle j|\left(\frac{S_1^2}{2} - S_2\right)U_{\text{diag}}(\tau)|\psi_{\text{at}}\rangle + \langle j|U_{\text{diag}}(\tau)\left(\frac{S_1^2}{2} + S_2\right)|\psi_{\text{at}}\rangle \right] + \dots, \quad (\text{B8})$$

where the last two terms in the first line and the second line correspond to the first- and second-order corrections. The operators S_1 and S_2 are given by Eqs. (B5) and (B6), which leads to the parity-conserving Kraus operators given by

$$M_1 = U_{\text{diag}}^{11}(\tau)c_g + U_{\text{diag}}^{13}(\tau)c_e + \frac{1}{2}\left(-aa^\dagger\frac{|g_1|^2}{\Delta_1^2} - a^\dagger a\frac{|g_2|^2}{\Delta_2^2}\right)[U_{\text{diag}}^{11}(\tau)c_g + U_{\text{diag}}^{13}(\tau)c_e] \\ + a^{\dagger 2}\frac{g_2^*g_3^*}{2\Delta_2\Delta_3}[U_{\text{diag}}^{31}(\tau)c_g + U_{\text{diag}}^{33}(\tau)c_e] \\ + \frac{1}{2}U_{\text{diag}}^{11}(\tau)\left[\left(-aa^\dagger\frac{|g_1|^2}{\Delta_1^2} - a^\dagger a\frac{|g_2|^2}{\Delta_2^2}\right)c_g + (a^\dagger)^2\frac{g_2^*g_3^*}{\Delta_2\Delta_3}c_e\right] \\ + \frac{1}{2}U_{\text{diag}}^{13}(\tau)\left[\left(-aa^\dagger\frac{|g_3|^2}{\Delta_3^2} - a^\dagger a\frac{|g_4|^2}{\Delta_4^2} - \frac{|G|^2}{\delta^2}\right)c_e + a^2\frac{g_2g_3}{\Delta_2\Delta_3}c_g\right] \\ + aU_{\text{diag}}^{00}(\tau)a^\dagger\frac{|g_1|^2}{\Delta_1^2}c_g + a^\dagger\frac{g_2^*}{\Delta_2}U_{\text{diag}}^{22}(\tau)\left(a\frac{g_2}{\Delta_2}c_g - a^\dagger\frac{g_3^*}{\Delta_3}c_e\right) + \dots, \quad (\text{B9})$$

$$\begin{aligned}
M_3 = & U_{\text{diag}}^{31}(\tau) c_g + U_{\text{diag}}^{33}(\tau) c_e + \frac{1}{2} \left(-aa^\dagger \frac{|g_3|^2}{\Delta_3^2} - a^\dagger a \frac{|g_4|^2}{\Delta_4^2} - \frac{|G|^2}{\delta^2} \right) [U_{\text{diag}}^{31}(\tau) c_g + U_{\text{diag}}^{33}(\tau) c_e] \\
& + a^2 \frac{g_2 g_3}{2\Delta_2 \Delta_3} [U_{\text{diag}}^{11}(\tau) c_g + U_{\text{diag}}^{13}(\tau) c_e] \\
& + \frac{1}{2} U_{\text{diag}}^{31}(\tau) \left[\left(-aa^\dagger \frac{|g_1|^2}{\Delta_1^2} - a^\dagger a \frac{|g_2|^2}{\Delta_2^2} \right) c_g + (a^\dagger)^2 \frac{g_2^* g_3^*}{\Delta_2 \Delta_3} c_e \right] \\
& + \frac{1}{2} U_{\text{diag}}^{33}(\tau) \left[\left(-aa^\dagger \frac{|g_3|^2}{\Delta_3^2} - a^\dagger a \frac{|g_4|^2}{\Delta_4^2} - \frac{|G|^2}{\delta^2} \right) c_e + a^2 \frac{g_2 g_3}{\Delta_2 \Delta_3} c_g \right] \\
& - a \frac{g_3}{\Delta_3} U_{\text{diag}}^{22}(\tau) \left(a \frac{g_2}{\Delta_2} c_g - a^\dagger \frac{g_3^*}{\Delta_3} c_e \right) + a^\dagger U_{\text{diag}}^{44}(\tau) a \frac{|g_4|^2}{\Delta_4^2} c_e + U_{\text{diag}}^{\text{aa}}(\tau) \frac{|G|^2}{\delta^2} c_e + \dots,
\end{aligned} \tag{B10}$$

and

$$M_a = -\frac{G}{\delta} [U_{\text{diag}}^{31}(\tau) c_g + U_{\text{diag}}^{33}(\tau) c_e - U_{\text{diag}}^{\text{aa}}(\tau) c_e] + \dots, \tag{B11}$$

where $U_{\text{diag}}^{jk}(\tau) \equiv \langle j|U_{\text{diag}}(\tau)|k \rangle$ for $j, k = 0, \dots, 4$, a [cf. Eq. (16)]. Note that M_1 and M_3 do not feature first-order corrections [the second and third term in (B8)], due to their parity conservation, as S_1 swaps the cavity parity, except for the atom in levels $|3\rangle$ and $|a\rangle$, so that M_a is of the first-order. For this reason, the parity-swapping Kraus operators are of the first-order,

$$M_0 = a^\dagger \frac{g_1^*}{\Delta_1} [U_{\text{diag}}^{11}(\tau) c_g + U_{\text{diag}}^{13}(\tau) c_e] - U_{\text{diag}}^{00}(\tau) a^\dagger \frac{g_1^*}{\Delta_1} c_g + \dots, \tag{B12}$$

$$M_2 = -a \frac{g_2}{\Delta_2} [U_{\text{diag}}^{11}(\tau) c_g + U_{\text{diag}}^{13}(\tau) c_e] + a^\dagger \frac{g_3^*}{\Delta_3} [U_{\text{diag}}^{31}(\tau) c_g + U_{\text{diag}}^{33}(\tau) c_e] + U_{\text{diag}}^{22}(\tau) \left(a \frac{g_2}{\Delta_2} c_g - a^\dagger \frac{g_3^*}{\Delta_3} c_e \right) + \dots, \tag{B13}$$

$$M_4 = -a \frac{g_4}{\Delta_4} [U_{\text{diag}}^{31}(\tau) c_g + U_{\text{diag}}^{33}(\tau) c_e] + U_{\text{diag}}^{44}(\tau) a \frac{g_4}{\Delta_4} c_e + \dots. \tag{B14}$$

Time-dependent corrections. We now discuss time-dependent corrections to $U_{\text{diag}}(\tau) = e^{-i\tau H_{\text{diag}}}$ from the diagonal Hamiltonian $H_{\text{diag}} = H_0 + H_2^{\text{diag}} + H_4^{\text{diag}} + \dots$, (B4), where H_k^{diag} denotes k th order corrections. As H_0 commutes by definition with H_{diag} , we have

$$U_{\text{diag}}(\tau) = e^{-i\tau H_0} e^{-i\tau(H_2^{\text{diag}} + H_4^{\text{diag}} + \dots)} = e^{-i\tau(H_0 + H_2^{\text{diag}})} \left(1 - i \int_0^\tau dt e^{itH_2^{\text{diag}}} H_4^{\text{diag}} e^{-itH_2^{\text{diag}}} + \dots \right), \tag{B15}$$

where in the last equality we used the Dyson series. The correction

$$\int_0^\tau dt e^{itH_2^{\text{diag}}} H_4^{\text{diag}} e^{-itH_2^{\text{diag}}} \equiv \tau \delta H_{\text{eff}}(\tau) \tag{B16}$$

can be considered as the contribution from the time-averaged H_4^{diag} in the rotating frame of H_2^{diag} . For the interaction time τ chosen so that the second-order dynamics in the two-level approximation [Eqs. (14) and (16)] is finite, the correction $\tau \delta H_{\text{eff}}(\tau)$ contributes as the second-order to $U_{\text{diag}}(\tau)$. We thus have [cf. Eq. (B15) and (16)]

$$U_{\text{diag}}^{11}(\tau) c_g + U_{\text{diag}}^{13}(\tau) c_e \equiv e^{-i\tau \Delta_1} [M_g + \delta M_g] + \dots \tag{B17a}$$

$$= e^{-i\tau \Delta_1} \langle 1|e^{-itH_2^{\text{diag}}} |\psi_{\text{at}}\rangle - i\tau e^{-i\tau \Delta_1} \left[\cos(\phi \sqrt{a^\dagger a^2}) \langle 1|\delta H_{\text{eff}}(\tau)|\psi_{\text{at}}\rangle - ia^{\dagger 2} \frac{\sin(\phi \sqrt{a^2 a^{\dagger 2}})}{\sqrt{a^2 a^{\dagger 2}}} \langle 3|\delta H_{\text{eff}}(\tau)|\psi_{\text{at}}\rangle \right] + \dots,$$

$$U_{\text{diag}}^{31}(\tau) c_g + U_{\text{diag}}^{33}(\tau) c_e \equiv e^{-i\tau \Delta_1} [M_e + \delta M_e] + \dots \tag{B17b}$$

$$= e^{-i\tau \Delta_1} \langle 3|e^{-itH_2^{\text{diag}}} |\psi_{\text{at}}\rangle - i\tau e^{-i\tau \Delta_1} \left[-ia^2 \frac{\sin(\phi \sqrt{a^\dagger a^2})}{\sqrt{a^\dagger a^2}} \langle 1|\delta H_{\text{eff}}(\tau)|\psi_{\text{at}}\rangle + \cos(\phi \sqrt{a^\dagger a^2}) \langle 3|\delta H_{\text{eff}}(\tau)|\psi_{\text{at}}\rangle \right] + \dots,$$

where we defined the zero-order Kraus operators M_g and M_e , cf. Eq. (16) [note that the Kraus operators in (16) differ by the global phase $e^{i\tau \frac{|g_2|^2}{\Delta_2}}$, which was additionally neglected in (14)]. For the Kraus operators in other micromaser setups, including 3-level model (see Appendix C).

Therefore, up to the second order in the coupling strength, the cavity dynamics (11) is determined by the first-order Kraus operators,

$$e^{i\tau\Delta_1} M_0 = a^\dagger \frac{g_1^*}{\Delta_1} M_g - e^{i\tau(\Delta_1 + \frac{|g_1|^2}{\Delta_1} a^\dagger a)} a^\dagger \frac{g_1^*}{\Delta_1} c_g + \dots, \quad (\text{B18})$$

$$e^{i\tau\Delta_1} M_2 = -a \frac{g_2}{\Delta_2} M_g + a^\dagger \frac{g_3^*}{\Delta_3} M_e + e^{-i\tau(\Delta_2 + a a^\dagger \frac{|g_2|^2}{\Delta_2} - a^\dagger a \frac{|g_3|^2}{\Delta_3})} \left(a \frac{g_2}{\Delta_2} c_g - a^\dagger \frac{g_3^*}{\Delta_3} c_e \right) + \dots, \quad (\text{B19})$$

$$e^{i\tau\Delta_1} M_4 = -a \frac{g_4}{\Delta_4} M_e + e^{-i\tau(\sum_{k=2}^4 \Delta_k + a a^\dagger \frac{|g_4|^2}{\Delta_4})} a \frac{g_4}{\Delta_4} c_e + \dots, \quad (\text{B20})$$

$$e^{i\tau\Delta_1} M_a = -\frac{G}{\delta} \left[M_e - e^{-i\tau(\sum_{k=2}^3 \Delta_k + \delta + \frac{|G|^2}{\delta})} c_e \right] + \dots, \quad (\text{B21})$$

where fourth-order corrections to H_{diag} in (B4) are neglected. Similarly,

$$\begin{aligned} e^{i\tau\Delta_1} M_1 &= M_g + \frac{1}{2} \left(-aa^\dagger \frac{|g_1|^2}{\Delta_1^2} - a^\dagger a \frac{|g_2|^2}{\Delta_2^2} \right) M_g + a^{\dagger 2} \frac{g_2^* g_3^*}{2\Delta_2 \Delta_3} M_e \\ &\quad + \frac{1}{2} M_{gg} \left[\left(-aa^\dagger \frac{|g_1|^2}{\Delta_1^2} - a^\dagger a \frac{|g_2|^2}{\Delta_2^2} \right) c_g + (a^\dagger)^2 \frac{g_2^* g_3^*}{\Delta_2 \Delta_3} c_e \right] \\ &\quad + \frac{1}{2} M_{ge} \left[\left(-aa^\dagger \frac{|g_3|^2}{\Delta_3^2} - a^\dagger a \frac{|g_4|^2}{\Delta_4^2} - \frac{|G|^2}{\delta^2} \right) c_e + a^2 \frac{g_2 g_3}{\Delta_2 \Delta_3} c_g \right] \\ &\quad + a e^{i\tau(\Delta_1 + \frac{|g_1|^2}{\Delta_1} a^\dagger a)} a^\dagger \frac{|g_1|^2}{\Delta_1^2} c_g + a^\dagger \frac{g_2^*}{\Delta_2} e^{-i\tau(\Delta_2 + a a^\dagger \frac{|g_2|^2}{\Delta_2} - a^\dagger a \frac{|g_3|^2}{\Delta_3})} \left(a \frac{g_2}{\Delta_2} c_g - a^\dagger \frac{g_3^*}{\Delta_3} c_e \right) \\ &\quad - i\tau \langle 1 | \delta H_{\text{eff}}(\tau) | \psi_{\text{at}} \rangle + \dots, \end{aligned} \quad (\text{B22})$$

$$\begin{aligned} e^{i\tau\Delta_1} M_3 &= M_e + \frac{1}{2} \left(-aa^\dagger \frac{|g_3|^2}{\Delta_3^2} - a^\dagger a \frac{|g_4|^2}{\Delta_4^2} - \frac{|G|^2}{\delta^2} \right) M_e + a^2 \frac{g_2 g_3}{2\Delta_2 \Delta_3} M_g \\ &\quad + \frac{1}{2} M_{eg} \left[\left(-aa^\dagger \frac{|g_1|^2}{\Delta_1^2} - a^\dagger a \frac{|g_2|^2}{\Delta_2^2} \right) c_g + (a^\dagger)^2 \frac{g_2^* g_3^*}{\Delta_2 \Delta_3} c_e \right] \\ &\quad + \frac{1}{2} M_{ee} \left[\left(-aa^\dagger \frac{|g_3|^2}{\Delta_3^2} - a^\dagger a \frac{|g_4|^2}{\Delta_4^2} - \frac{|G|^2}{\delta^2} \right) c_e + a^2 \frac{g_2 g_3}{\Delta_2 \Delta_3} c_g \right] \\ &\quad - a \frac{g_3}{\Delta_3} e^{-i\tau(\Delta_2 + a a^\dagger \frac{|g_2|^2}{\Delta_2} - a^\dagger a \frac{|g_3|^2}{\Delta_3})} \left(a \frac{g_2}{\Delta_2} c_g - a^\dagger \frac{g_3^*}{\Delta_3} c_e \right) + a^\dagger e^{-i\tau(\sum_{k=2}^4 \Delta_k + a a^\dagger \frac{|g_4|^2}{\Delta_4})} a \frac{|g_4|^2}{\Delta_4^2} c_e \\ &\quad + e^{-i\tau(\sum_{k=2}^3 \Delta_k + \delta + \frac{|G|^2}{\delta})} \frac{|G|^2}{\delta^2} c_e - i\tau \langle 3 | \delta H_{\text{eff}}(\tau) | \psi_{\text{at}} \rangle + \dots, \end{aligned} \quad (\text{B23})$$

and we defined $M_{\mu\nu} \equiv M_\mu$ with $c_\nu = 1$, where $\mu, \nu = g, e$. The global phase factor $e^{i\tau\Delta_1}$ in Eqs. (B18-B23) corresponds to a global phase neglected in (12). Furthermore, for the (5+1)-model, the conditions in Eq. (13) leading to cancellation of the Stark shifts, establish dependent variables: $g_1^*/\Delta_1 = g_2/\sqrt{\Delta_1\Delta}$, $-g_4/\Delta_4 = g_3/\sqrt{\Delta_4\Delta}$, and $-G/\delta = \sqrt{|g_2|^2 + |g_3|^2}/\sqrt{\Delta\delta}$.

For completeness, we now provide fourth-order corrections to (B4), which contribute to Eq. (B16), for the case $g_1 = g_2 = g_3 = g_4 = g$, $\Delta_1 = \Delta_2 = -\Delta_3 = -\Delta_4 = \Delta$, and $G^2/\delta = -2g^2/\Delta$,

$$H_4^{\text{diag}} = \left[\begin{array}{cc} \frac{4g^4[a^\dagger a(a^\dagger a - 3) - 1]}{3\Delta^3} & a^\dagger \frac{8g^4(g^2 + G^2 a^\dagger a)}{3G^2\Delta^3} a^\dagger \\ a \frac{8g^4(g^2 + G^2 a^\dagger a)}{3G^2\Delta^3} & -\frac{4g^4[4g^2 - G^2(a^\dagger a a a^\dagger + 1)]}{3G^2\Delta^3} \end{array} \right], \quad (\text{B24})$$

which are expressed for $e^S(|1\rangle \otimes |n\rangle)$ and $e^S(|3\rangle \otimes |n\rangle)$, i.e., the diagonal basis of the atom-cavity Hamiltonian [cf. Eq. (B1)]. Here (B24) was obtained from (B1) by considering the expansion of S up to the fourth-order, i.e., $S = S_1 + S_2 + S_3 + S_4 + \dots$.

Higher-order corrections in the 3-level model. In the 3-level model [see Eq. (14) with $g_1 = 0, g_4 = 0, G = 0$] at resonance (7), the stationary state is known to be *pure* for all detunings, and given by the squeezed vacuum [42, 44]. We will now recover this result by showing that this state is not affected by the parity swapping Kraus operator M_2

[cf. Eq. (48)]. Indeed, beyond adiabatic limit we have [cf. Eq. (B19)]

$$M_2 = -a \frac{g_2}{\Delta} M_g - a^\dagger \frac{g_3^*}{\Delta} M_e + e^{-i\tau \left(\Delta + a a^\dagger \frac{|g_2|^2}{\Delta} + a^\dagger a \frac{|g_3|^2}{\Delta} \right)} \left(a \frac{g_2}{\Delta} c_g + a^\dagger \frac{g_3^*}{\Delta} c_e \right) + \dots \quad (\text{B25})$$

where M_g and M_e correspond to 3-level dynamics. M_2 operator, however, is 0 in the first-order on the squeezed vacuum state $|\Psi_+\rangle$, as

$$\begin{aligned} \left(-a \frac{g_2}{\Delta} M_g - a^\dagger \frac{g_3^*}{\Delta} M_e \right) |\Psi_+\rangle &= - \left(a \frac{g_2}{\Delta} c_g + a^\dagger \frac{g_3^*}{\Delta} c_e \right) |\Psi_+\rangle \\ &= \sum_{n=0}^{\infty} \left(\sqrt{2n+2} \frac{g_2}{\Delta} c_g c_{2n+2} + \sqrt{2n+1} \frac{g_3^*}{\Delta} c_e c_{2n} \right) |2n+1\rangle = 0, \end{aligned} \quad (\text{B26})$$

where in the first equality we used that in 3-level model we have $M_e|\psi_\pm\rangle = c_e$ and $M_g|\psi_\pm\rangle = c_g$ (up to a global phase) (see Appendix C). The last equality follows from the recurrence relation for the pure stationary states (cf. Appendix C)

$$\frac{c_{n+2}}{c_n} = -\frac{c_e}{c_g} \frac{g_3^*}{g_2} \frac{\sqrt{n+1}}{\sqrt{n+2}}. \quad (\text{B27})$$

It is worth to emphasize that for the state of the negative parity (odd n), the parity-swapping Kraus operator M_2 does not vanish on its one-photon component, thus leading to its decay and a unique stationary state of the dynamics given by the squeezed vacuum [42] (see also Appendix G).

APPENDIX C: PURE STATIONARY STATES OF TWO-PHOTON MICROMASERS

In Appendix B we derived the effective two-photon Hamiltonian, Eq. (12), describing the far-detuned limit of the cavity interaction with a multi-level atom in the ladder configuration [see Fig. 1(a)]. Here we discuss pure stationary states of *general two-photon dynamics*, with a Hamiltonian of the same functional form as (12) but with arbitrary Stark shifts and two-photon couplings. We show that beyond the stationary states in Eq. (26), the only pure states correspond to the stationary states of 3-level model [42, 44, 68].

Effective Hamiltonian. Within RWA, i.e., for dynamics based single-photon Jaynes-Cummings interactions, the adiabatic limit of far-detuned levels with a two-photon resonance [Eq. (7)] leads in the second-order to the effective Hamiltonian

$$H_{\text{eff}} = \begin{bmatrix} Aa^\dagger a + B \mathbb{1} & C^* a^{\dagger 2} \\ C a^2 & D a^\dagger a + E \mathbb{1} \end{bmatrix}, \quad (\text{C1})$$

where $A, B, D, E \in \mathbb{R}$ and $C \in \mathbb{C}$ and the basis is given by the resonant levels $|1\rangle, |3\rangle$ [cf. Appendix B and Eq. (12)]. The constants A, B, D and E describe the Stark shifts, while C determines the effective two-photon coupling strength.

Pure stationary states. We are interested in the case when the two Kraus operators corresponding to the Hamiltonian (C1) feature the same cavity state $|\Psi_{\text{ss}}\rangle = \sum_{n=0}^{\infty} c_n |n\rangle$ as an eigenvector. This corresponds to the following set of equations [cf. Eqs. (16) and (24)]

$$\alpha c_{n+2} = c_g e^{-i\varphi_n} \left[\cos(\phi_n) - i s_n^z \frac{\sin(\phi_n)}{\phi_n} \right] c_{n+2} - i c_e e^{-i\varphi_n} (s_n^x)^* \frac{\sin(\phi_n)}{\phi_n} c_n, \quad (\text{C2a})$$

$$\beta c_n = -i c_g e^{-i\varphi_n} s_n^x \frac{\sin(\phi_n)}{\phi_n} c_{n+2} + c_e e^{-i\varphi_n} \left[\cos(\phi_n) + i s_n^z \frac{\sin(\phi_n)}{\phi_n} \right] c_n, \quad (\text{C2b})$$

where

$$s_n^z = \frac{A(n+2) + B - Dn - E}{2}, \quad s_n^x = C \sqrt{(n+1)(n+2)}, \quad (\text{C3})$$

$$\phi_n = \tau \sqrt{(s_n^z)^2 + (s_n^x)^2}, \quad \varphi_n = \tau \frac{(A+D)n + 2A + B + E}{2}. \quad (\text{C4})$$

Eqs. (C2) feature non-trivial solution when the corresponding determinant is 0 independently of n ,

$$e^{-i\varphi_n} \left[\alpha \beta e^{i\varphi_n} + c_e c_g e^{-i\varphi_n} - \cos(\phi_n) (\alpha c_e + \beta c_g) - i s_n^z \frac{\sin(\phi_n)}{\phi_n} (\alpha c_e - \beta c_g) \right] = 0, \quad (\text{C5})$$

where on l.h.s. we used the fact $(s_n^z)^2 + (s_n^x)^2 = \phi_n^2$.

Note that in the absence of coupling, $C = 0$, we obtain that $s_n^x \equiv 0$, and dynamics corresponds to the dephasing of coherences, which is caused by the Stark shifts in (C1). This leads to a stationary state of the cavity given by the diagonal of an initial state (a classical state without coherences), unless both ϕ_n and φ_n are independent of n (this takes place when $A = 0 = D$, in which case the Stark shift is independent from the cavity field, and instead of dephasing the passage of atoms only changes the global phase).

For the case of $C \neq 0$, the last term in Eq. (C4), $s_n^z \sin(\phi_n)/\phi_n$, is *independent* function of n , from both $\cos(\phi_n)$ and $e^{i\varphi_n}$, $e^{-i\varphi_n}$, i.e., it cannot be cancelled by the other terms for all n . Therefore, for Eq. (C4) to hold, it is necessary for the last term to vanish for all n , which takes place when $s_n^z = 0$ or $\alpha c_e - \beta c_g = 0$, which define *two complementary cases* we now discuss.

Case 1. Lets first consider $s_n^z = 0$, which from (C3) yields the effective Hamiltonian coefficients as

$$A = D \quad \text{and} \quad B = E + 2A, \quad (\text{C6})$$

As $C \neq 0$, ϕ_n depends on n , and furthermore $\cos(\phi_n)$ is an independent function from $e^{i\varphi_n}$ and $e^{-i\varphi_n}$. Therefore, it is required that $\alpha c_e + \beta c_g = 0$, so that the outgoing state of atoms are given by [cf. Eq. (25)]

$$\alpha = c_g e^{-i\varphi}, \quad \beta = -c_e e^{-i\varphi}, \quad (\text{C7})$$

This in turn simplifies the first two terms in (C4) as $\alpha \beta e^{i\varphi_n} + c_e c_g e^{-i\varphi_n} = -2i c_e c_g e^{-i\varphi} \sin(\varphi_n - \varphi)$, which thus requires $\varphi_n = \varphi + k\pi$, where $k \in \mathbb{Z}$, so that

$$A = -D = 0 \quad \text{and} \quad \varphi = 2B\tau + k\pi, \quad (\text{C8})$$

and there are no Stark shifts (except the global phase φ): $A = D = 0$, $B = E$. This is exactly the case discussed at length in this work, which leads to the stationary states given by the recurrence relation (26) [by choosing $k = 0, 1$ in φ].

Case 2. In order to remove the amplitude of the last term in Eq. (C4), we now consider $\alpha c_e - \beta c_g = 0$, which determines the outgoing state of atoms as [cf. Eq. (C7)]

$$\alpha = c_g e^{-i\varphi}, \quad \beta = c_e e^{-i\varphi}. \quad (\text{C9})$$

In this case we have for the remaining terms

$$\begin{aligned} \alpha \beta e^{i\varphi_n} + c_e c_g e^{-i\varphi_n} - \cos(\phi_n) (\alpha c_e + \beta c_g) &= c_e c_g e^{-i\varphi} [\cos(\varphi_n - \varphi) - \cos(\phi_n)] \\ &= -2c_e c_g e^{-i\varphi} \sin\left(\frac{\varphi_n + \phi_n - \varphi}{2}\right) \sin\left(\frac{\varphi_n - \phi_n - \varphi}{2}\right). \end{aligned} \quad (\text{C10})$$

Therefore, we require $\varphi_n - \varphi + 2k\pi = \pm\phi_n$, where $k \in \mathbb{Z}$, which expression squared (and divided by τ^2) yields

$$n^2 (AD - |C|^2) + n [2AD - 3|C|^2 + AE + DB - (A + D)\omega] + (2A + B)E - 2|C|^2 - (2A + B + E)\omega + \omega^2 = 0, \quad (\text{C11})$$

where $\omega = (\varphi - 2k\pi)/\tau$. Requiring that the above expression holds for all n , we arrive at the following conditions on the effective Hamiltonian coefficients,

$$|C|^2 = AD > 0, \quad \omega = \frac{A(-D + E) + DB}{A + D}, \quad (B + D - E)(A + B + 2D - E) = 0 \quad (\text{C12})$$

where $A + D \neq 0$ follows from $A \neq -D$ as $AD > 0$. Interestingly, both solutions of the last condition, $B = -D + E$ ($\varphi = \tau B + 2k\pi$) and $B + A + D = -D + E$ [$\varphi = \tau(A + B) + 2k\pi$], yield the same stationary state given by the recurrence relation [cf. Eq. (26)]

$$\frac{c_{n+2}}{c_n} = -\frac{c_e}{c_g} \frac{C^*}{A} \sqrt{\frac{n+1}{n+2}} \quad (\text{C13})$$

which in the even-parity subspace yields the squeezed vacuum state, whose squeezing can be regulated by the ratio of the dynamical shifts $\frac{|C|}{A} = \sqrt{\frac{A}{D}}$. In particular, for the micromaser with 3-level atoms [42, 44, 68] we have $A = -\frac{|g_2|^2}{\Delta}$, $B = 0$, $C = -\frac{g_2 g_3}{\Delta}$ and $D = E = -\frac{|g_3|^2}{\Delta}$ [cf. Eq. (15)]. Therefore, the squeezing is regulated by the ratio $|\frac{g_3}{g_2}|$.

APPENDIX D: HARD WALLS AND PELL EQUATION

In Sec. IV D we have discussed hard-walls in the cavity dynamics, i.e., when the integrated coupling strength ϕ leads to $\sin_m(\phi) = 0$ for certain m , so that the cavity states $|m\rangle$ and $|m+2\rangle$ are no longer coupled. Here we show that the condition in Eq. (41) corresponds for the subsequent walls to Pell equation [80, 81], and derive the recurrence relation for positions of these hard walls.

Pell equation. For a given integrated coupling strength ϕ , let us assume that m is the position of the *first* wall with the corresponding K . Any other wall at $m' > m$ must fulfill, from (41),

$$(m' + 1)(m' + 2) = \left(\frac{K'}{K}\right)^2 (m + 1)(m + 2). \quad (\text{D1})$$

for a certain integer K' . By setting $D := (m+1)(m+2)$, $x := 2m' + 3$ and $y := 2K'/K$, we get the Pell equation [80, 81]

$$x^2 - Dy^2 = 1. \quad (\text{D2})$$

We assume $\phi > 0$ and thus $K > 0$ [cf. Eq. (41)] (otherwise we equivalently consider positive integers $-K$ and $-K'$). Since D is not a perfect square, Eq. (D2) has infinitely many positive integer solutions (x_n, y_n) , $n \geq 1$. If the solutions are ordered by the magnitude of x_n , the n th solution is given by the recurrence relation [82]

$$x_n = x_1 x_{n-1} + D y_1 y_{n-1}, \quad (\text{D3a})$$

$$y_n = x_1 y_{n-1} + y_1 x_{n-1}, \quad (\text{D3b})$$

or equivalently

$$x_n + \sqrt{D} y_n = (x_1 + \sqrt{D} y_1)^n, \quad (\text{D4})$$

where $(x_1, y_1) = (2m + 3, 2)$ is the first non-zero integer solution, called the fundamental solution.

Recurrence relation for hard walls. From Eq. (D3) we note that, since x_1 is odd, x_n is always odd, while y_n is always even as y_1 is even [this is a consequence of D being even; cf. Eq. (D2)]. Therefore, each solution with x_n and y_n , corresponds directly to a hard wall in the dynamics at $m_n = (x_n - 3)/2$, and with $K_n = y_n K/2$ being a multiple of K . Furthermore, Eq. (D3) yields the recurrence relation

$$m_n = m_{n-1}(2m + 3) + 3(m + 1) + 2(m + 1)(m + 2) K_{n-1}/K, \quad (\text{D5a})$$

$$K_n = K_{n-1}(2m + 3) + K(2m_{n-1} + 3), \quad (\text{D5b})$$

and we conclude there are infinitely many hard walls in the dynamics.

We need to note, however, that we are also interested in solutions of (D2), in which x is an (odd) integer, while y is a rational number, i.e., when $2K'$ is not a multiple of K . As we show below, however, the position of walls fulfils the recurrence relation (D5) and K is always a multiplicity of K .

Proof. Suppose that there exists a hard wall at m' with $2K'$ not divisible by K , $\bar{K} := \gcd(K, 2K') < K$. We have

$$(2m' + 3)^2 - 1 = D \left(\frac{\bar{K}}{K}\right)^2 \left(\frac{2K'}{\bar{K}}\right)^2. \quad (\text{D6})$$

Since the greatest common factor of the integers $2K'/\bar{K}$ and $\tilde{K} := K/\bar{K}$ is 1 by definition, it follows, from the left-hand side of (D6) being an integer, that D must be divisible by \tilde{K}^2 . Therefore, $\tilde{D} := D/\tilde{K}^2 < D$ is an integer, and since D was not a square of integer, neither is \tilde{D} . We thus arrive at a new Pell equation

$$\tilde{x}^2 - \tilde{D}\tilde{y}^2 = 1, \quad (\text{D7})$$

where the new integer variable $\tilde{y} := \tilde{K}y$, while $\tilde{x} := x$ as before. We will now show that, as $\tilde{x} = x$ remains unchanged, the recurrence relation (D5) stays the same.

The position of the first hard wall m , together with K , yield an integer solution of Eq. (D7): $\tilde{x} = 2m + 3$, $\tilde{y} = 2\tilde{K}$. Therefore, it must appear in the recurrence relation in Eq. (D3) with D replaced by \tilde{D} . If \tilde{x}_1 is odd (i.e. when \tilde{D} is even), \tilde{x}_n is also odd, and thus corresponds to a hard wall at an integer \tilde{m}_n . In particular, the fundamental solution corresponds to the first hard wall, i.e. $m = (\tilde{x}_1 - 3)/2$ [where $\tilde{x}_1 \geq 3$ follows from $\tilde{y}_1 > 0$ required by the assumed positive integrated coupling $\phi > 0$, cf. Eq. (41)]. Thus, we again obtain the recurrence relation in Eq. (D5) [as in the recurrence equation for $\tilde{x}_n \equiv x_n$ we have that \tilde{D} simplifies with $\tilde{y}_1\tilde{y}_{n-1}$ to Dy_ny_{n-1} in Eq. (D3a), while the recurrence equation for \tilde{y}_n can be divided by \tilde{K} yielding Eq. (D3b), since \tilde{y}_n is divisible by \tilde{K} as so is \tilde{y}_1].

When \tilde{D} is odd, it is possible that x_1 is even (and y_1 odd), in which case the parity of x_n (and y_n) oscillates with period 2. In particular, the first hard wall corresponds to the second solution, $m = (\tilde{x}_2 - 3)/2 = (\tilde{x}_1^2 + \tilde{D}\tilde{y}_1^2 - 3)/2$, while other hard walls correspond to x_{2n} . Nevertheless, from (D4) we have

$$\tilde{x}_{2n} + \sqrt{\tilde{D}}\tilde{y}_{2n} = \left(\tilde{x}_2 + \sqrt{\tilde{D}}\tilde{y}_2\right)^n, \quad (\text{D8})$$

so that the odd solutions also obey the recurrence relation Eq. (D3), but with the fundamental solution chosen as x_2 and y_2 , instead of x_1 and y_1 . Therefore, analogously as in the case of \tilde{D} being even, the walls are again determined by Eq. (D5). This concludes the proof.

APPENDIX E: SOFT WALLS

In Sec. IV D we introduced the notion of a soft wall. Here we discuss the structure of stationary states in the cavity in the presence of soft walls, and also discuss the induced long-time dynamics leading to those stationary states.

1. Distribution of pure stationary states between soft walls

We now discuss the structure of the stationary state between soft walls and argue that they are supported only after the walls corresponding to the boundary condition Eq. (27). We assume coherent dynamics $c_e, c_g \neq 0$.

Dynamics with soft walls features pure states given in Eq. (29). In general, the, say, even state can be written as a sum of contributions with support between subsequent pairs of walls located at m_k^+ and m_{k+1}^+ as

$$\begin{aligned} |\Psi_+\rangle &= \sum_{n=0}^{m_1^+/2} c_{2n} |2n\rangle + \sum_{k=1}^{\infty} \sum_{n=1+m_k^+/2}^{m_{k+1}^+/2} c_{2n} |2n\rangle \\ &= \sum_{n=0}^{m_1^+/2} c_{2n} |2n\rangle + \sum_{k=1}^{\infty} c_{m_k^+} (-i) \frac{c_e}{c_g} \frac{\sin_{m_k^+}(\phi)}{1 - \cos_{m_k^+}(\phi)} \sum_{n=1+m_k^+/2}^{m_{k+1}^+/2} \frac{c_{2n}}{c_{m_k^++2}} |2n\rangle \\ &= c_0 \left\{ \mathcal{N}_0^+ |\Psi_0^+\rangle + \sum_{k=1}^{\infty} \left[\prod_{l=1}^k \frac{c_{m_l^+}}{c_{m_{l-1}^++2}} \right] (-i)^k \left(\frac{c_e}{c_g} \right)^k \left[\prod_{l=1}^k \frac{\sin_{m_l^+}(\phi)}{1 - \cos_{m_l^+}(\phi)} \right] \mathcal{N}_k^+ |\Psi_k^+\rangle \right\}, \end{aligned} \quad (\text{E1})$$

where m_k^+ labels the walls of the even parity [cf. Eq. (26)] and we introduced normalisation $(\mathcal{N}_k^+)^2 = \sum_{n=1+m_k^+/2}^{m_{k+1}^+/2} |c_{2n}/c_{m_k^++2}|^2$ and the state after the k th even wall $|\Psi_k^+\rangle = \sum_{n=1+m_k^+/2}^{m_{k+1}^+/2} c_{2n} |2n\rangle / c_{m_k^++2} / \mathcal{N}_k^+$ (where for $|\Psi_0^+\rangle$ we formally define $m_0^+ = -2$). The analogous construction holds for the odd state $|\Psi_-\rangle$ in Eq. (29).

In Eq. (E1) we can identify $c_{m_{k+1}^+}/c_{m_k^++2}$ is the ratio between the last and the first coefficients in the state after k th wall, $|\Psi_k^+\rangle$ and thus we expect it to be finite (as there are no soft walls within the state). Similarly, the norm \mathcal{N}_k^+ of the k th state is finite. In contrary, the remaining terms Eq. (E1) can lead either to the suppression or the increase of the k th state contribution, depending whether the boundary condition after k th even soft wall, Eq. (46), coincides

Case	Soft walls			Hard walls ($\delta_1, \delta_2 = 0$)		
	$\cos_{m_1^+}(\phi)$	$\cos_{m_2^+}(\phi)$	$ \Psi_+\rangle$	ρ_0^+	ρ_1^+	ρ_2^+
1.	$-1 + \frac{\delta_1^2}{2}$	$-1 + \frac{\delta_2^2}{2}$	$ \Psi_0^+\rangle + \mathcal{O}(\delta_1)$	$ \Psi_0^+\rangle$	mixed	mixed
2.	$1 - \frac{\delta_1^2}{2}$	$-1 + \frac{\delta_2^2}{2}$	$ \Psi_1^+\rangle + \mathcal{O}(\delta_1, \delta_2)$	mixed	$ \Psi_1^+\rangle$	mixed
3.	$-1 + \frac{\delta_1^2}{2}$	$1 - \frac{\delta_2^2}{2}$	$\beta_0^+ \Psi_0^+\rangle + \beta_2^+ \Psi_2^+\rangle + \mathcal{O}[\min(\delta_1, \delta_2)]$	$ \Psi_0^+\rangle$	$ \Psi_1^+\rangle$	$ \Psi_2^+\rangle$
4.	$1 - \frac{\delta_1^2}{2}$	$1 - \frac{\delta_2^2}{2}$	$ \Psi_2^+\rangle + \mathcal{O}(\delta_2)$	mixed	mixed	$ \Psi_2^+\rangle$

TABLE II. **Steady state between two soft walls vs. two hard walls.** The stationary state with soft walls approximately corresponds only to the pure stationary states of hard walls that obey the same boundary conditions. For soft walls: $|\Psi_+\rangle$ from Eqs. (E1) and (E2). In case 3. $\beta_2^+/\beta_0^+ = -(c_e/c_g)^2 \mathcal{N}_2^+/\mathcal{N}_0^+ [c_{m_2^+}/c_{m_1^++2}] [c_{m_1^+}/c_0] \times 4 \lim \delta_1/\delta_2$. For hard walls: $|\Psi_k^+\rangle$ refers to the k th pure stationary state with with boundary conditions at the $(k-1)$ -th and k -th wall which are opposite to Eq. (27). For the finite number of walls, we have assumed a third even wall to be hard, with $\cos_{m_3^+}(\phi) = -1$, so that pure stationary states before that wall exist [cf. Eqs. (27) and (45)]. The same results hold for the odd stationary state.

with the boundary condition of the state $|\Psi_+\rangle$ in Eq. (27),

$$\text{when } \cos_{m_k^+}(\phi) \approx 1, \quad \frac{\sin_{m_k^+}(\phi)}{1 - \cos_{m_k^+}(\phi)} \approx \frac{2}{\sin_{m_k^+}(\phi)} \rightarrow \pm\infty \quad (\text{E2a})$$

$$\text{when } \cos_{m_k^+}(\phi) \approx -1, \quad \frac{\sin_{m_k^+}(\phi)}{1 - \cos_{m_k^+}(\phi)} \approx \frac{\sin_{m_k^+}(\phi)}{2} \rightarrow 0 \quad (\text{E2b})$$

where the arrows correspond to the limit of soft wall being hard. Noticing that c_0 in Eq. (E1) also changes with the height of the walls in order to keep the norm of $|\Psi_+\rangle$ equal 1, we arrive at the following approximation

$$\begin{aligned} |\Psi_+\rangle &\approx \alpha_0^+ \mathcal{N}_0^+ |\Psi_0^+\rangle + \sum_{k=1}^{\infty} \left[\prod_{l=1}^k \frac{c_{m_l^+}}{c_{m_{l-1}^++2}} \right] (-i)^k \left(\frac{c_e}{c_g} \right)^k \alpha_k^+ \mathcal{N}_k^+ |\Psi_k^+\rangle \\ &=: \beta_0^+ |\Psi_0^+\rangle + \sum_{k=1}^{\infty} \beta_k^+ |\Psi_k^+\rangle, \end{aligned} \quad (\text{E3})$$

where we defined the *hard wall limit* as

$$c_0 \prod_{l=1}^k \frac{\sin_{m_l^+}(\phi)}{1 - \cos_{m_l^+}(\phi)} \rightarrow \alpha_k^+, \quad (\text{E4})$$

so that we choose $\alpha_k^+ = 0$ if $\cos_{m_k^+}(\phi) \approx -1$ [cf. Eq. (E2)].

In Eq. (E3) only the states after the soft walls with the boundary condition $\cos_{m_k^+}(\phi) \approx 1$ can be present [cf. Fig. 2(b) and see the example in Tab. II]. Therefore, the state $|\Psi_0^+\rangle$ can be present only for the first wall with $\cos_{m_1^+}(\phi) \approx -1$ [cf. Fig. 2(b) for the states (ii, viii)]. We further note that several subsequent walls with $\cos_{m_k^+}(\phi) \approx 1$ may be needed to counteract the suppression due to an earlier wall, in which case only the state after the last such a wall is present, see Fig. 2(b) for the states (iii,vi,vii,ix). The same results follows from considering soft walls as a perturbation away from auxiliary hard walls (see below).

Finally we note that for finite walls, the coefficients β_k^+ in Eq. (E3) depend also on the distribution of the states $|\Psi_k^+\rangle$ between the walls, e.g., whether the state is supported only close to one of the walls. In particular, in the case of $|c_g| = 1$, we simply have $|\Psi_+\rangle = |\Psi_0\rangle = |0\rangle$.

2. Dynamics due to soft walls

Here we discuss timescales of achieving pure stationary states, Eq. (E3), by considering dynamics in the presence of soft walls as a perturbation of auxiliary dynamics with hard walls.

a. *Dynamics of soft walls as perturbation of hard walls*

The dynamics of the cavity with soft walls can be formally considered as a *perturbation of* an auxiliary dynamics $M_g^{(0)}$, $M_e^{(0)}$ with *hard walls* replacing soft walls,

$$M_g - M_g^{(0)} \equiv \delta M_g = \sum_{k=1}^{\infty} (-ic_e \sin_{m_k}(\phi) |m_k+2\rangle\langle m_k| + c_g [\cos_{m_k}(\phi) \mp 1] |m_k+2\rangle\langle m_k+2|), \quad (\text{E5a})$$

$$M_e - M_e^{(0)} \equiv \delta M_e = \sum_{k=1}^{\infty} (c_e [\cos_{m_k}(\phi) \mp 1] |m_k\rangle\langle m_k| - ic_g \sin_{m_k}(\phi) |m_k\rangle\langle m_k+2|), \quad (\text{E5b})$$

where we consider $\cos_{m_k}(\phi) \approx \pm 1$, so that $\cos_{m_k}(\phi) \mp 1 \approx 0$. In this appendix we discuss the order of the perturbation in the powers of a small parameter δ_k of k th wall where

$$\cos_{m_k}(\phi) \approx \pm \left(1 - \frac{\delta_k^2}{2}\right), \quad \sin_{m_k}(\phi) \approx \pm \delta_k \quad (\text{E6})$$

[see Eq. (E5) and Tab. II].

b. *Steady state with soft walls vs. stationary states of hard walls*

The stationary state in Eq. (29) is pure and fulfills the boundary condition (27). In contrast, each soft wall present in the dynamics can be approximated by a hard wall that determines boundary conditions for a state before and after that wall [Eqs. (45) and (46)].

Steady states of hard walls. First, the k th stationary state ρ_k^{\pm} , between subsequent walls of the same parity at m_k^{\pm} and m_{k+1}^{\pm} , is pure only if $\cos_{m_k^{\pm}}(\phi) = -\cos_{m_{k+1}^{\pm}}(\phi)$. Otherwise, that stationary state is mixed. Second, even if the stationary state is pure, when its boundary condition differs from (27), it does not correspond to the stationary state with soft walls $|\Psi_{\pm}\rangle$, i.e., it differs from its projection $|\Psi_k^{\pm}\rangle$ between the k th and $(k+1)$ th walls, as $|\langle \bar{\Psi}_k^{\pm} | \Psi_k^{\pm} \rangle|^2 < 1$, unless $m_{k+1}^+ - m_k^+ = 2$ and it is a fixed photon state, $|\bar{\Psi}_k^{\pm}\rangle = |m_{k+1}^{\pm}\rangle$. Indeed, from Eq. (26), when $c_e, c_g \neq 0$, $|\langle \bar{\Psi}_k^{\pm} | \Psi_k^{\pm} \rangle|^2 = 1$ requires $\cot_k(\phi/2) = -\tan_k(\phi/2)$ [for all $m_k^{\pm} + 2 < k \leq m_{k+1}^{\pm}$ such that $(-1)^k = \pm 1$], which is never true. Furthermore, the coherences between pure stationary states corresponding to opposite boundary condition [i.e., opposite eigenvalues of Kraus operators, see Eq. (25)], and between the pure and mixed stationary states, are not stationary (cf. Sec. IV D).

Consequences for stationary state with soft walls. The perturbative dynamics defined in Eq. (E5) should recover the true stationary state in Eq. (29). In particular, in the zero order, the solution is a linear combination of the stationary states between hard walls [50, 88]. Therefore, in agreement with Eq. (E3), the stationary states in Eq. (29) can be *approximated* only by the *pure stationary states between hard walls that are consistent with the boundary conditions* (27), i.e., $\cos_{m_k^{\pm}}(\phi) = 1 = -\cos_{m_{k+1}^{\pm}}(\phi)$. See Tab. II for the example of two walls.

c. *Perturbative dynamics*

Below we derive the long-time dynamics due to the presence of the soft walls. We prove that this dynamics is second-order in $\sin_{m_n}(\phi)$. Due to locality of the perturbation in Eq. (E5) only neighbouring states get connected, or coherences between states separated by two walls are created. Furthermore, the perturbation depends on the amplitude of the states directly next to the walls. We discuss how the closed form of the long-time dynamics generator can be found using the structure of the stationary state Eq. (E3).

First and second-order perturbation. The difference $\delta \mathcal{L}$ between the dynamics generated by M_g , M_e (16) and the modified Kraus operators with hard walls $M_g^{(0)}$ and $M_e^{(0)}$ feature the first and second order perturbation in δM_g and δM_e [cf. (E5)]

$$\begin{aligned} \nu^{-1} \mathcal{L}(\rho) &= M_g \rho M_g^{\dagger} + M_g \rho M_g^{\dagger} - \rho = M_g^{(0)} \rho [M_g^{(0)}]^{\dagger} + M_e^{(0)} \rho [M_e^{(0)}]^{\dagger} - \rho + \\ &+ \left\{ \delta M_g \rho [M_g^{(0)}]^{\dagger} + \delta M_e \rho [M_e^{(0)}]^{\dagger} + \text{H.c.} \right\} + \delta M_g \rho \delta M_g^{\dagger} + \delta M_e \rho \delta M_e^{\dagger}, \end{aligned} \quad (\text{E7})$$

cf. Eq. (11). The perturbations in the Kraus operators themselves, δM_g and δM_e in Eq. (E5), feature first and second-order perturbations [cf. Eq. (E6)]

$$\delta M_g^{(1)} = -ic_e \sum_{k=1}^{\infty} \sin_{m_k}(\phi) |m_k+2\rangle\langle m_k|, \quad \delta M_g^{(2)} = c_g \sum_{k=1}^{\infty} [\cos_{m_k}(\phi) \mp 1] |m_k+2\rangle\langle m_k+2|, \quad (\text{E8a})$$

$$\delta M_e^{(1)} = -ic_g \sum_{k=1}^{\infty} \sin_{m_k}(\phi) |m_k\rangle\langle m_k+2|, \quad \delta M_e^{(2)} = c_e \sum_{k=1}^{\infty} [\cos_{m_k}(\phi) \mp 1] |m_k\rangle\langle m_k|. \quad (\text{E8b})$$

Therefore, we can identify the first and second-order perturbation to the master equation (E7) as

$$\delta \mathcal{L}_1 = \delta M_g^{(1)} \rho [M_g^{(0)}]^\dagger + \delta M_e^{(1)} \rho [M_e^{(0)}]^\dagger + \text{H.c.}, \quad (\text{E9})$$

$$\delta \mathcal{L}_2 = \delta M_g^{(1)} \rho [\delta M_g^{(1)}]^\dagger + \delta M_e^{(1)} \rho [\delta M_e^{(1)}]^\dagger + \left\{ \delta M_g^{(2)} \rho [M_g^{(0)}]^\dagger + \delta M_e^{(2)} \rho [M_e^{(0)}]^\dagger + \text{H.c.} \right\}. \quad (\text{E10})$$

Below we focus on the second-order corrections to the dynamics, and thus we neglect the third and-forth order perturbations in (E7).

Absence of first-order corrections. We show now that dynamics feature no contribution from \mathcal{L}_1 in (E9). We consider only even or odd states, but we drop the superscript \pm in $|\Psi_k^\pm\rangle$, ρ_k^\pm and m_k^\pm for convenience.

Noting that for pure stationary state between the k th and $(k+1)$ th walls we have $M_g^{(0)}|\Psi_k\rangle = \pm c_g$ and $M_e^{(0)}|\Psi_k\rangle = \mp c_e$,

$$\nu^{-1} \delta \mathcal{L}_1 (|\Psi_k\rangle\langle\Psi_k|) = \pm ic_g c_e^* c_{m_k+2}^{(k)} \sin_{m_k}(\phi) |m_k\rangle\langle\Psi_k| \mp ic_e c_g^* c_{m_{k+1}}^{(k)} \sin_{m_{k+1}}(\phi) |m_{k+1}+2\rangle\langle\Psi_k| + \text{H.c.}, \quad (\text{E11})$$

where $c_n^{(k)}$ is the amplitude (coefficient) of n photons in the pure stationary state between the k th and $(k+1)$ th walls. Analogously, for the coherences between the states with the same boundary conditions,

$$\begin{aligned} \nu^{-1} \delta \mathcal{L}_1 (|\Psi_{k_1}\rangle\langle\Psi_{k_2}|) = & \pm ic_g c_e^* c_{m_{k_1}+2}^{(k_1)} \sin_{m_{k_1}}(\phi) |m_{k_1}\rangle\langle\Psi_{k_2}| \mp ic_e c_g^* c_{m_{k_1+1}}^{(k_1)} \sin_{m_{k_1+1}}(\phi) |m_{k_1+1}+2\rangle\langle\Psi_{k_2}| \\ & \mp ic_g^* c_e \left(c_{m_{k_2}+2}^{(k_2)} \right)^* \sin_{m_{k_2}}(\phi) |\Psi_{k_1}\rangle\langle m_{k_2}| \pm ic_e^* c_g \left(c_{m_{k_2+1}}^{(k_2)} \right)^* \sin_{m_{k_2+1}}(\phi) |\Psi_{k_1}\rangle\langle m_{k_2+1}+2|. \end{aligned} \quad (\text{E12})$$

Similarly, for the mixed state ρ_k (mixed due to different boundary conditions implied by k th and $(k+1)$ th walls) we have

$$\nu^{-1} \delta \mathcal{L}_1 (\rho_k) = -ic_g \sin_{m_k}(\phi) |m_k\rangle\langle m_k+2| \rho_k [M_e^{(0)}]^\dagger - ic_e \sin_{m_{k+1}}(\phi) |m_{k+1}+2\rangle\langle m_{k+1}| \rho_k [M_g^{(0)}]^\dagger + \text{H.c.} \quad (\text{E13})$$

As stationary coherences can only exist between pure stationary states which are separated by at least two walls [cf. Eqs. (45) and (46) and [83]], there are no first-order corrections to the dynamics [cf. Eq. (G2) and [50, 88, 91]]

$$\Pi_0 \delta \mathcal{L}_1 (|\Psi_k\rangle\langle\Psi_k|) = 0, \quad (\text{E14})$$

$$\Pi_0 \delta \mathcal{L}_1 (|\Psi_{k_1}\rangle\langle\Psi_{k_2}|) = 0, \quad (\text{E15})$$

$$\Pi_0 \delta \mathcal{L}_1 (\rho_k) = 0, \quad (\text{E16})$$

where Π_0 denotes the projection onto the stationary states of dynamics \mathcal{L}_0 with hard walls.

Second-order corrections. We now derive the effective dynamics in the second-order of the corrections in δM_g and δM_e , Eq. (E5). We consider both the corrections from \mathcal{L}_2 , as well as the contribution from \mathcal{L}_1 in Eqs. (E9) and (E10), as the second-order corrections are given by [50, 88, 91]

$$\Pi_0 \mathcal{L}_2 \Pi_0 - \Pi_0 \mathcal{L}_1 \mathcal{S}_0 \mathcal{L}_1 \Pi_0, \quad (\text{E17})$$

where \mathcal{S}_0 is the resolvent for the dynamics \mathcal{L}_0 with hard walls (evaluated at 0), i.e., $\mathcal{S}_0 \mathcal{L}_0 = \mathcal{L}_0 \mathcal{S}_0 = \mathcal{I} - \Pi_0$.

First, we consider second-order corrections $\Pi_0 \mathcal{L}_2 \Pi_0$ due to the second-order perturbation \mathcal{L}_2 [cf. Eq. (G2) and [50, 88, 91]]. We have

$$\begin{aligned} \nu^{-1} \Pi_0 \delta \mathcal{L}_2 (|\Psi_k\rangle\langle\Psi_k|) = & |c_e|^2 \sin_{m_{k+1}}^2(\phi) |c_{m_{k+1}}^{(k)}|^2 \rho_{k+1} + |c_g|^2 \sin_{m_k}^2(\phi) |c_{m_k+2}^{(k)}|^2 \rho_{k-1} \\ & \pm 2 \left\{ |c_g|^2 [\cos_{m_k}(\phi) \mp 1] |c_{m_k+2}^{(k)}|^2 - |c_e|^2 [\cos_{m_{k+1}}(\phi) \pm 1] |c_{m_{k+1}}^{(k)}|^2 \right\} |\Psi_k\rangle\langle\Psi_k|, \end{aligned} \quad (\text{E18})$$

where $\rho_{k\mp 1}$ denotes (note necessarily mixed) $(k\mp 1)$ th stationary state. We used the fact that the projection Π_0 on the states between the hard walls is given by the supports between the walls, so that $\Pi_0(|m_{k+1}\rangle\langle\Psi_k|) = (c_{m_{k+1}}^{(k)})^*|\Psi_k\rangle\langle\Psi_k|$ and $\Pi_0(|m_k+2\rangle\langle\Psi_k|) = (c_{m_k+2}^{(k)})^*|\Psi_k\rangle\langle\Psi_k|$. We assumed the boundary conditions $\cos_{m_k}(\phi) \approx \pm 1 \approx -\cos_{m_{k+1}}(\phi)$, so that up to the second order of perturbation, we have $\cos_{m_k}(\phi)\mp 1 = \mp \sin_{m_k}^2(\phi)/2$ and $\cos_{m_{k+1}}(\phi)\pm 1 = \pm \sin_{m_{k+1}}^2(\phi)/2$ [cf. Eq. (E6)].

Similarly, for the coherences between states $|\Psi_{k_1}\rangle$ and $|\Psi_{k_2}\rangle$ with the same boundary conditions,

$$\begin{aligned} \nu^{-1} \Pi_0 \delta \mathcal{L}_2 (|\Psi_{k_1}\rangle\langle\Psi_{k_2}|) &= |c_e|^2 \sin_{m_{k_1+1}}(\phi) \sin_{m_{k_2+1}}(\phi) c_{m_{k_1+1}}^{(k_1)} \left[c_{m_{k_2+1}}^{(k_2)} \right]^* \eta_{k_1, k_2}^+ |\Psi_{k_1+1}\rangle\langle\Psi_{k_2+1}| \\ &\quad + |c_g|^2 \sin_{m_{k_1}}(\phi) \sin_{m_{k_2}}(\phi) c_{m_{k_1}+2}^{(k_1)} \left[c_{m_{k_2}+2}^{(k_2)} \right]^* \eta_{k_1, k_2}^- |\Psi_{k_1-1}\rangle\langle\Psi_{k_2-1}| \\ &\quad \pm |c_g|^2 \left\{ [\cos_{m_{k_1}}(\phi) \mp 1] |c_{m_{k_1}+2}^{(k_1)}|^2 + [\cos_{m_{k_2}}(\phi) \mp 1] |c_{m_{k_2}+2}^{(k_2)}|^2 \right\} |\Psi_{k_1}\rangle\langle\Psi_{k_2}| \\ &\quad \mp |c_e|^2 \left\{ [\cos_{m_{k_1+1}}(\phi) \pm 1] |c_{m_{k_1+1}}^{(k_1)}|^2 + [\cos_{m_{k_2+1}}(\phi) \pm 1] |c_{m_{k_2+1}}^{(k_2)}|^2 \right\} |\Psi_{k_1}\rangle\langle\Psi_{k_2}|. \end{aligned} \quad (\text{E19})$$

where we introduced $\eta_{k_1, k_2}^+ = \langle\Psi_{k_1+1}|\Pi_0(|m_{k_1+1}+2\rangle\langle m_{k_2+1}+2|)|\Psi_{k_2+1}\rangle$ and $\eta_{k_1, k_2}^- = \langle\Psi_{k_1-1}|\Pi_0(|m_{k_1}\rangle\langle m_{k_2}|)|\Psi_{k_2-1}\rangle$, which are 0 if the pure stationary states $|\Psi_{k_1+1}\rangle$, $|\Psi_{k_2+1}\rangle$, or $|\Psi_{k_1-1}\rangle$, $|\Psi_{k_2-1}\rangle$, do not exist. In derivation of Eq. (E19) we used the fact that pure stationary states are necessarily dark in shifted dynamics [cf. Eq. (31) for the boundary conditions in Eq. (27)], and thus the coherences to them are orthogonally projected by Π_0 [cf. Eq. (G12) and see [118]], e.g., $\Pi_0(|m_{k_1}+2\rangle\langle\Psi_{k_2}|) = (c_{m_{k_1}+2}^{(k)})^*|\Psi_{k_1}\rangle\langle\Psi_{k_2}|$.

Finally, for the mixed stationary state ρ_k [due to mixed boundary conditions from after k th and before $(k+1)$ th wall; cf. Eqs. (45) and (46)],

$$\begin{aligned} \nu^{-1} \Pi_0 \delta \mathcal{L}_2 (\rho_k) &= |c_e|^2 \sin_{m_{k+1}}^2(\phi) \langle m_{k+1}|\rho_k|m_{k+1}\rangle \rho_{k+1} + |c_g|^2 \sin_{m_k}^2(\phi) \langle m_k+2|\rho_k|m_k+2\rangle \rho_{k-1} \\ &\quad \pm 2 \left\{ |c_g|^2 [\cos_{m_k}(\phi) \mp 1] \langle m_k+2|\rho_k|m_k+2\rangle - |c_e|^2 [\cos_{m_{k+1}}(\phi) \pm 1] \langle m_{k+1}|\rho_k|m_{k+1}\rangle \right\} \rho_k, \end{aligned} \quad (\text{E20})$$

where we again used the fact that the projection Π_0 on the states between the hard walls is given by the support between the walls, and from Eq. (E5) $\langle m_k+2|\rho_k[M_g^{(0)}]^\dagger|m_k+2\rangle = \pm c_g \langle m_k+2|\rho_k|m_k+2\rangle$ and $\langle m_{k+1}|\rho_k[M_e^{(0)}]^\dagger|m_{k+1}\rangle = \mp c_e^* \langle m_{k+1}|\rho_k|m_{k+1}\rangle$.

Second, we consider the second-order corrections from the first-order perturbation \mathcal{L}_1 in Eq. (E9), which contributes as $-\Pi_0 \mathcal{L}_1 \mathcal{S}_0 \mathcal{L}_1 \Pi_0$ [50, 88, 91] [cf. Eq. (E17)].

From Eqs. (E11) and (E12) for pure stationary states and coherences between them the first-order perturbation creates coherences to pure stationary states. As a pure stationary state corresponds to the dark state of shifted dynamics, the coherences to such state decay with the corresponding effective Hamiltonian [118]

$$H_\pm \equiv -i\nu[\mathbb{1} \pm (-c_g^* M_g - c_g M_g^\dagger + c_e^* M_e + c_e M_e^\dagger)/2], \quad (\text{E21})$$

where we assumed the state with boundary condition the same/opposite to Eq. (27) [see Eq. (31)]. In particular, the coherence $|\psi\rangle\langle\Psi_k|$ between the dark state and any state between hard walls with different boundary conditions to $|\Psi_k\rangle$ decays to 0, i.e., $\Pi_0|\psi\rangle\langle\Psi_k| = 0$. Furthermore, as $\mathcal{S}_0 = -\int_0^\infty dt (e^{t\mathcal{L}_0} - \Pi_0)$, we have that the resolvent \mathcal{S}_0 simplifies to the *pseudo-inverse* of the effective Hamiltonian

$$\begin{aligned} \mathcal{S}_0(|\psi\rangle\langle\Psi_k|) &= -\int_0^\infty dt e^{-iH_\pm} |\psi\rangle\langle\Psi_k| = (-iH_\pm)^{-1} |\psi\rangle\langle\Psi_k| \\ &= -\nu^{-1} \left[\mathbb{1} \pm \frac{-c_g^* M_g - c_g M_g^\dagger + c_e^* M_e + c_e M_e^\dagger}{2} \right]^{-1} |\psi\rangle\langle\Psi_k| \end{aligned} \quad (\text{E22})$$

As the effective Hamiltonian (E21) does not change the support of the state between the hard walls we have

$$\begin{aligned}
\nu^{-1}\Pi_0\delta\mathcal{L}_1\mathcal{S}_0\delta\mathcal{L}_1(|\Psi_k\rangle\langle\Psi_k|) &= \\
&= \left[|c_g c_e^*|^2 |c_{m_k+2}^{(k)}|^2 \sin_{m_k}^2(\phi) \langle m_k | (-iH_{\pm})^{-1} | m_k \rangle + |c_g c_e^*|^2 |c_{m_{k+1}}^{(k)}|^2 \sin_{m_{k+1}}^2(\phi) \langle m_{k+1}+2 | (-iH_{\pm})^{-1} | m_{k+1}+2 \rangle \right] |\Psi_k\rangle\langle\Psi_k| \\
&\quad - (c_g c_e^*)^2 \left[c_{m_{k-1}}^{(n-2)} \right]^* c_{m_k+2}^{(k)} \sin_{m_{k-1}}(\phi) \sin_{m_k}(\phi) \langle m_{k-1}+2 | (-iH_{\pm})^{-1} | m_k \rangle |\Psi_{k-2}\rangle\langle\Psi_k| \\
&\quad - (c_e c_g^*)^2 \left[c_{m_{k+2}+2}^{(k+2)} \right]^* c_{m_{k+1}}^{(k)} \sin_{m_{k+2}}(\phi) \sin_{m_{k+1}}(\phi) \langle m_{k+2} | (-iH_{\pm})^{-1} | m_{k+1}+2 \rangle |\Psi_{k+2}\rangle\langle\Psi_k| \\
&\quad - |c_g c_e^*|^2 |c_{m_k+2}^{(k)}|^2 \sin_{m_k}^2(\phi) \langle m_k | (-iH_{\pm})^{-1} | m_k \rangle \rho_{k-1} \\
&\quad - |c_e c_g^*|^2 |c_{m_{k+1}}^{(k)}|^2 \sin_{m_{k+1}}^2(\phi) \langle m_{k+1}+2 | (-iH_{\pm})^{-1} | m_{k+1}+2 \rangle \rho_{k+1} \\
&\quad + (c_g c_e^*)^2 c_{m_k+2}^{(k)} \left[c_{m_{k+1}}^{(k)} \right]^* \sin_{m_k}(\phi) \sin_{m_{k+1}}(\phi) \eta_k^{-+} |\Psi_{k-1}\rangle\langle\Psi_{k+1}| \\
&\quad + (c_e c_g^*)^2 c_{m_{k+1}}^{(k)} \left[c_{m_k+2}^{(k)} \right]^* \sin_{m_{k+1}}(\phi) \sin_{m_k}(\phi) \eta_k^{+-} |\Psi_{k+1}\rangle\langle\Psi_{k-1}| \\
&\quad + \text{H.c.}
\end{aligned} \tag{E23}$$

where we introduced $\eta_k^{-+} = \mp c_g^{-1} \langle \Psi_{k-1} | \Pi_0 [M_g^{(0)} (-iH_{\pm})^{-1} | m_k \rangle \langle m_{k+1}+2 |] | \Psi_{k+1} \rangle$ and $\eta_k^{+-} = \pm c_e^{-1} \langle \Psi_{k+1} | \Pi_0 [M_e^{(0)} (-iH_{\pm})^{-1} | m_{k+1}+2 \rangle \langle m_k |] | \Psi_{k-1} \rangle$ and $\eta_k^{\pm\mp} = 0$ if the pure stationary states $|\Psi_{k-1}\rangle$ and $|\Psi_{k+1}\rangle$ do not exist. We also assumed that the pure states $|\Psi_{k-2}\rangle$ and $|\Psi_{k+2}\rangle$ with same boundary condition as $|\Psi_k\rangle$ exist, otherwise the terms with corresponding coherences are absent in Eq. (E23). To derive 1st, 4th and 5th line we used the fact that the projection Π_0 on the states between the hard walls is given by the supports between the walls, and in the 2nd and 3rd line, that the projection Π_0 of the coherence to the dark state reduces to the orthogonal projection on dark states.

Similarly, for the coherences between states $|\Psi_{k_1}\rangle$ and $|\Psi_{k_2}\rangle$ with the same boundary conditions [cf. Eq. (E12)]

$$\begin{aligned}
\nu^{-1}\Pi_0\delta\mathcal{L}_1\mathcal{S}_0\delta\mathcal{L}_1(|\Psi_{k_1}\rangle\langle\Psi_{k_2}|) &= \\
&= |c_g c_e^*|^2 |c_{m_{k_1}+2}^{(k_1)}|^2 \sin_{m_{k_1}}^2(\phi) \langle m_{k_1} | (-iH_{\pm})^{-1} | m_{k_1} \rangle |\Psi_{k_1}\rangle\langle\Psi_{k_2}| \\
&\quad + |c_g c_e^*|^2 |c_{m_{k_1+1}}^{(k_1)}|^2 \sin_{m_{k_1+1}}^2(\phi) \langle m_{k_1+1}+2 | (-iH_{\pm})^{-1} | m_{k_1+1}+2 \rangle |\Psi_{k_1}\rangle\langle\Psi_{k_2}| \\
&\quad - (c_g c_e^*)^2 \left[c_{m_{k_1-1}}^{(k_1-2)} \right]^* c_{m_{k_1}+2}^{(k_1)} \sin_{m_{k_1-1}}(\phi) \sin_{m_{k_1}}(\phi) \langle m_{k_1-1}+2 | (-iH_{\pm})^{-1} | m_{k_1} \rangle |\Psi_{k_1-2}\rangle\langle\Psi_{k_2}| \\
&\quad - (c_e c_g^*)^2 \left[c_{m_{k_1+2}+2}^{(k_1+2)} \right]^* c_{m_{k_1+1}}^{(k_1)} \sin_{m_{k_1+2}}(\phi) \sin_{m_{k_1+1}}(\phi) \langle m_{k_1+2} | (-iH_{\pm})^{-1} | m_{k_1+1}+2 \rangle |\Psi_{k_1+2}\rangle\langle\Psi_{k_2}| \\
&\quad - |c_g c_e^*|^2 c_{m_{k_1}+2}^{(k_1)} [c_{m_{k_2}+2}^{(k_2)}]^* \sin_{m_{k_1}}(\phi) \sin_{m_{k_2}}(\phi) \eta_{k_1,k_2}^{-+} |\Psi_{k_1-1}\rangle\langle\Psi_{k_2-1}| \\
&\quad - |c_e c_g^*|^2 c_{m_{k_1+1}}^{(k_1)} [c_{m_{k_2+1}}^{(k_2)}]^* \sin_{m_{k_1+1}}(\phi) \sin_{m_{k_2+1}}(\phi) \eta_{k_1,k_2}^{++} |\Psi_{k_1+1}\rangle\langle\Psi_{k_2+1}| \\
&\quad + (c_g c_e^*)^2 c_{m_{k_1}+2}^{(k_1)} \left[c_{m_{k_2+1}}^{(k_2)} \right]^* \sin_{m_{k_1}}(\phi) \sin_{m_{k_2+1}}(\phi) \eta_{k_1,k_2}^{-+} |\Psi_{k_1-1}\rangle\langle\Psi_{k_2+1}| \\
&\quad + (c_e c_g^*)^2 c_{m_{k_1+1}}^{(k_1)} \left[c_{m_{k_2}+2}^{(k_2)} \right]^* \sin_{m_{k_1+1}}(\phi) \sin_{m_{k_2}}(\phi) \eta_{k_1,k_2}^{+-} |\Psi_{k_1+1}\rangle\langle\Psi_{k_2-1}| \\
&\quad + (\text{H.c.})^{k_1 \leftrightarrow k_2}.
\end{aligned} \tag{E24}$$

where we introduced $\eta_{k_1,k_2}^{++} = \pm c_e^{-1} \langle \Psi_{k_2+1} | \Pi_0 [M_e^{(0)} (-iH_{\pm})^{-1} | m_{k_1+1}+2 \rangle \langle m_{k_2+1}+2 |] | \Psi_{k_2+1} \rangle$, $\eta_{k_1,k_2}^{-+} = \mp c_g^{-1} \langle \Psi_{k_2-1} | \Pi_0 [(-iH_{\pm})^{-1} | m_{k_1} \rangle \langle m_{k_2} |] | \Psi_{k_2-1} \rangle$, $\eta_{k_1,k_2}^{-+} = \mp c_g^{-1} \langle \Psi_{k_1-1} | \Pi_0 [M_g^{(0)} (-iH_{\pm})^{-1} | m_{k_2} \rangle \langle m_{k_1+1}+2 |] | \Psi_{k_2+1} \rangle$ and $\eta_{k_1,k_2}^{+-} = \pm c_e^{-1} \langle \Psi_{k_1+1} | \Pi_0 [M_e^{(0)} (-iH_{\pm})^{-1} | m_{k_1+1}+2 \rangle \langle m_{k_2} |] | \Psi_{k_2-1} \rangle$, while $(\text{H.c.})^{k_1 \leftrightarrow k_2}$ denotes the Hermitian conjugate but with swapped indices k_1 and k_2 .

Finally, for the mixed state ρ_k

$$\begin{aligned}
\nu^{-1}\Pi_0\delta\mathcal{L}_1\mathcal{S}_0\delta\mathcal{L}_1(\rho_k) &= \mp |c_g|^2 c_e \sin_{m_k}^2(\phi) \langle m_k | \mathcal{S}_0 \left[|m_k\rangle\langle m_k+2 | \rho_k [M_e^{(0)}]^\dagger \right] | m_k+2 \rangle (\rho_k - \rho_{k-1}) \\
&\quad \pm |c_e|^2 c_g \sin_{m_{k+1}}^2(\phi) \langle m_{k+1}+2 | \mathcal{S}_0 \left[|m_{k+1}+2\rangle\langle m_{k+1} | \rho_k [M_g^{(0)}]^\dagger \right] | m_{k+1} \rangle (\rho_k - \rho_{k+1}) + \text{H.c.}
\end{aligned} \tag{E25}$$

Additional information from stationary state. Although in Eqs. (E23-E25) we do not give closed formulas for the terms corresponding to the resolvent (with H_{\pm} or \mathcal{S}_0) and the projection on the coherences, the knowledge of the stationary state in Eqs. (29) and (E3) can be used to further determine the second-order corrections to the dynamics

across soft walls. Namely, the condition $\mathcal{L}_{\text{eff}}\rho_{ss} = 0$, gives D conditions on the effective second-order dynamics \mathcal{L}_{eff} , where D is the dimension of the subspace, on which the dynamics takes place:

Example of two walls. We consider Case 3. from Tab. II where we have three pure stationary states between the walls $|\Psi_0\rangle$, $|\bar{\Psi}_0\rangle$, and $|\Psi_2\rangle$ with the coherences $|\Psi_0\rangle\langle\Psi_2|$ and $|\Psi_2\rangle\langle\Psi_0|$ also stationary ($D = 5$) (cf. Sec. IV B).

We have [cf. Eq. (E18)] $\Pi_0\delta\mathcal{L}_2(|\Psi_0\rangle\langle\Psi_0|, |\Psi_1\rangle\langle\Psi_1|, |\Psi_2\rangle\langle\Psi_2|) =$

$$\nu \begin{bmatrix} -|c_e|^2 \sin_{m_1}^2(\phi) |c_{m_1}^{(0)}|^2 & |c_g|^2 \sin_{m_1}^2(\phi) |c_{m_1+2}^{(1)}|^2 & 0 \\ |c_e|^2 \sin_{m_1}^2(\phi) |c_{m_1}^{(0)}|^2 & -|c_g|^2 \sin_{m_1}^2(\phi) |c_{m_1+2}^{(1)}|^2 - |c_e|^2 \sin_{m_2}^2(\phi) |c_{m_2}^{(1)}|^2 & |c_g|^2 \sin_{m_2}^2(\phi) |c_{m_2+2}^{(2)}|^2 \\ 0 & |c_e|^2 \sin_{m_2}^2(\phi) |c_{m_2}^{(1)}|^2 & -|c_g|^2 \sin_{m_2}^2(\phi) |c_{m_2+2}^{(2)}|^2 \end{bmatrix} \begin{pmatrix} |\Psi_0\rangle\langle\Psi_0| \\ |\Psi_1\rangle\langle\Psi_1| \\ |\Psi_2\rangle\langle\Psi_2| \end{pmatrix}, \quad (\text{E26})$$

and [cf. Eq. (E19)]

$$\Pi_0\delta\mathcal{L}_2(|\Psi_0\rangle\langle\Psi_2|) = -\frac{\nu}{2} \left[|c_e|^2 \sin_{m_1}^2(\phi) |c_{m_1}^{(0)}|^2 + |c_g|^2 \sin_{m_2}^2(\phi) |c_{m_2+2}^{(2)}|^2 \right] |\Psi_0\rangle\langle\Psi_2|. \quad (\text{E27})$$

On the other hand, [cf. Eq. (E23)]

$$\begin{aligned} \nu^{-1}\Pi_0\delta\mathcal{L}_1\mathcal{S}_0\delta\mathcal{L}_1(|\Psi_0\rangle\langle\Psi_0|) &= \\ &= 2|c_g c_e^*|^2 |c_{m_1}^{(0)}|^2 \sin_{m_1}^2(\phi) \langle m_1+2|(-iH_+)^{-1}|m_1+2\rangle (|\Psi_0\rangle\langle\Psi_0| - |\Psi_1\rangle\langle\Psi_1|) \\ &\quad - \left\{ (c_e c_g^*)^2 \left[c_{m_2+2}^{(2)} \right]^* c_{m_1}^{(0)} \sin_{m_2}(\phi) \sin_{m_1}(\phi) \langle m_2|(-iH_+)^{-1}|m_1+2\rangle |\Psi_2\rangle\langle\Psi_0| + \text{H.c.} \right\}, \end{aligned} \quad (\text{E28})$$

$$\begin{aligned} \nu^{-1}\Pi_0\delta\mathcal{L}_1\mathcal{S}_0\delta\mathcal{L}_1(|\Psi_1\rangle\langle\Psi_1|) &= \\ &= 2 \left[|c_g c_e^*|^2 |c_{m_1+2}^{(1)}|^2 \sin_{m_1}^2(\phi) \langle m_1|(-iH_-)^{-1}|m_1\rangle + |c_g c_e^*|^2 |c_{m_2}^{(1)}|^2 \sin_{m_2}^2(\phi) \langle m_2+2|(-iH_-)^{-1}|m_2+2\rangle \right] |\Psi_1\rangle\langle\Psi_1| \\ &\quad - 2|c_g c_e^*|^2 |c_{m_1+2}^{(1)}|^2 \sin_{m_1}^2(\phi) \langle m_1|(-iH_-)^{-1}|m_1\rangle |\Psi_0\rangle\langle\Psi_0| \\ &\quad - 2|c_e c_g^*|^2 |c_{m_2}^{(1)}|^2 \sin_{m_2}^2(\phi) \langle m_2+2|(-iH_-)^{-1}|m_2+2\rangle |\Psi_2\rangle\langle\Psi_2| \\ &\quad + 2(c_e c_g^*)^2 c_{m_1+2}^{(1)} \left[c_{m_2}^{(1)} \right]^* \sin_{m_1}(\phi) \sin_{m_2}(\phi) \eta_1^{-+} |\Psi_0\rangle\langle\Psi_2| \\ &\quad + 2(c_e c_g^*)^2 c_{m_2}^{(1)} \left[c_{m_1+2}^{(1)} \right]^* \sin_{m_2}(\phi) \sin_{m_1}(\phi) \eta_1^{+-} |\Psi_2\rangle\langle\Psi_0|, \end{aligned} \quad (\text{E29})$$

and

$$\begin{aligned} \nu^{-1}\Pi_0\delta\mathcal{L}_1\mathcal{S}_0\delta\mathcal{L}_1(|\Psi_2\rangle\langle\Psi_2|) &= \\ &= 2|c_g c_e^*|^2 |c_{m_2+2}^{(2)}|^2 \sin_{m_2}^2(\phi) \langle m_2|(-iH_+)^{-1}|m_2\rangle (|\Psi_2\rangle\langle\Psi_2| - |\Psi_1\rangle\langle\Psi_1|) \\ &\quad - \left\{ (c_g c_e^*)^2 \left[c_{m_1}^{(0)} \right]^* c_{m_2+2}^{(2)} \sin_{m_1}(\phi) \sin_{m_2}(\phi) \langle m_1+2|(-iH_+)^{-1}|m_2\rangle |\Psi_0\rangle\langle\Psi_2| + \text{H.c.} \right\}, \end{aligned} \quad (\text{E30})$$

while

$$\begin{aligned} \nu^{-1}\Pi_0\delta\mathcal{L}_1\mathcal{S}_0\delta\mathcal{L}_1(|\Psi_0\rangle\langle\Psi_2|) &= \\ &= |c_g c_e^*|^2 \left[|c_{m_2+2}^{(2)}|^2 \sin_{m_2}^2(\phi) \langle m_2|(-iH_+)^{-1}|m_2\rangle + |c_{m_1}^{(0)}|^2 \sin_{m_1}^2(\phi) \langle m_1+2|(-iH_+)^{-1}|m_1+2\rangle \right] |\Psi_0\rangle\langle\Psi_2| \\ &\quad - (c_e c_g^*)^2 c_{m_1}^{(0)} \left[c_{m_2+2}^{(2)} \right]^* \sin_{m_1}(\phi) \sin_{m_2}(\phi) \langle m_2|(-iH_+)^{-1}|m_1+2\rangle (|\Psi_0\rangle\langle\Psi_0| + |\Psi_2\rangle\langle\Psi_2|) \\ &\quad + 2(c_e c_g^*)^2 c_{m_1}^{(0)} \left[c_{m_2+2}^{(2)} \right]^* \sin_{m_1}(\phi) \sin_{m_2}(\phi) \langle m_2|(-iH_+)^{-1}|m_1+2\rangle |\Psi_1\rangle\langle\Psi_1|, \end{aligned} \quad (\text{E31})$$

cf. Eq. (E24). In the above expression we used the fact that $-iH_{\pm}$ is Hermitian [cf. Eq. (E21)].

The stationary state is [cf. Tab. II]

$$\rho_{ss} = |\beta_0|^2 |\Psi_0\rangle\langle\Psi_0| + |\beta_2|^2 |\Psi_2\rangle\langle\Psi_2| + \beta_0\beta_2^* |\Psi_0\rangle\langle\Psi_2| + \beta_2\beta_0^* |\Psi_2\rangle\langle\Psi_0|, \quad (\text{E32})$$

where $|\beta_0|^2 + |\beta_2|^2 = 1$. Therefore, from Eq. (E17), we have $\Pi_0\delta\mathcal{L}_2(\rho_{ss}) = \Pi_0\delta\mathcal{L}_1\mathcal{S}_0\delta\mathcal{L}_1(\rho_{ss})$, which can be written as

$$Y \begin{bmatrix} \sin_{m_1}^2(\phi) \langle m_1+2|(-iH_+)^{-1}|m_1+2\rangle \\ \sin_{m_2}^2(\phi) \langle m_2|(-iH_+)^{-1}|m_2\rangle \\ \sin_{m_1}(\phi) \sin_{m_2}(\phi) \langle m_2|(-iH_+)^{-1}|m_1+2\rangle \\ \sin_{m_1}(\phi) \sin_{m_2}(\phi) \langle m_1+2|(-iH_+)^{-1}|m_2\rangle \end{bmatrix} = \begin{bmatrix} -|c_e|^2 \sin_{m_1}^2(\phi) |c_{m_1}^{(0)}|^2 |\beta_0|^2 \\ - \left[|c_e|^2 \sin_{m_1}^2(\phi) |c_{m_1}^{(0)}|^2 + |c_g|^2 \sin_{m_2}^2(\phi) |c_{m_2+2}^{(2)}|^2 \right] \beta_0\beta_2^*/2 \\ |c_e|^2 \sin_{m_1}^2(\phi) |c_{m_1}^{(0)}|^2 |\beta_0|^2 + |c_g|^2 \sin_{m_2}^2(\phi) |c_{m_2+2}^{(2)}|^2 |\beta_2|^2 \\ - \left[|c_e|^2 \sin_{m_1}^2(\phi) |c_{m_1}^{(0)}|^2 + |c_g|^2 \sin_{m_2}^2(\phi) |c_{m_2+2}^{(2)}|^2 \right] \beta_2\beta_0^*/2 \\ -|c_g|^2 \sin_{m_2}^2(\phi) |c_{m_2+2}^{(2)}|^2 |\beta_2|^2 \end{bmatrix}, \quad (\text{E33})$$

where

$$Y = \begin{bmatrix} 2|c_g c_e^*|^2 |c_{m_1+2}^{(1)}|^2 |\beta_0|^2 & 0 & -(c_e c_g^*)^2 c_{m_1}^{(0)} [c_{m_2+2}^{(2)}]^* \beta_0 \beta_2^* & -(c_e^* c_g)^2 [c_{m_1}^{(0)}]^* c_{m_2+2}^{(2)} \beta_2 \beta_0^* \\ |c_g c_e^*|^2 |c_{m_1}^{(0)}|^2 \beta_0 \beta_2^* & |c_g c_e^*|^2 |c_{m_2+2}^{(2)}|^2 \beta_0 \beta_2^* & 0 & -(c_e^* c_g)^2 [c_{m_1}^{(0)}]^* c_{m_2+2}^{(2)} \\ -2|c_g c_e^*|^2 |c_{m_1+2}^{(1)}|^2 |\beta_0|^2 & -2|c_g c_e^*|^2 |c_{m_2+2}^{(2)}|^2 |\beta_2|^2 & 2(c_e c_g^*)^2 c_{m_1}^{(0)} [c_{m_2+2}^{(2)}]^* \beta_0 \beta_2^* & 2(c_e^* c_g)^2 [c_{m_1}^{(0)}]^* c_{m_2+2}^{(2)} \beta_2 \beta_0^* \\ |c_g c_e^*|^2 |c_{m_1}^{(0)}|^2 \beta_2 \beta_0^* & |c_g c_e^*|^2 |c_{m_2+2}^{(2)}|^2 \beta_2 \beta_0^* & -(c_e c_g^*)^2 c_{m_1}^{(0)} [c_{m_2+2}^{(2)}]^* & 0 \\ 0 & 2|c_g c_e^*|^2 |c_{m_2+2}^{(2)}|^2 |\beta_2|^2 & -(c_e c_g^*)^2 c_{m_1}^{(0)} [c_{m_2+2}^{(2)}]^* \beta_0 \beta_2^* & -(c_e^* c_g)^2 [c_{m_1}^{(0)}]^* c_{m_2+2}^{(2)} \beta_2 \beta_0^* \end{bmatrix}, \quad (\text{E34})$$

so that we can find analytically the columns of the dynamics generator that correspond to the support of the stationary state (E32) [cf. Eqs. (E28), (E30) and (E31)].

APPENDIX F: REVIEW OF METASTABILITY THEORY

Here we summarise the properties of Markovian dynamics of open quantum systems which lead to metastability [50, 87].

Markovian dynamics. We consider an open quantum system dynamics described by a Markovian master equation [59, 60],

$$\frac{d}{dt}\rho(t) = \mathcal{L}[\rho(t)] = -i[H, \rho(t)] + \frac{1}{2} \sum_j \left[2 J_j \rho(t) J_j^\dagger - J_j^\dagger J_j \rho(t) - \rho(t) J_j^\dagger J_j \right], \quad (\text{F1})$$

where H is the system Hamiltonian, while J_j denote so called jump operators which describe the interaction of the system with the environment. In the case of the dynamics of micromaser, Eq. (11), the system is the cavity which interacts with the environment constituted by passing atoms. The Hamiltonian $H = 0$ (dynamics is considered in the rotating frame with the Hamiltonian as explained in Sec. II B), while the jump operators are given by the Kraus operators, Eq. (48).

Timescales of the dynamics in (F1) are given by the spectrum of the master operator \mathcal{L} . Although in general \mathcal{L} is not Hermitian, and thus not necessarily diagonalisable, in all studied cases it could be diagonalised. We label the corresponding eigenvalues as $\{\lambda_k\}_{k \geq 1}$, ordered in the decreasing order of their real part, $\text{Re } \lambda_1 \geq \text{Re } \lambda_2 \geq \dots$, and the corresponding left- and right-eigenmodes L_k and R_k , $\mathcal{L} R_k = \lambda_k R_k$, $L_k \mathcal{L} = \lambda_k L_k$ [normalised as $\text{Tr}(L_j R_k) = \delta_{jk}$]. For an initial state ρ_{in} we have that the system state at time t is given by

$$\rho(t) = e^{t\mathcal{L}}(\rho_{\text{in}}) = \rho_{\text{ss}} + \sum_{k \geq 2} e^{t\lambda_k} \text{Tr}(L_k \rho_{\text{in}}) R_k \quad (\text{F2})$$

where we used the fact that $\lambda_1 = 0$, which corresponds to a stationary state $R_1 = \rho_{\text{ss}}$, and $L_1 = \mathbb{1}$ due to trace-preservation. When the stationary state is unique, $\rho(t)$ relaxes to ρ_{ss} at the timescale given by the inverse of the gap to the second eigenvalue, $\tau = (-\text{Re } \lambda_2)^{-1}$.

Metastability. When there exists a separation between real parts of the eigenvalues, $-\text{Re } \lambda_m \ll -\text{Re } \lambda_{m+1}$, there exists a time regime $(-\text{Re } \lambda_{m+1})^{-1} \ll t \ll (-\text{Re } \lambda_m)^{-1}$, where after the initial fast relaxation of modes $k > m$, the system state appears steady, i.e., is *metastable*, and can be approximated as [cf. Eq. (F2)]

$$\rho(t) \approx \rho_{\text{ss}} + \sum_{k=2}^m \text{Tr}(L_k \rho_{\text{in}}) R_k \equiv \Pi(\rho_{\text{in}}), \quad (\text{F3})$$

where we denoted by Π the projection on the low-lying eigenmodes of the dynamics. The manifold of metastable states is described by the coefficients $\{\text{Tr}(L_k \rho_{\text{in}})\}_{k=2}^m$ that depend on the initial state ρ_{in} , and thus this manifold is $(m-1)$ -dimensional. Beyond the metastable regime, $t \gtrsim (-\text{Re } \lambda_m)^{-1}$, the decay of low-lying eigenmodes can no longer be neglected, and the system undergoes final relaxation inside the metastable manifold [cf. Eq. (F2)]

$$\rho(t) \approx \rho_{\text{ss}} + \sum_{k=2}^m e^{t\lambda_k} \text{Tr}(L_k \rho_{\text{in}}) R_k = e^{t\mathcal{L}_{\text{eff}}} \Pi(\rho_{\text{in}}) \quad (\text{F4})$$

which is governed by the low-lying modes as

$$\mathcal{L}_{\text{eff}} = \Pi \mathcal{L} \Pi. \quad (\text{F5})$$

We note that several metastable regimes can exist if there are multiple separations in the spectrum of \mathcal{L} , which leads to hierarchy of the corresponding metastable manifolds. In the next Appendix G, we consider the case in which metastability is a consequence of perturbing dynamics which features multiple stationary states.

APPENDIX G: DERIVATIONS OF METASTABLE DYNAMICS

Here we consider metastability and effective long-time dynamics in the case of perturbing the dynamics which features multiple stationary states. We derive the effective dynamics due to parity-conserving and parity-swapping perturbations, which leads to Eqs. (51) and (60). We also discuss the corresponding dynamics in the presence of hard walls.

Metastability due to perturbations of multiple stationary states. One class of open quantum dynamics where metastability arises, is the case when the dynamics \mathcal{L}_0 , which features multiple stationary states, is perturbed by $\delta\mathcal{L}$, i.e., $\mathcal{L} = \mathcal{L}_0 + \delta\mathcal{L}$. By means of non-Hermitian perturbation theory, it can be shown [88], that the slow (low-lying) eigenmodes which contribute to the metastable states, Eq. (F3), correspond to the stationary states of \mathcal{L}_0 ,

$$\Pi = \Pi_0 + \dots \quad (\text{G1})$$

where Π_0 is the projection on the stationary states of \mathcal{L}_0 . Furthermore, the effective long-time dynamics, Eq. (F5), is well-approximated by

$$\Pi \mathcal{L} \Pi = \Pi_0 \delta\mathcal{L} \Pi_0 + \dots, \quad (\text{G2})$$

which corresponds to completely positive and trace-preserving dynamics of the metastable states [50, 90, 91, 119].

1. Metastable dynamics with weak parity symmetry

Here we derive Eqs. (51) and (60).

Projection on stationary subspace. In this work we consider dynamics of the cavity, \mathcal{L}_0 in (18), which conserves the parity $P = (-1)^{a^\dagger a}$, Eq. (20), and features a stationary DFS spanned by states $|\Psi_+\rangle$ and $|\Psi_-\rangle$ of the opposite parity. In this case the projection on the stationary subspace also conserves the parity, and is given by

$$\Pi_0(\rho) = |\Psi_+\rangle\langle\Psi_+|\text{Tr}(\mathbb{1}_+\rho) + |\Psi_-\rangle\langle\Psi_-|\text{Tr}(\mathbb{1}_-\rho) + |\Psi_+\rangle\langle\Psi_-|\text{Tr}(L_{+-}\rho) + |\Psi_-\rangle\langle\Psi_+|\text{Tr}(L_{-+}\rho). \quad (\text{G3})$$

where $\mathbb{1}_-$ and $\mathbb{1}_+$ are identity operators on the odd and even subspace, while $L_{+-} = L_{-+}^\dagger$ is a conserved quantity supported in odd-even coherences, see Sec. IV B. For discussion of metastability in the case with hard wall in the dynamics (see Appendix G 4).

Effective dynamics with weak parity symmetry. We consider a perturbation by the purely dissipative dynamics with jumps J [cf. Eq. (F1)]

$$\delta\mathcal{L}(\rho) = J\rho J^\dagger - \frac{1}{2}J^\dagger J\rho - \frac{1}{2}\rho J^\dagger J. \quad (\text{G4})$$

We furthermore assume that the action of a jump J flips/swaps the cavity parity $P = (-1)^{a^\dagger a}$,

$$JP + PJ = 0, \quad (\text{G5})$$

as it is the case for a single-photon loss $J = \sqrt{\kappa_{1\text{ph}}}a$ in Eq. (57). Therefore, $\mathcal{L} = \mathcal{L}_0 + \delta\mathcal{L}$ features the weak-parity symmetry [cf. Eqs. (50) and (59)].

Effective dynamics. Below we prove that the first-order dynamics due to (G4) is given by (in the basis $\{|\Psi_+\rangle\langle\Psi_+|, |\Psi_-\rangle\langle\Psi_-|, |\Psi_+\rangle\langle\Psi_-|, |\Psi_-\rangle\langle\Psi_+|\}$)

$$\frac{d}{dt}\rho(t) = \begin{bmatrix} -\langle J^\dagger J \rangle_+ & \langle J^\dagger J \rangle_- & 0 & 0 \\ \langle J^\dagger J \rangle_+ & -\langle J^\dagger J \rangle_- & 0 & 0 \\ 0 & 0 & -\frac{1}{2}(\langle J^\dagger J \rangle_+ + \langle J^\dagger J \rangle_-) & \eta(\langle J^\dagger J \rangle_+ \langle J^\dagger J \rangle_-)^{1/2} \\ 0 & 0 & \eta^*(\langle J^\dagger J \rangle_+ \langle J^\dagger J \rangle_-)^{1/2} & -\frac{1}{2}(\langle J^\dagger J \rangle_+ + \langle J^\dagger J \rangle_-) \end{bmatrix} \rho(t), \quad (\text{G6})$$

where

$$\eta = \frac{\text{Tr}(L_{+-}J|\Psi_{-}\rangle\langle\Psi_{+}|J^{\dagger})}{(\langle J^{\dagger}J\rangle_{+}\langle J^{\dagger}J\rangle_{-})^{1/2}} \quad \text{and} \quad |\eta| \leq 1. \quad (\text{G7})$$

This gives Eq. (60) and the dissipative contribution in Eq. (51). Although L_{+-} is not known in general (i.e., beyond the weak-coupling limit [39]), η can be determined *numerically* for a given coupling strength ϕ as [cf. Eq. (G3)]

$$\text{Tr}(L_{+-}J|\Psi_{-}\rangle\langle\Psi_{+}|J^{\dagger}) = \langle\Psi_{+}|[\Pi_0(J|\Psi_{-}\rangle\langle\Psi_{+}|J^{\dagger})]|\Psi_{-}\rangle = \langle\Psi_{+}|\left(\lim_{t\rightarrow\infty} e^{t\mathcal{L}_0}J|\Psi_{-}\rangle\langle\Psi_{+}|J^{\dagger}\right)|\Psi_{-}\rangle. \quad (\text{G8})$$

Effective master equation. Eq. (G6) corresponds to *biased bit flip noise* in the DFS,

$$\frac{d}{dt}\rho(t) = \sum_{j=1,2} \gamma_j \left[s_j \rho(t) s_j^{\dagger} - \frac{1}{2} \left(s_j^{\dagger} s_j \rho(t) + \rho(t) s_j^{\dagger} s_j \right) \right], \quad (\text{G9})$$

$$s_{1,2} = \frac{e^{i\varphi}(\epsilon + 2\gamma \pm \sqrt{\epsilon^2 + 4|\gamma|^2})|\Psi_{+}\rangle\langle\Psi_{-}| + e^{-i\varphi}(-\epsilon + 2\gamma \pm \sqrt{\epsilon^2 + 4|\gamma|^2})|\Psi_{-}\rangle\langle\Psi_{+}|}{N_{1,2}}. \quad (\text{G10})$$

Here $\gamma_{1,2} = (2\kappa \pm \sqrt{\epsilon^2 + 4|\gamma|^2})/4$ are the individual spin-flip rates, $N_{1,2}^2 = \epsilon^2 + [2\gamma \pm \sqrt{\epsilon^2 + 4|\gamma|^2}]^2$ are the normalization factors, and we have introduced: $\epsilon = \langle J^{\dagger}J\rangle_{+} - \langle J^{\dagger}J\rangle_{-}$, $\gamma = \eta(\langle J^{\dagger}J\rangle_{+}\langle J^{\dagger}J\rangle_{-})^{1/2}$, and the phase $e^{2i\varphi}|\eta| = \eta$. Note that the total dissipation rate $\kappa = (\langle J^{\dagger}J\rangle_{+} + \langle J^{\dagger}J\rangle_{-})/2$. When $|\eta| = 1$, there is only a single jump, s_1 . This corresponds to the case when the jump J leaves the cavity state within the DFS [cf. Eq. (G13)]. This takes place for single-photon losses and the cavity dynamics in the weak-coupling limit (see Sec. VB and Refs. [52–54]).

Steady state. The effective dynamics in Eq. (G6) features a *unique stationary state*,

$$\rho_{\text{ss}} = \frac{\langle J^{\dagger}J\rangle_{-}|\Psi_{+}\rangle\langle\Psi_{+}| + \langle J^{\dagger}J\rangle_{+}|\Psi_{-}\rangle\langle\Psi_{-}|}{\langle J^{\dagger}J\rangle_{+} + \langle J^{\dagger}J\rangle_{-}}, \quad (\text{G11})$$

which approximates, in the zero order of the perturbation by J , the stationary state of the dynamics $\mathcal{L} = \mathcal{L}_0 + \delta\mathcal{L}$.

Derivation of Eq. (G6). As Π_0 conserves the parity, the first-order corrections (G2) must also feature the weak-parity symmetry. Indeed, in the basis $\{|\Psi_{+}\rangle\langle\Psi_{+}|, |\Psi_{-}\rangle\langle\Psi_{-}|, |\Psi_{+}\rangle\langle\Psi_{-}|, |\Psi_{-}\rangle\langle\Psi_{+}|\}$, the effective dynamics is *block-diagonal*, $\frac{d}{dt}\rho(t) =$

$$\begin{bmatrix} -\langle J^{\dagger}J\rangle_{+} & \text{Tr}(\mathbb{1}_{+}J|\Psi_{-}\rangle\langle\Psi_{-}|J^{\dagger}) & 0 & 0 \\ \text{Tr}(\mathbb{1}_{-}J|\Psi_{+}\rangle\langle\Psi_{+}|J^{\dagger}) & -\langle J^{\dagger}J\rangle_{-} & 0 & 0 \\ 0 & 0 & -\frac{1}{2}\text{Tr}[L_{+-}(J^{\dagger}J|\Psi_{+}\rangle\langle\Psi_{-}| - |\Psi_{+}\rangle\langle\Psi_{-}|J^{\dagger}J)] & \text{Tr}(L_{+-}J|\Psi_{+}\rangle\langle\Psi_{-}|J^{\dagger}) \\ 0 & 0 & \text{Tr}(L_{-+}J|\Psi_{-}\rangle\langle\Psi_{+}|J^{\dagger}) & -\frac{1}{2}\text{Tr}[L_{-+}(J^{\dagger}J|\Psi_{-}\rangle\langle\Psi_{+}| - |\Psi_{-}\rangle\langle\Psi_{+}|J^{\dagger}J)] \end{bmatrix} \rho(t).$$

The diagonal terms stem from the parity-conserving terms in (G4), i.e., $(J^{\dagger}J\rho + \rho J^{\dagger}J)/2$, while the off-diagonal terms originate from the parity swap $J\rho J^{\dagger}$. Here, we denoted the averages as $\langle J^{\dagger}J\rangle_{\pm} \equiv \text{Tr}(\mathbb{1}_{\pm}J^{\dagger}J|\Psi_{\pm}\rangle\langle\Psi_{\pm}|) = \langle\Psi_{\pm}|J^{\dagger}J|\Psi_{\pm}\rangle$.

We can further simplify the effective dynamics. First, from the trace-preservation of Eq. F5, we have that $\text{Tr}(\mathbb{1}_{\mp}J|\Psi_{\pm}\rangle\langle\Psi_{\pm}|J^{\dagger}) = \langle J^{\dagger}J\rangle_{\pm}$. Second, we note that $|\Psi_{+}\rangle$ and $|\Psi_{-}\rangle$ are the dark states of the dynamics (31) and (32), i.e., $\widetilde{M}_g|\Psi_{\pm}\rangle = \widetilde{M}_e|\Psi_{\pm}\rangle = 0$. Therefore, as the dynamics of coherences to a dark state is governed by the effective Hamiltonian of (32), $\frac{i}{2}(\widetilde{M}_g^{\dagger}\widetilde{M}_g + \widetilde{M}_e^{\dagger}\widetilde{M}_e)$, the projection Π_0 reduces to the orthogonal projection onto the dark states $|\Psi_{+}\rangle, |\Psi_{-}\rangle$ [118]

$$\Pi_0(J^{\dagger}J|\Psi_{+}\rangle\langle\Psi_{-}|) = \lim_{t\rightarrow\infty} e^{t\mathcal{L}_0}(J^{\dagger}J|\Psi_{+}\rangle\langle\Psi_{-}|) = \lim_{t\rightarrow\infty} [e^{-\frac{1}{2}(\widetilde{M}_g^{\dagger}\widetilde{M}_g + \widetilde{M}_e^{\dagger}\widetilde{M}_e)t}J^{\dagger}J|\Psi_{+}\rangle]\langle\Psi_{-}| = \langle J^{\dagger}J\rangle_{+}|\Psi_{+}\rangle\langle\Psi_{-}|. \quad (\text{G12})$$

Finally, as the effective dynamics is completely-positive [50, 90, 91, 119], we have that

$$\text{Tr}(L_{+-}J|\Psi_{-}\rangle\langle\Psi_{+}|J^{\dagger}) = \eta(\langle J^{\dagger}J\rangle_{+}\langle J^{\dagger}J\rangle_{-})^{1/2} \quad \text{where} \quad |\eta| \leq 1. \quad (\text{G13})$$

Moreover, when $\mathcal{L}_0 + \delta\mathcal{L}$ corresponds to the real dynamics (see Sec. IIIB), η is also real.

2. Metastable dynamics with parity conservation

Effective dynamics with parity conservation. We now consider a perturbation $\delta\mathcal{L}$ of the cavity dynamics \mathcal{L}_0 and assume that $\delta\mathcal{L}$ conserves the photon-number parity (see Sec. IIIB). As we derive below the effective first-order dynamics in

the DFS basis $|\Psi_+\rangle\langle\Psi_+|$, $|\Psi_-\rangle\langle\Psi_-|$, $|\Psi_+\rangle\langle\Psi_-|$, $|\Psi_-\rangle\langle\Psi_+|$ is *diagonal*,

$$\frac{d}{dt}\rho(t) = \begin{bmatrix} 0 & 0 & 0 & 0 \\ 0 & 0 & 0 & 0 \\ 0 & 0 & -i\Omega - \frac{\gamma_{\text{deph}}}{2} & 0 \\ 0 & 0 & 0 & i\Omega - \frac{\gamma_{\text{deph}}}{2} \end{bmatrix} \rho(t), \quad (\text{G14})$$

where $-i\Omega - \frac{\gamma_{\text{deph}}}{2} = \text{Tr}(L_{+-}\delta\mathcal{L}|\Psi_+\rangle\langle\Psi_-|)$, which corresponds to effective *dephasing* at the rate γ_{deph} and *unitary rotation* at frequency Ω , along the direction of the DFS parity,

$$\frac{d}{dt}\rho(t) = -i\Omega[s_z, \rho(t)] + \gamma_{\text{deph}}\left[s_z \rho(t) s_z^\dagger - \frac{1}{2}(s_z^\dagger s_z \rho(t) + \rho(t) s_z^\dagger s_z)\right], \quad (\text{G15})$$

$$s_z = (|\Psi_+\rangle\langle\Psi_+| - |\Psi_-\rangle\langle\Psi_-|)/2. \quad (\text{G16})$$

Steady states. Any dynamics conserving the parity features at least two stationary states [77], corresponding to the conserved quantities $\mathbb{1}_+$ and $\mathbb{1}_-$ (cf. Sec. III B). Indeed, in (G14) the even-odd coherences dephase to 0 whenever $\gamma_{\text{deph}} > 0$ (cf. Fig. 6) and asymptotic states are mixtures of the odd and even stationary states

$$\rho_{\text{ss}} = p|\Psi_+\rangle\langle\Psi_+| + (1-p)|\Psi_-\rangle\langle\Psi_-|, \quad (\text{G17})$$

where p is determined by the initial support in the even parity subspace. ρ_{ss} approximates (in the zero order of $\delta\mathcal{L}$) the asymptotic state of $\mathcal{L} = \mathcal{L}_0 + \delta\mathcal{L}$.

Derivation of Eq. (G14). As the projection on the stationary subspace Π_0 also conserves the parity, Eq. (G3), so does the first-order effective dynamics, Eq. (G2). Therefore, in the basis $|\Psi_+\rangle\langle\Psi_+|$, $|\Psi_-\rangle\langle\Psi_-|$, $|\Psi_+\rangle\langle\Psi_-|$, $|\Psi_-\rangle\langle\Psi_+|$, the effective dynamics must be diagonal. The first two terms on the diagonal are 0 from the trace-preservation of the effective dynamics [50, 90, 91, 119]. Furthermore, from $\mathcal{L}_0 + \mathcal{L}\delta$ being Hermiticity-preserving we have $[\text{Tr}(L_{+-}\delta\mathcal{L}|\Psi_-\rangle\langle\Psi_+|)]^* = \text{Tr}(L_{+-}\delta\mathcal{L}|\Psi_+\rangle\langle\Psi_-|)$ which is in general complex so that we set $\text{Tr}(L_{+-}\delta\mathcal{L}|\Psi_+\rangle\langle\Psi_-|) \equiv -i\Omega - \frac{\gamma_{\text{deph}}}{2}$.

a. Parity conserving higher-order corrections in far-detuned regime

Here we derive the Hamiltonian contribution to Eq. (51). We also prove that relaxing the conditions in Eq. (13) leads to corrections which are of higher order than the (second order) effective dynamics in Eq. (51).

Unitary first-order dynamics of dark states. We now consider the case of $\delta\mathcal{L}$ corresponding to the perturbation of the Hamiltonian H by δH and a jump J by δJ in the master equation (F1),

$$\begin{aligned} \mathcal{L}(\rho) &= (\mathcal{L}_0 + \delta\mathcal{L})(\rho) = -i[H + \delta H, \rho] + (J + \delta J)\rho(J + \delta J)^\dagger - \frac{1}{2}\{(J + \delta J)^\dagger(J + \delta J), \rho\} \\ &= -i[H, \rho] + J\rho J^\dagger - \frac{1}{2}\{J^\dagger J, \rho\} \\ &\quad -i[\delta H, \rho] + \delta J\rho J^\dagger + J\rho\delta J^\dagger - \frac{1}{2}\{\delta J^\dagger J + J^\dagger\delta J, \rho\} + \delta J\rho\delta J^\dagger - \frac{1}{2}\{\delta J^\dagger\delta J, \rho\}, \end{aligned} \quad (\text{G18})$$

where $\{X, Y\} = XY + YX$ denotes the anti-commutator, which corresponds to the first $\delta\mathcal{L}_1$ and second order corrections $\delta\mathcal{L}_2$ in δH and δJ . In the case when stationary states of \mathcal{L}_0 are pure, $|\Psi_+\rangle$ and $|\Psi_-\rangle$, and dark with respect to the jump operator J , i.e., $J|\Psi_\pm\rangle = 0$, so that they form a DFS, the first-order corrections to the dynamics in the DFS are unitary [89, 90] and only due to the Hamiltonian δH ,

$$\begin{aligned} \Pi_0 \delta\mathcal{L}_1(|\Psi_+\rangle\langle\Psi_-|) &= \Pi_0 \left(-i[\delta H, |\Psi_+\rangle\langle\Psi_-|] + \delta J|\Psi_+\rangle\langle\Psi_-|J^\dagger + J|\Psi_+\rangle\langle\Psi_-|\delta J^\dagger - \frac{1}{2}\{\delta J^\dagger J + J^\dagger\delta J, |\Psi_+\rangle\langle\Psi_-|\} \right) \\ &= \Pi_0 \left(-i[\delta H, |\Psi_+\rangle\langle\Psi_-|] - \frac{1}{2}J^\dagger\delta J|\Psi_+\rangle\langle\Psi_-| - \frac{1}{2}|\Psi_+\rangle\langle\Psi_-|\delta J^\dagger J \right) \\ &= -i(\langle\delta H\rangle_+ - \langle\delta H\rangle_-)|\Psi_+\rangle\langle\Psi_-| - i\langle\delta H\rangle_{-+}(|\Psi_-\rangle\langle\Psi_-| - |\Psi_+\rangle\langle\Psi_+|), \end{aligned} \quad (\text{G19})$$

where $\langle\delta H\rangle_{-+} = \langle\Psi_-|\delta H|\Psi_+\rangle$, and in the last line we used the fact that coherences to dark states are orthogonally projected on the dark states [cf. Eq. (G12) and see [118]]. When both \mathcal{L}_0 and \mathcal{L} conserve the parity, the parity is necessarily conserved by H , J and δH , δJ [77], and thus the first order correction is given by [cf. Eq. (G14)]

$$\Pi_0 \delta\mathcal{L}_1(|\Psi_+\rangle\langle\Psi_-|) = -i(\langle\delta H\rangle_+ - \langle\delta H\rangle_-)|\Psi_+\rangle\langle\Psi_-| = -i\Omega|\Psi_+\rangle\langle\Psi_-|. \quad (\text{G20})$$

Higher-order corrections in far-detuned regime. The result in Eq. (G20) is directly used in Eq. (53), which corresponds to the higher-order corrections in the parity conserving Kraus operators due to finite-detuning, Eqs. (B22) and (B23). The parity conserving operators can be shifted so that $|\Psi_+\rangle$ and $|\Psi_-\rangle$ are the dark states of the adiabatic dynamics [see Eq. (31) and (32)]. In this case, we can identify $H = 0$ and

$$\delta H = \frac{i}{2} \left(c_g^* e^{i\tau \frac{|g_2|^2}{\Delta}} M_1 - c_g e^{-i\tau \frac{|g_2|^2}{\Delta}} M_1^\dagger - c_e^* e^{i\tau \frac{|g_2|^2}{\Delta}} M_3 + c_e e^{-i\tau \frac{|g_2|^2}{\Delta}} M_e^\dagger \right), \quad (\text{G21})$$

while the changes in the shifted Kraus operators

$$\widetilde{M}_1 = M_1 - c_g e^{-i\tau \frac{|g_2|^2}{\Delta}} \mathbb{1}, \quad (\text{G22a})$$

$$\widetilde{M}_3 = M_3 + c_e e^{-i\tau \frac{|g_2|^2}{\Delta}} \mathbb{1}, \quad (\text{G22b})$$

that play the role of jump operators, do not contribute. Note that here we use definition of the Kraus operators M_1 and M_3 from Eqs. (B22) and (B23), which differ from the Kraus operators defined in the main text, Eq. (16), by the global phase $e^{i\tau \frac{|g_2|^2}{\Delta}}$ due to constant terms neglected in (14).

Corrections to (5+1)-model. Analogously, as the fourth-order corrections to the atom-cavity interactions, Eq. (B24), contribute to δH via M_1 and M_3 , Eqs. (B22) and (B23), relaxing the conditions in Eq. (13), which cancel the Stark shifts from the atom-cavity interactions, Eq. (14), also leads to the higher-order Hamiltonian corrections [cf. Eq. (12)]. Therefore, in the lowest order, the perturbation away from Eq. (13), contributes to the unitary dynamics, Eq. (G21), while in the higher order leads to dephasing of coherences, Eq. (G14), due to parity-conservation. Furthermore, the corrections in Eq. (54), which stem from other Kraus operators, Eqs. (B18) and (B21), are expressed for any choice of detunings and coupling strength, and thus also apply to the case without Eq. (13).

b. Mixed atom states

In the main text we discussed the properties of two-photon micromaser dynamics under the assumption that all atoms entering the cavity are prepared in an identical pure state, Eq. (8). Here we investigate, how the imperfections of the atom preparation influence the resulting cavity dynamics.

Micromaser dynamics with mixed atom state. The most general state of the atom invariant to the Hamiltonian (4a) (as required by the Assumption 3. in Sec. IIB) is

$$\rho_{\text{at}} = p_a |\psi_a\rangle\langle\psi_a| + p_b |\psi_b\rangle\langle\psi_b| + \sum_{j=0,2,4,a} p_j |j\rangle\langle j|, \quad (\text{G23})$$

where $p_a + p_b + \sum_{j=0,2,4,a} p_j = 1$ and coherent superpositions

$$|\psi_a\rangle = c_g |1\rangle + c_e |3\rangle, \quad |\psi_b\rangle = c_e^* |1\rangle - c_g^* |3\rangle \quad (\text{G24})$$

are allowed due to the two-photon resonance in Eq. (7) [cf. Eq. (8)]. Note that the states $|\psi_a\rangle$ and $|\psi_b\rangle$ are orthonormal.

The cavity dynamics due to a passage of a single atom in the mixed state (G23) is given by [cf. Eq. (10)]

$$\rho^{(k)} = \sum_{\substack{j=g,e \\ l=a,b}} p_l M_{jl} \rho^{(k-1)} M_{jl}^\dagger + \sum_{j=0,2,4,a} p_j M_j \rho^{(k-1)} M_j^\dagger \equiv \mathcal{M} \left[\rho^{(k-1)} \right], \quad (\text{G25})$$

where for the initial states $|\psi_a\rangle$ and $|\psi_b\rangle$ we have two pairs of Kraus operators [cf. Eqs. (9) and (16)],

$$M_{ga} = \langle 1 | U_{\text{eff}}(\tau) | \psi_a \rangle, \quad M_{ea} = \langle 3 | U_{\text{eff}}(\tau) | \psi_a \rangle, \quad \text{and} \quad (\text{G26a})$$

$$M_{gb} = \langle 1 | U_{\text{eff}}(\tau) | \psi_b \rangle, \quad M_{eb} = \langle 3 | U_{\text{eff}}(\tau) | \psi_b \rangle \quad (\text{G26b})$$

with the effective Hamiltonian H_{eff} coupling the resonant levels given by (14), while

$$M_0 = e^{i\tau a^\dagger a \frac{|g_2|^2}{\Delta}}, \quad M_2 = e^{-i\tau a^\dagger a \frac{|g_2|^2 + |g_3|^2}{\Delta}}, \quad M_4 = e^{i\tau a^\dagger a \frac{|g_3|^2}{\Delta}}, \quad \text{and} \quad M_a = \mathbb{1}, \quad (\text{G27})$$

up to a global phase [see Eqs. (9), (13), and (B4)]. The continuous dynamics is then given by Eq. (11).

We note that, exactly as in the case of a pure atom state, the cavity dynamics is *parity-conserving*, which is due to the far-detuned limit, Eq. (14). Furthermore, it also corresponds to real-valued dynamics when $p_0 = p_2 = p_4 = 0$, as in this case the relative phase between coefficients of both atom states $|\psi_a\rangle$ and $|\psi_b\rangle$ is the same (see Sec. III B).

Mixed stationary states of the dynamics. As discussed in Sec. IV A, a pair of Kraus operators in Eq. (16) corresponding to a pure atom state in Eq. (8) features two even and odd pure eigenstates, which are determined by the recurrence relation in Eq. (23). In order for stationary states of the cavity to be pure in the dynamics with the mixed atom state (G23) it is necessary for it to be an eigenstate of all Kraus operators in Eqs. (G26) and (G27). However, for the orthogonal states $|\psi_a\rangle$ and $|\psi_b\rangle$, Eq. (G24), the corresponding recurrence relations features the factors c_e/c_g and $-c_g^*/c_e^*$, respectively, which are always different, as $|c_g|^2 \neq |c_e|^2$. Furthermore, even if $p_a = 0$ (or $p_b = 0$), the Kraus operators M_0 , M_2 and M_4 in Eq. (G27) cannot feature pure cavity states as eigenstates unless the cavity state is a fixed photon number state or the interaction time τ is such that $\frac{|g_2|^2}{\Delta}\tau = \frac{|g_3|^2}{\Delta}\tau = 2\pi$, so that $M_0 = M_2 = M_4 = \mathbb{1}$. Therefore, *no pure stationary states exist* if the atom state is mixed between levels $|j\rangle$ with $j = 0, \dots, 4$ (i.e., except $|a\rangle$). Nevertheless, the cavity features at least two, odd and even, mixed stationary states, since the photon-number parity is conserved [77].

Coherent stationary state of cavity from coherent states of atoms. We now prove that whenever the atom state, Eq. (G23), is coherent ($p_a \neq p_b$ and $|c_e| \neq 1, 0$), the even and odd stationary states of the cavity are coherent as well, i.e., they are not diagonal in the photon number basis. In contrast, for a diagonal atom state, two odd and even stationary states are diagonal in photon number basis (see Appendix H).

Proof. Consider a diagonal even state $\rho^+ = \sum_{n=0}^{\infty} p_{2n} |2n\rangle\langle 2n|$. We have [cf. Eqs. (10) and (16)]

$$\mathcal{M}(\rho_+) = \mathcal{M}_{\text{diag}}(\rho_+) + \sum_{n=0}^{\infty} \left\{ -ic_e c_g^* \sin_{2n}(\phi) (\sqrt{p_a} - \sqrt{p_b}) [\cos_{2n-1}(\phi) p_{2n} - \cos_{2n+2}(\phi) p_{2n+2}] |2n+2\rangle\langle 2n| + \text{H.c.} \right\}, \quad (\text{G28})$$

where $\mathcal{M}_{\text{diag}}$ is the dynamics with a diagonal atom state, $\sum_{j=0,2,4,a} p_j |j\rangle\langle j| + [p_a |c_g|^2 + p_b |c_e|^2] |1\rangle\langle 1| + [p_a |c_e|^2 + p_b |c_g|^2] |3\rangle\langle 3|$, which leaves diagonal states diagonal. Therefore, for ρ^+ to be a stationary state, no coherences can appear in Eq. (G28), and thus $c_e c_g^* = 0$, or $p = 1 - p$, or $\cos_{2n-1}(\phi) p_{2n} - \cos_{2n+2}(\phi) p_{2n+2} = 0$. The first two conditions correspond to incoherent states of the atom, while the last condition cannot be fulfilled for a stationary state of diagonal dynamics $\mathcal{M}_{\text{diag}}$, as it is effectively thermal with the temperature determined as $p_a |c_e|^2 + p_b |c_g|^2 / (p_a |c_g|^2 + p_b |c_e|^2) = \exp[-2\omega/(k_B T)]$ (see Appendix H) and thus independent from the interaction strength. The proof for odd stationary state is analogous.

Metastable dephasing dynamics for almost pure states. When atom state in Eq. (G23) is almost pure, $p_a \approx 1$ (or $p_b \approx 1$) so that $\rho_{\text{at}} \approx |\psi_a\rangle\langle\psi_a|$ (or $|\psi_b\rangle\langle\psi_b|$), the Kraus operators M_0 , M_2 , M_4 , and M_{gb} and M_{eb} (or M_{ga} and M_{ea}) can be treated as the perturbation of the dynamics with the pure states $|\Psi_+\rangle$, $|\Psi_-\rangle$ [which takes place at the modified rate νp_a (or νp_b)]. As derived above in Eq. (G14) this parity-conserving perturbation necessarily leads to *dephasing* of the even-odd coherences $|\Psi_+\rangle\langle\Psi_-|$ and $|\Psi_-\rangle\langle\Psi_+|$ at the rate $\gamma_{\text{deph}} \propto \nu$. Furthermore, when the atom state is only supported on the levels $|1\rangle$ and $|3\rangle$, there is no additional unitary dynamics, $\Omega = 0$, as the dynamics corresponds to real-valued dynamics. The dephasing manifests the fact that the even and odd stationary states of the dynamics mixed (although in the zero-order they are approximated by the pure state $|\Psi_+\rangle$ and $|\Psi_-\rangle$), and coherences between them are not stationary.

Dynamics in weak coupling limit. In the limit of small integrated coupling, $|\phi| \ll 1$, when the stationary state of the dynamics with a pure atom state are given by Schrödinger cat states [cf. Eqs. (36) and (40)], we obtain for the mixed state of the levels $|1\rangle$ and $|3\rangle$ ($p_a = 1 - p_b$) for $p_a \approx 1$

$$\gamma_{\text{deph}} = \nu(1-p) |c_g|^2 \phi^2 \{ |\alpha|^4 + |\alpha|^2 [\tanh(|\alpha|^2) + \coth(|\alpha|^2)] + 1 - \text{Tr}(L_{+-} a^{\dagger 2} |\Psi_+\rangle\langle\Psi_-| a^2) \}, \quad (\text{G29})$$

which corresponds to *two-photon injections* to the cavity (see also [39, 40, 52]),

$$\frac{d}{dt} \rho = -i[g_{2\text{ph}}^* a^2 + g_{2\text{ph}} a^{\dagger 2}, \rho] + \kappa_{2\text{ph}} \left(a^2 \rho a^{\dagger 2} - \frac{1}{2} \{ a^2 \rho a^{\dagger 2}, \rho \} \right) + \gamma_{2\text{ph}} \left(a^{\dagger 2} \rho a^2 - \frac{1}{2} \{ a^{\dagger 2} \rho a^2, \rho \} \right), \quad (\text{G30})$$

where $g_{2\text{ph}} = \nu c_g^* c_e \phi$, $\kappa_{2\text{ph}} = \nu p |c_g|^2 \phi^2$, and $\gamma_{2\text{ph}} = \nu(1-p) |c_g|^2 \phi^2$, since for $|c_e| \ll 1$ we have $M_{g2}/\sqrt{1-p+c_e^*} \approx 2c_e^* \mathbb{1} + ic_g^* \phi a^{\dagger 2}$ and $M_{e2}/\sqrt{1-p+c_g^*} \approx 0$ [cf. Eqs. (32) and (38)].

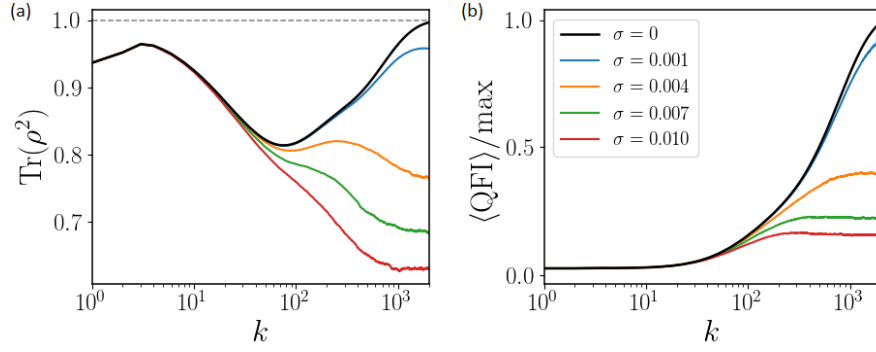


FIG. 11. **Effects of the non-monochromaticity of atomic beam.** Dynamics of the purity (a), $\text{Tr}(\rho^2)$, and the QFI (b) [Eq. (79), normalized by the maximum value $F_Q(\rho)/4\langle n \rangle = 7.39$ in dynamics with the monochromatic beam], with the number of atoms k passing the cavity, is shown for different widths σ of the integrated coupling distribution, which for simplicity is assumed normal, $p(\phi) = \exp[-(\phi - \langle \phi \rangle)^2/2\sigma^2]/\sqrt{2\pi\sigma^2}$. The initial state is the vacuum $|0\rangle$ the atom state is $c_e = 0.65$ and the coupling $\langle \phi \rangle = \phi_{20,5} \approx 0.73707$ [equal to the parameters of the stationary state (iii) in Figs. 2 and Fig. 9]. Dynamics was averaged over 100 random trajectories [cf. Eq. (G31)]. Note the control of the order of 0.1% in the velocity spread is required in order to achieve $\text{Tr}(\rho^2) > 0.9$ and $> 90\%$ of the QFI obtained with a monochromatic beam.

c. Non-monochromatic atom beam

In Sections III-V we assumed that the atomic beam is monochromatic, i.e., the velocity v of all atoms passing through the cavity is the same, leading to identical time τ spent in the cavity, and thus the uniform value of the integrated coupling strength ϕ [see Eqs. (9) and (11), and cf. Appendix A]. Here, we discuss how the micromaser dynamics is changed for a non-monochromatic atomic beam.

Micromaser dynamics. We consider atom velocities drawn from a probability distribution $p(v)$, which can be for example a Maxwell-Boltzmann distribution, i.e., a Gaussian distribution with thermal width $\sqrt{k_B T/m}$ and the corresponding average velocity of the atoms $\langle v \rangle$. The velocity distribution determines the probability distribution of the integrated coupling given by $g(\phi)d\phi = p(l/\phi)l/\phi^2 d\phi$, where l is the length of the cavity (note that in general $\langle \phi \rangle = l\langle v^{-1} \rangle \neq l/\langle v \rangle$). The dynamics of the cavity due to a single atom passage is now described by the average [cf. Eqs. (10) and (17)]

$$\langle \mathcal{M} \rangle = \int d\phi g(\phi) \mathcal{M}(\phi), \quad (\text{G31})$$

where $\mathcal{M}(\phi)$ denotes the dynamics with integrated coupling strength ϕ [see Eq. (16)].

Mixed stationary states of even and odd parity. As the recurrence relation in Eq. (26) obeyed by pure stationary states depends on ϕ , it can no longer be fulfilled for all velocities so that the stationary state becomes in general mixed [cf. the previous Appendix G] b. Nevertheless, due to the far-detuned limit in Eq. (14) the parity is conserved by the dynamics, and thus there exists two even and odd stationary states [77], which are mixed [cf. Fig. 11(a)].

Metastable dephasing dynamics. In the case in which the distribution of the integrated coupling is sufficiently peaked around its average, we expect $\delta\mathcal{M} \equiv \langle \mathcal{M} \rangle - \mathcal{M}(\langle \phi \rangle)$ can be treated as a perturbation of $\mathcal{M}(\langle \phi \rangle)$. In such case, it induces the dephasing dynamics within the DFS of the pure stationary states of $\mathcal{M}(\langle \phi \rangle)$, as the parity is conserved [see Eq. (G14)]. Furthermore, as the dynamics of $\mathcal{M}(\phi)$ corresponds to real-valued dynamics for all ϕ (cf. Sec. III B), there is no associated Hamiltonian contribution and $\Omega = 0$ in Eq. (G14). Note that the effective dephasing dynamics manifests the fact that the even and odd stationary states of the dynamics with $\langle \mathcal{M} \rangle$ are mixed (and only in zero-order they are approximated by the pure states $|\Psi_+\rangle$ and $|\Psi_-\rangle$), and coherences between them are not stationary.

In the weak-coupling limit, however, from Eq. (G31), we obtain the dynamics described by Eq. (40) with the averaged coefficients $g_{2\text{ph}} = \nu c_g^* c_e \langle \phi \rangle$, $\kappa_{2\text{ph}} = \nu |c_g|^2 \langle \phi^2 \rangle$. Therefore, in the weak-coupling limit, the stationary states are pure Schrödinger-cat states of Eq. (36), and their coherences are stationary as well. We note this approximation requires the weak coupling-limit of Eq. (37) to be valid for all values of ϕ attainable in the distribution $g(\phi)$.

Phase estimation precision. In the lowest-order in $\delta\mathcal{M}$, the non-monochromaticity of the atom beam leads to the

dephasing of the odd-even coherences, so that the QFI of the states of fixed parity is not affected. However, those stationary states are only approximately pure [cf. Fig. 11(a)] with corrections proportional to $\delta\mathcal{M}$ and the relaxation time of $\mathcal{M}(\langle\phi\rangle)$ (cf. Sec. VIB). This mixedness introduced by the non-monochromaticity of atom beam affects the QFI in phase estimation, (79) [cf. Fig. 11(b)].

This can be understood as follows. The enhancement in estimation precision and the long relaxation time is due to the presence of soft walls (cf. Sec. VI). The height and position of soft walls, $\sin_m(\phi) \approx 0$, however, depends on ϕ , leading to strong variations of the structure of the stationary states of $M(\phi)$ (see Fig. 2) and thus also the QFI (cf. Fig. 9). Therefore, for a broad enough distribution $g(\phi)$, the individual stationary states of $M(\phi)$ differ significantly from the stationary state of $M(\langle\phi\rangle)$, and the state of the averaged dynamics, Eq. (G31), is mixed. But, importantly, even when the purity of the final state is significantly reduced, it can still yield an enhancement over the standard quantum limit [cf. Fig. 11(b)].

3. Metastable dynamics due to single-photon losses and corrections to far-detuned limit in the presence of hard walls

Here we derive the effective dynamics due to single-photon losses, Eq. (60), and corrections to the far-detuned limit, Eq. (51), in the case when the unperturbed dynamics features hard walls (see Sec. VC for the discussion).

Multiple stationary states for hard walls. Hard walls in the far-detuned dynamics of Eq. (16) lead to presence of multiple stationary states (see Sec. IV D). If the first wall appears at even m_1 , $\sin_{m_1}(\phi) = 0$, there are infinitely many stationary states of both parities, as the parity of subsequent walls alternates. If the first wall appears at odd m_1 , however, there are only odd walls, leading to multiple odd stationary states [cf. Tab. I]. Furthermore, pure stationary states exist only when the first wall is odd with the integrated coupling strength such that $\cos_{m_1}(\phi) = 1$. In this case also the coherences between the pure stationary states with the same boundary conditions are stationary.

In derivations below we *assume* there is a unique stationary state between each two walls. In such case, for the first hard wall at even m_1 , the asymptotic state is given by

$$\lim_{t \rightarrow \infty} \rho(t) = \sum_{k=0}^{\infty} p_k^+ \rho_k^+ + \sum_{k=0}^{\infty} p_k^- \rho_k^-, \quad (\text{G32})$$

where ρ_k^+ [ρ_k^-] denotes k th even (odd) stationary states, i.e., the stationary state supported between walls at m_{2k-1} and m_{2k+1} (at m_{2k} and m_{2k+2}), and we formally expressed the boundary conditions (of non-negative photon number) as $m_{-1} = -2$ and $m_0 = -1$. The probabilities are given by the initial support between the hard walls, $p_k^\pm = \text{Tr}(\mathbb{1}_k^\pm \rho_{\text{in}})$ with $\mathbb{1}_k^+ = \sum_{m=m_{2k-1}+2}^{m_{2k+1}} |m\rangle\langle m|$ and $\mathbb{1}_k^- = \sum_{m=m_{2k}+2}^{m_{2k+2}} |m\rangle\langle m|$. Similarly, for the first wall being odd,

$$\begin{aligned} \lim_{t \rightarrow \infty} \rho(t) &= p^+ |\Psi_+\rangle\langle\Psi_+| + \sum_{k=0}^{\infty} p_k^- \rho_k^- \\ &+ \sum_{k=0}^{\infty} (c_{2k}^{+-} |\Psi_+\rangle\langle\Psi_{2k}^-| + \text{H.c.}) + \sum_{k=0}^{\infty} \sum_{\substack{k' > k: \\ (k'-k)|2}} (c_{k,k'}^- |\Psi_k^- \rangle\langle\Psi_{k'}^-| + \text{H.c.}), \end{aligned} \quad (\text{G33})$$

and $p^+ = \text{Tr}(\mathbb{1}^+ \rho_{\text{in}})$ with $\mathbb{1}^+ = \sum_{m=0}^{\infty} |2m\rangle\langle 2m|$. The second line in Eq. (G33) is present only when the first wall corresponds to $\cos_{m_1}(\phi) = 1$, i.e., the odd stationary states are pure, $\rho_k^- = |\Psi_k^- \rangle\langle\Psi_k^-|$ allowing for stationary coherences with $c_{2k}^{+-} = \text{Tr}(L_{2k}^{+-} \rho_{\text{in}})$ and $c_{k,k'}^+ = \text{Tr}(L_{k,k'}^+ \rho_{\text{in}})$, where L_{2k}^{+-} is a conserved quantity in odd-even coherences with the odd part within the support of ρ_{2k}^- , while $L_{k,k'}^+$ is the conserved quantity between the supports of ρ_k^- and $\rho_{k'}^-$ [where $k' > k$ such that the difference $k' - k$ is divisible by 2].

a. Effective dynamics due to single-photon losses

As a single-photon loss changes the parity of a state, consequently only the states of opposite parity in Eqs. (G32) and (G33) get connected. Furthermore, a single-photon loss reduces photon number by 1 in each state. Therefore, for the states to get connected, their supports need to overlap after the loss.

Case of the even first wall. For the probability p_k^\pm of being in the state ρ_k^\pm [cf. Eq. (G32)] single-photon losses induce

the following dynamics [see Eq. (G6)]

$$\frac{d}{dt} \begin{pmatrix} p_0^+ \\ p_0^- \\ p_1^+ \\ p_1^- \\ \vdots \end{pmatrix} = \kappa \begin{pmatrix} -\langle n \rangle_0^+ & \langle n \rangle_{0,0}^- & & & \\ \langle n \rangle_0^+ & -\langle n \rangle_0^- & \langle n \rangle_{1,0}^+ & & \\ & \langle n \rangle_{0,1}^- & -\langle n \rangle_1^+ & \langle n \rangle_{1,1}^- & \\ & & \langle n \rangle_{1,1}^+ & -\langle n \rangle_1^- & \ddots \\ & & & \ddots & \ddots \end{pmatrix} \begin{pmatrix} p_0^+ \\ p_0^- \\ p_1^+ \\ p_1^- \\ \vdots \end{pmatrix}, \quad (\text{G34})$$

where $\langle n \rangle_k^\pm = \text{Tr}(n \rho_k^\pm)$, $\langle n \rangle_{k,k'}^\pm = \text{Tr}(\mathbb{1}_{k'}^\mp a \rho_k^\pm a^\dagger)$, and empty entries correspond to 0. Since the parity of the subsequent walls alternates, the support of a given state between two walls shifted by 1 overlaps only with two states of opposite parity, so that $\langle n \rangle_{k,k}^\pm + \langle n \rangle_{k,k\mp 1}^\pm = \langle n \rangle_k^\pm$ (except the case of ρ_0^+).

The dynamics in Eq. (G34) obeys *detailed balance*, leading to the *unique stationary state* given by

$$\rho_{ss} = \sum_{k=0}^{\infty} (p_{ss,k}^+ \rho_k^+ + p_{ss,k}^- \rho_k^-), \quad \text{where} \quad \frac{p_{ss,k}^+}{p_{ss,k-1}^-} = \frac{\langle n \rangle_{k-1,k}^-}{\langle n \rangle_{k,k-1}^+} \quad \text{and} \quad \frac{p_{ss,k}^-}{p_{ss,k}^+} = \frac{\langle n \rangle_{k,k}^+}{\langle n \rangle_{k,k}^-}, \quad (\text{G35})$$

and $p_{ss,0}^+$ is determined by the normalisation $\sum_{k=0}^{\infty} (p_{ss,k}^+ + p_{ss,k}^-) = 1$, and $\langle n \rangle_{0,0}^+ \equiv \langle n \rangle_0^+$. Eq. (G35) follows from Eq. (G34) corresponding to the classical *birth-death process*.

Trapping states. In the case when the cavity is being pumped by the atoms in the excited state ($|c_e| = 1$), the stationary states of the cavity are pure and correspond to the position of hard walls $\rho_k^+ = |m_{2k+1}\rangle\langle m_{2k+1}|$ and $\rho_k^- = |m_{2k+2}\rangle\langle m_{2k+2}|$. In this case a single photon loss transforms the states into $|m_{2k+1} - 1\rangle\langle m_{2k+1} - 1|$ and $|m_{2k+2} - 1\rangle\langle m_{2k+2} - 1|$, which evolve into ρ_k^- and ρ_{k+1}^+ , respectively. Therefore, the effective dynamics due to single-photon losses leads to the stochastic increase of the photon number of the cavity [cf. Eq. (G34)]

$$\frac{d}{dt} \begin{pmatrix} p_0^+ \\ p_0^- \\ p_1^+ \\ p_1^- \\ \vdots \end{pmatrix} = \kappa \begin{pmatrix} -m_1 & & & & \\ & m_1 & -m_2 & & \\ & & m_2 & -m_3 & \\ & & & m_3 & -m_4 \\ & & & & \ddots & \ddots \end{pmatrix} \begin{pmatrix} p_0^+ \\ p_0^- \\ p_1^+ \\ p_1^- \\ \vdots \end{pmatrix}, \quad (\text{G36})$$

and no stationary state exists. This is due to the assumption, that $\kappa \ll \nu$, so that cavity is pumped at much higher rate, than it loses photons. Furthermore, the formerly stationary coherences between trapping states of the same parity decay as

$$\frac{d}{dt} \begin{pmatrix} \vdots \\ c_{k,k'}^{++} \\ c_{k,k'}^{--} \\ c_{k+1,k'+1}^{++} \\ \vdots \end{pmatrix} = \kappa \begin{pmatrix} \ddots & & & & \\ \ddots & -\frac{m_{2k+1}+m_{2k'+1}}{2} & & & \\ & \bar{\eta}_{k,k'}^{++} & -\frac{m_{2k+2}+m_{2k'+2}}{2} & & \\ & & \bar{\eta}_{k,k'}^{--} & -\frac{m_{2k+3}+m_{2k'+3}}{2} & \\ & & & \ddots & \ddots \end{pmatrix} \begin{pmatrix} \vdots \\ c_{k,k'}^{++} \\ c_{k,k'}^{--} \\ c_{k+1,k'+1}^{++} \\ \vdots \end{pmatrix} \quad (\text{G37})$$

where $c_{k,k'}^{++}$ is the coefficient corresponding to the even-even coherence $|m_{2k+1}\rangle\langle m_{2k'+1}|$ and $c_{k,k'}^{--}$ is the coefficient for the odd-odd coherence $|m_{2k+2}\rangle\langle m_{2k'+2}|$. We have defined $\bar{\eta}_{k,k'}^{++} = \sqrt{m_{2k+1}m_{2k'+1}}\langle m_{2k'+1}-1|L_{k,k'}^-|m_{2k+1}-1\rangle$ and $\bar{\eta}_{k,k'}^{--} = \sqrt{m_{2k+2}m_{2k'+2}}\langle m_{2k'+2}-1|L_{k+1,k'+1}^+|m_{2k+2}-1\rangle$, where $L_{k,k'}^-$ and $L_{k,k'}^+$ are the conserved quantities corresponding to $|m_{2k+2}\rangle\langle m_{2k'+2}|$ and $|m_{2k+1}\rangle\langle m_{2k'+1}|$, respectively. Furthermore, when $\cos_{m_1}(\phi) = 1$, the formerly stationary even-odd and odd-even coherences similarly decay as

$$\frac{d}{dt} \begin{pmatrix} \vdots \\ c_{k,k'}^{+-} \\ c_{k,k'+1}^{++} \\ c_{k+1,k'+1}^{+-} \\ \vdots \end{pmatrix} = \kappa \begin{pmatrix} \ddots & & & & \\ \ddots & -\frac{m_{2k+1}+m_{2k'+2}}{2} & & & \\ & \bar{\eta}_{k,k'}^{+-} & -\frac{m_{2k+2}+m_{2k'+3}}{2} & & \\ & & \bar{\eta}_{k,k'+1}^{--} & -\frac{m_{2k+3}+m_{2k'+4}}{2} & \\ & & & \ddots & \ddots \end{pmatrix} \begin{pmatrix} \vdots \\ c_{k,k'}^{+-} \\ c_{k,k'+1}^{++} \\ c_{k+1,k'+1}^{+-} \\ \vdots \end{pmatrix}, \quad (\text{G38})$$

where $c_{k,k'}^{+-}$ is the coefficient corresponding to the even-odd coherence $|m_{2k+1}\rangle\langle m_{2k'+2}|$, $c_{k,k'}^{-+}$ is the coefficient corresponding to the odd-even coherence $|m_{2k+2}\rangle\langle m_{2k'+1}|$ and we have defined $\bar{\eta}_{k,k'}^{+-} = \sqrt{m_{2k+1}m_{2k'+2}}\langle m_{2k'+2} - 1 | L_{k,k'+1}^{+-} | m_{2k+1} - 1 \rangle$ and $\bar{\eta}_{k,k'}^{-+} = \sqrt{m_{2k+2}m_{2k'+1}}\langle m_{2k'+1} - 1 | L_{k+1,k'}^{+-} | m_{2k+2} - 1 \rangle$ with $L_{k,k'}^{+-}$ and $L_{k,k'}^{-+}$ being the conserved quantities corresponding to $|m_{2k+2}\rangle\langle m_{2k'+1}|$ and $|m_{2k+1}\rangle\langle m_{2k'+2}|$, respectively.

Case of the odd first wall. For the case of the first wall with $\cos_{m_1}(\phi) = -1$, there exist a single even pure stationary state and multiple odd mixed stationary states between odd hard walls (cf. Tab. 43). In the presence of single-photon losses the corresponding probabilities [cf. Eq. (G33)] undergo the following dynamics [see Eq. (G6)]

$$\frac{d}{dt} \begin{pmatrix} p^+ \\ p_0^- \\ p_1^- \\ \vdots \end{pmatrix} = \kappa \begin{pmatrix} -\langle n \rangle_+ & \langle n \rangle_0^- & \langle n \rangle_1^- & \cdots \\ \langle n \rangle_0^+ & -\langle n \rangle_0^- & & \\ \langle n \rangle_1^+ & & -\langle n \rangle_1^- & \\ \vdots & & & \ddots \end{pmatrix} \begin{pmatrix} p^+ \\ p_0^- \\ p_1^- \\ \vdots \end{pmatrix}, \quad (\text{G39})$$

where $\langle n \rangle_+ = \langle \Psi_+ | n | \Psi_+ \rangle$, $\langle n \rangle_k^- = \text{Tr}(n \rho_k^-)$, and $\langle n \rangle_k^+ = \text{Tr}(\mathbb{1}_k^- a | \Psi_+ \rangle \langle \Psi_+ | a^\dagger)$. For the first wall with $\cos_{m_1}(\phi) = -1$, the dynamics in Eq. (G39) leads to the stationary state

$$\rho_{ss} = p_{ss}^+ |\Psi_+ \rangle \langle \Psi_+| + \sum_{k=0}^{\infty} p_{ss,k}^- \rho_k^-, \quad \text{where} \quad \frac{p_{ss,k}^-}{p_{ss}^+} = \frac{\langle n \rangle_k^+}{\langle n \rangle_k^-}, \quad (\text{G40})$$

which structure is due to the dynamics obeying the *detailed balance*, as the odd states are only coupled to the unique even state. In Eq. (G40) p_{ss}^+ is determined by the normalisation $p_{ss}^+ + \sum_{k=0}^{\infty} p_{ss,k}^- = 1$.

For the first wall with $\cos_{m_1}(\phi) = 1$, coherences can also be stationary in the absence of single-photon losses [cf. Eq. (G33)], but the single photon losses lead to their decay, as follows. For the coherences between the even state and odd states we have

$$\frac{d}{dt} \begin{pmatrix} c_0^{+-} \\ c_0^{-+} \\ c_2^{+-} \\ c_2^{-+} \\ \vdots \end{pmatrix} = \kappa \begin{pmatrix} -\frac{\langle n \rangle_+ + \langle n \rangle_0^-}{2} & \bar{\eta}_{0,0} & & \bar{\eta}_{2,0} & \cdots \\ \bar{\eta}_{0,0} & -\frac{\langle n \rangle_+ + \langle n \rangle_0^-}{2} & \bar{\eta}_{2,0} & & \ddots \\ & \bar{\eta}_{0,2} & -\frac{\langle n \rangle_+ + \langle n \rangle_2^-}{2} & \bar{\eta}_{2,2} & \\ \bar{\eta}_{0,2} & & \bar{\eta}_{2,2} & -\frac{\langle n \rangle_+ + \langle n \rangle_2^-}{2} & \ddots \\ \vdots & \ddots & & \ddots & \ddots \end{pmatrix} \begin{pmatrix} c_0^{+-} \\ c_0^{-+} \\ c_2^{+-} \\ c_2^{-+} \\ \vdots \end{pmatrix}, \quad (\text{G41})$$

where c_{2k}^{+-} , c_{2k}^{-+} are the coefficients for the coherences $|\Psi_{2k}^- \rangle \langle \Psi_+|$ and $|\Psi_+ \rangle \langle \Psi_{2k}^-|$, respectively, and we have defined $\bar{\eta}_{2k,2k'} = \text{Tr}[(L_{2k'}^+)^{\dagger} a | \Psi_+ \rangle \langle \Psi_{2k}^- | a^\dagger]$, $k, k' = 0, 1, \dots$. Furthermore, the coherence between odd states decay as

$$\frac{d}{dt} c_{k,k'}^{--} = -\kappa \frac{\langle n \rangle_+ + \langle n \rangle_0^-}{2} c_{k,k'}^{--}, \quad (\text{G42})$$

where $c_{k,k'}^{--}$ is the coefficient for the coherences $|\Psi_k^- \rangle \langle \Psi_{k'}^-|$ and $(k' - k)$ is divisible by 2 (then they correspond to states with the same boundary conditions). Finally, coherences between the odd states can be created by the single-photon loss from the even state [cf. Eq. (G39)]

$$\frac{d}{dt} |\Psi_+ \rangle \langle \Psi_+| = -\langle n \rangle^+ |\Psi_+ \rangle \langle \Psi_+| + \sum_{k=0}^{\infty} \langle n \rangle_k^+ |\Psi_k^- \rangle \langle \Psi_k^-| + \sum_{k=0}^{\infty} \sum_{\substack{k' > k: \\ (k' - k)|2}} \left[\text{Tr} \left(L_{k,k'}^- a | \Psi_+ \rangle \langle \Psi_+ | a^\dagger \right) |\Psi_k^- \rangle \langle \Psi_{k'}^-| + \text{H.c.} \right]. \quad (\text{G43})$$

Nevertheless, the coherences decay at long times [cf. Eq. (G42)], thus leading to the same structure of the stationary state as in the case without coherence [$\cos_{m_1}(\phi) = -1$], i.e., Eq. (G40).

b. Dynamics due to corrections to the far-detuned limit

The corrections to the far-detuned limit lead to the introduction of the parity-swapping Kraus operators M_0 , M_2 and M_4 , and modification of the parity-conserving Kraus operators M_1 , M_3 (as well as the introduction of M_a) [cf. Eq. (48) and Appendix B].

Dissipative dynamics. The parity-swapping Kraus operators M_0 , M_2 and M_4 can change the support of a state between hard walls only by a single photon number (analogously to adding or removing a single-photon) in the first order of the ratio between couplings and detunings (see Appendix B 2). Therefore, repeating the arguments for the dynamics with single-photon losses, we conclude that the parity swapping Kraus operators lead to the second-order dynamics as in Eqs. (G34-G42), but with $\sqrt{\kappa}a$ replaced by $\sqrt{\nu}M_0$, $\sqrt{\nu}M_2$ or $\sqrt{\nu}M_4$, and then summed [compare Eqs. (51) and (56) and Eqs. (60), (61)].

Unitary dynamics. The parity-conserving Kraus operators M_1 , M_3 change the support of a state between hard walls by two photons in the second order of the ratio between couplings and detunings (see Appendix B 2). Therefore, these corrections contribute unitarily to the dynamics of coherences as follows [cf. Eqs. (51) and (53)]. For the first wall being even and trapping states [cf. Eqs. (G37) and (G38)]

$$\frac{d}{dt}c_{k,k'}^{++} = -i [\langle \delta H \rangle_k^+ - \langle \delta H \rangle_{k'}^+] c_{2k}^{++}, \quad (\text{G44})$$

$$\frac{d}{dt}c_{k,k'}^{--} = -i [\langle \delta H \rangle_k^- - \langle \delta H \rangle_{k'}^-] c_{2k}^{--} \times \cos_{m_1}(\phi), \quad (\text{G45})$$

$$\frac{d}{dt}c_{k,k'}^{+-} = -i [\langle \delta H \rangle_k^+ - \langle \delta H \rangle_{k'}^-] c_{k,k'}^{+-}, \quad (\text{G46})$$

where δH is given by Eq. (G21). For the first wall being odd [cf. Eqs. (G41) and (G42)]

$$\frac{d}{dt}c_{2k}^{+-} = -i [\langle \delta H \rangle_+ - \langle \delta H \rangle_k^-] c_{2k}^{+-}, \quad (\text{G47})$$

$$\frac{d}{dt}c_{k,k'}^{--} = -i [\langle \delta H \rangle_k^- - \langle \delta H \rangle_{k'}^-] c_{k,k'}^{--} \times \cos_{m_k}(\phi), \quad (\text{G48})$$

and we further have $\cos_{m_k}(\phi) = (-1)^k$.

Steady states. From the above considerations, the stationary state for the first wall being even is, cf. Eq. (G35),

$$\rho_{ss} = \sum_{k=0}^{\infty} (p_{ss,k}^+ \rho_k^+ + p_{ss,k}^- \rho_k^-), \quad \text{where} \quad \frac{p_{ss,k}^+}{p_{ss,k-1}^-} = \frac{\langle X \rangle_{k-1,k}^-}{\langle X \rangle_{k,k-1}^+} \quad \text{and} \quad \frac{p_{ss,k}^-}{p_{ss,k}^+} = \frac{\langle X \rangle_{k,k}^+}{\langle X \rangle_{k,k}^-}, \quad (\text{G49})$$

where $\langle X \rangle_{k,k'}^{\pm} = \sum_{j=0,2,4} \text{Tr}(\mathbb{1}_{k'}^{\mp} M_j \rho_k^{\pm} M_j^{\dagger})$, while for the first wall being odd [cf. Eq. (G40)]

$$\rho_{ss} = p_{ss}^+ |\Psi_+\rangle\langle\Psi_+| + \sum_{k=0}^{\infty} p_{ss,k}^- \rho_k^-, \quad \text{where} \quad \frac{p_{ss,k}^-}{p_{ss}^+} = \frac{\langle X \rangle_k^+}{\langle X \rangle_k^-}, \quad (\text{G50})$$

where $X = \sum_{j=0,2,4} M_j^{\dagger} M_j$, $\langle X \rangle_k^- = \text{Tr}(X \rho_k^-)$ and $\langle X \rangle_k^+ = \sum_{j=0,2,4} \text{Tr}(\mathbb{1}_k^- M_j |\Psi_+\rangle\langle\Psi_+| M_j^{\dagger})$.

APPENDIX H: CLASSICAL MICROMASER DYNAMICS FOR THERMAL ATOMS

Here we consider the micromaser dynamics, Eq. (11), in the case of thermal atoms. The dynamics in the far-detuned limit is *classical* and obeys *detailed balance*, resulting in thermal stationary states of the even and the odd parity, which are independent from the integrated coupling.

Classical detailed-balance dynamics. Consider an atom in a thermal state

$$\rho_{\text{at}} = \sum_{j=0,\dots,4,a} p_j |j\rangle\langle j|, \quad p_j \propto e^{-\frac{E_j}{k_B T}} \quad (\text{H1})$$

where T denotes the atom temperature and E_j is the energy of the atomic level (see Sec. II).

There are eight Kraus operators [cf. Eqs. (9), (16) and (G27)]

$$M_{gg} = \cos\left(\phi\sqrt{a^\dagger a}\right), \quad M_{eg} = -i a^2 \frac{\sin\left(\phi\sqrt{a^\dagger a}\right)}{\sqrt{a^\dagger a}}, \quad (\text{H2a})$$

$$M_{ge} = -i a^\dagger \frac{\sin\left(\phi\sqrt{a^\dagger a}\right)}{\sqrt{a^\dagger a}}, \quad M_{ee} = \cos\left(\phi\sqrt{a^\dagger a}\right), \quad (\text{H2b})$$

$$M_0 = e^{i\tau a^\dagger a \frac{|g_2|^2}{\Delta}}, \quad M_2 = e^{-i\tau a^\dagger a \frac{|g_2|^2 + |g_3|^2}{\Delta}}, \quad M_4 = e^{i\tau a^\dagger a \frac{|g_3|^2}{\Delta}}, \quad \text{and} \quad M_a = \mathbb{1}, \quad (\text{H2c})$$

which describe the change in the cavity state due to a passage of the atom as [cf. Eq. (10)]

$$\rho^{(k)} = \sum_{j,l=g,e} p_l M_{jl} \rho^{(k-1)} M_{jl}^\dagger + \sum_{j=0,2,4,a} p_j M_j \rho^{(k-1)} M_j^\dagger \equiv \mathcal{M} \left[\rho^{(k-1)} \right]. \quad (\text{H3})$$

The resulting continuous cavity dynamics in Eq. (11) conserves the parity, Eq. (21), due to the approximation of far-detuned limit (cf. Eq. (14)). Furthermore, the dynamics is classical, with diagonal states in the photon number basis remaining diagonal, and thus evolving independently from the coherences. In particular, for diagonal states, Eqs. (H2) describes a detailed-balance process between the photon number states of fixed parity, which corresponds to the so called *birth-death process* with the birth referring to the change from $|n\rangle\langle n|$ to $|n+2\rangle\langle n+2|$ due to the Kraus operator M_{ge} , and the death - from $|n\rangle\langle n|$ to $|n-2\rangle\langle n-2|$ - due to the Kraus operator M_{eg} , while the other Kraus operators do not contribute. The respective rates are given by

$$b_n = \nu p_3 \sin_n^2(\phi), \quad d_n = \nu p_1 \sin_{n-2}^2(\phi). \quad (\text{H4})$$

Thermal stationary states. From the detailed balance it follows that two stationary states $\rho^+ = \sum_{n=0}^{\infty} p_{2n} |2n\rangle\langle 2n|$ and $\rho^- = \sum_{n=0}^{\infty} h_{2n+1} |2n+1\rangle\langle 2n+1|$ are thermal with the probabilities determined by the recurrence relation

$$\frac{h_{n+2}}{h_n} = \frac{b_n}{d_{n+2}} = \frac{p_3}{p_1} = e^{\frac{-2\omega}{k_B T}}, \quad (\text{H5})$$

where $2\omega = E_1 - E_3$ due to the two-photon resonance in Eq. (7). Furthermore, the detailed balance dynamics is present for any diagonal, not necessarily thermal, state of the atom. In this case Eq. (H5) defines the effective temperature T .

The sequence of probabilities h_n is convergent if $e^{-2\omega/k_B T} < 1$, which takes place for positive temperatures $T > 0$ (or for a diagonal state when $p_1 > p_3$). In the case of an initial state of the cavity ρ_{in} with the support on both the even and odd subspace, the asymptotic state is a probabilistic mixture of the even and odd stationary states

$$\rho_{\text{ss}} = p \rho^+ + (1-p) \rho^- = \frac{1}{1 + e^{\frac{-2\omega}{k_B T}}} \sum_{n=0}^{\infty} e^{\frac{-2n\omega}{k_B T}} \left[p |2n\rangle\langle 2n| + (1-p) |2n+1\rangle\langle 2n+1| \right], \quad (\text{H6})$$

where the probability $p = \text{Tr}(\mathbb{1}_+ \rho_{\text{in}})$ is determined by the initial support on the even subspace.

Interaction dependent timescales of dynamics. Due to the initial atomic state being thermal, Eq. (H1), the stationary states of the cavity are independent from the integrated coupling strength ϕ . However, the dynamics of relaxation towards the stationary state depends crucially on the value of ϕ . This follows from the birth and death rates, Eq. (H4) being dependent on $\sin_n^2(\phi)$. Therefore, the presence of a soft wall at $n = m$, $\sin_m(\phi) \approx 0$, leads to slowing down of the dynamics, similarly as it was the case for the quantum micromaser dynamics discussed in Sec. IV D. In particular, the relaxation timescales to the stationary state are dominated by the slowest pairs of the birth and death rates, i.e., such m within the support of the stationary state for which $b_m, d_{m+2} \propto \sin_m^2(\phi) \approx 0$. Treating b_m, d_{m+2} as a perturbation of the dynamics with $b_m^{(0)} = 0, d_{m+2}^{(0)} = 0$, from Eq. (G2) we obtain the long-time dynamics between thermal states supported before and after a wall as [87]

$$\begin{aligned} \frac{d}{dt} p_k(t) = & - \left[p_1 \sin_{m_k}^2(\phi) p_{m_k+2}^{(k)} + p_3 \sin_{m_{k+1}}^2(\phi) p_{m_{k+1}}^{(k)} \right] p_k(t) \\ & + p_1 \sin_{m_k}^2(\phi) p_{m_k+2}^{(k)} p_{k-1}(t) + p_3 \sin_{m_{k+1}}^2(\phi) p_{m_{k+1}}^{(k)} p_{k+1}(t), \end{aligned} \quad (\text{H7})$$

where $p_k(t)$ denotes the probability of being in the k th state supported after k th wall, while $h_n^{(k)}$ denotes the probability of finding n photons in the k th state (for simplicity we dropped the indices denoting the parity, but only the states of the same parity are coupled) (see also Appendix E). Note that the final stationary state is again given by Eq. (H6).

APPENDIX I: CONTINUOUS VERSUS DISCRETE CAVITY DYNAMICS

In this Appendix we discuss similarities and differences between continuous dynamics, Eqs. (11) and (18), and the discrete dynamics, Eqs. (10) and (17), where the number of atoms that has passed is known explicitly. In particular, the numerical simulations in Figures 1-3, 5-8, 9 and 11 utilize the discrete dynamics.

Discrete dynamics. The master equations (11) and (18) represent *continuous dynamics* of the density matrix, which describes the cavity state averaged both over the possible measurement outcomes of the outgoing atomic states - i.e., when the atoms are traced out - and over the exponentially-distributed arrival times of atoms into the cavity (see Appendix A). The former average procedure results precisely in Kraus operators in Eqs. (10) and (48), while the latter average yields the master equation (11) governing continuous evolution of the cavity in time. Note that by counting the number of atoms that have passed through the cavity, its state after the passage of k atoms is simply given by [cf. Eqs. (10) and (17)]

$$\rho^{(k)} = \mathcal{M}^k(\rho_{\text{in}}), \quad (\text{I1})$$

where $\rho_{\text{in}} \equiv \rho^{(0)}$ denotes the initial state of the cavity. Note that the conditional *discrete dynamics* in (I1) is independent from the atom rate ν , but the probability of the passage of k atoms up to time t is given by $e^{-\nu t} (\nu t)^k / k!$, which depends solely on νt , as described by the Poisson point process (see also Appendix A).

Timescales of dynamics. We first note that, in the far-detuned limit, the stationary states of the discrete dynamics (17) corresponding to the eigenvalue 1 of \mathcal{M}_0 are also the stationary states of the continuous dynamics \mathcal{L}_0 , (18), which is also the case beyond the adiabatic approximation for \mathcal{M} and \mathcal{L} , Eqs. (10) and (11). Actually, all eigenmodes of the discrete dynamics are also eigenmodes of continuous dynamics, with eigenvalues $\lambda_m^{\text{discrete}}$ of \mathcal{M} rescaled to the eigenvalues λ_m of \mathcal{L} as [120]

$$\lambda_m = \nu(\lambda_m^{\text{discrete}} - 1), \quad (\text{I2})$$

since $\mathcal{L} = \nu(\mathcal{M} - \mathcal{I})$. The relation (I2) plays an important role in the presence of a hard wall (see Sec. IV D). For the discrete dynamics all eigenmodes of \mathcal{M} with eigenvalue of absolute value 1 are non-decaying, while for the continuous dynamics only the modes corresponding to the eigenvalue 1 are stationary. In particular, for a hard wall leading to different boundary conditions before and after the wall, the coherence between the pure stationary states after and before the wall is non-decaying in the discrete dynamics, but the coherence phase is flipped, i.e. is shifted by π , with each passing atom, which in the continuous case leads to its dephasing (see Sec. IV D).

Discrete dynamics in the presence of losses. In Sec. V B we consider cavity dynamics in the presence of single-photon losses at rate κ . In the derivation of the dynamics governed by the master equation (58) it is assumed that photon loss takes place when there is no atom within the cavity, i.e., $\kappa\tau \ll 1$ for the atom passage time τ , so that the single-photon losses can be considered independent of the atom-cavity dynamics [31, 57]. For the discrete dynamics this assumption leads to the state of the cavity after the passage of k atoms given by

$$\rho^{(k)} = (\mathcal{M}_{1\text{ph}})^k (\mathcal{I} - \mathcal{L}_{1\text{ph}}/\nu)^{-1} (\rho_{\text{in}}), \quad \text{where} \quad \mathcal{M}_{1\text{ph}} \equiv (\mathcal{I} - \mathcal{L}_{1\text{ph}}/\nu)^{-1} \mathcal{M}_0. \quad (\text{I3})$$

Note that $\mathcal{M}_{1\text{ph}}$ describes the joint effect of the passage of an atom in the far-detuned limit given by \mathcal{M}_0 , and the losses that can occur afterwards, but before the passage of the next atom, $\int_0^\infty dt \nu e^{-\nu t} e^{t\mathcal{L}_{1\text{ph}}} = [\mathcal{I} - \mathcal{L}_{1\text{ph}}/\nu]^{-1}$. Eq. (I3) can be used to derive the master dynamics (58) in the limit $\kappa \ll \nu$ (cf. Appendix A in [31]). Therefore, from Eq. (I3), the stationary state of continuous dynamics in the presence of losses (58) corresponds to the stationary state of the discrete dynamics,

$$\rho_{\text{ss}}^{\text{discrete}} = (\mathcal{I} - \mathcal{L}_{1\text{ph}}/\nu) \rho_{\text{ss}}, \quad (\text{I4})$$

since $\mathcal{L}\rho_{\text{ss}} = 0$, where $\mathcal{L} \equiv \nu(\mathcal{M}_0 - \mathcal{I}) + \mathcal{L}_{1\text{ph}}$, so that $\mathcal{M}_0\rho_{\text{ss}} = (\mathcal{I} - \mathcal{L}_{1\text{ph}}/\nu)\rho_{\text{ss}}$ and, thus, $\mathcal{M}_{1\text{ph}}\rho_{\text{ss}} = \rho_{\text{ss}}$.

Metastability in discrete dynamics. In the metastable limit of a small rate of the single-photon losses, $\kappa \ll \nu$, we recover $\rho_{\text{ss}}^{\text{discrete}} \approx \rho_{\text{ss}}$ from Eq. (I4). Furthermore, the continuous dynamics of all the metastable modes discussed in Sec. V B, will be approximately the same in the discrete case, as follows. Recall from above that, without the losses, the DFS of pure stationary states $|\Psi_+\rangle$ and $|\Psi_-\rangle$, Eq. (29), is stationary both in the continuous case of \mathcal{L}_0 and discrete case of \mathcal{M}_0 . Expanding $\mathcal{M}_{1\text{ph}}$ in (I3) we have

$$\mathcal{M}_{1\text{ph}} = \mathcal{M}_0 + \mathcal{L}_{1\text{ph}}\mathcal{M}_0/\nu + \mathcal{O}(\kappa^2/\nu^2). \quad (\text{I5})$$

Therefore, within the DFS, the eigenvalues and eigenmodes of $\mathcal{M}_{1\text{ph}}$ in the lowest order of the expansion in κ/ν correspond to the eigenmodes of the continuous effective first-order dynamics in Eq. (60), as

$$\Pi_0 \mathcal{M}_{1\text{ph}} \Pi_0 = \Pi_0 + \Pi_0 \mathcal{L}_{1\text{ph}} \Pi_0 / \nu + \mathcal{O}(\kappa^2/\nu^2), \quad (I6)$$

where Π_0 denotes the projection on the formerly stationary DFS (cf. Sec. IV B and Appendix G), while the initial term $[\mathcal{I} - \mathcal{L}_{1\text{ph}}/\nu]^{-1}$ in (I3) contributes only as the higher-order corrections to the eigenmodes of the discrete dynamics.

Similarly, in the case of the metastability due the higher-order corrections to the two-photon cavity dynamics, Sec. V A, the long-time discrete dynamics beyond adiabatic limit \mathcal{M} can be approximated within the metastable DFS exactly as in Eq. (I6), but with $\Pi_0 \mathcal{L}_{1\text{ph}} \Pi_0$ replaced by the master operator of Eq. (51), which corresponds to $\nu(\Pi_0 \mathcal{M} \Pi_0 - \Pi_0)$.

APPENDIX J: IDENTIFYING POSSIBLE LEVEL SCHEME IN RYDBERG ATOMS

As described in Sec. VII, we have used the ARC package [105, 106] in order to evaluate the energies of levels $|j\rangle$, $j = 0, \dots, 4$, as well as the corresponding dipole moments $d_{j-1,j} = \langle j-1 | e\hat{r} | j \rangle$, $j > 0$, where e is the electron charge and \hat{r} the position operator. The dipole moments are related to the single photon Rabi frequencies g_j through $g_j = d_{j-1,j} E_{1\text{ph}}/\hbar$, where $E_{1\text{ph}} = \sqrt{\hbar\omega/2\varepsilon_0 V}$ with ω , ε_0 and V being the cavity frequency, vacuum permittivity and volume of the cavity mode respectively. In the following estimations we take $V = 70 \text{ mm}^3$ as a benchmark from the reference [32]. The parameter λ in Eq. (14) is then the two-photon Rabi frequency. The number of possible transitions grows rapidly with the number of basis states considered. To limit our search, we have considered again the reference [32] which used a ladder configuration $39\text{S}_{\frac{1}{2}} \leftrightarrow 39\text{P}_{\frac{3}{2}} \leftrightarrow 40\text{S}_{\frac{1}{2}}$ and use a set of 30 basis states $|n, l, j\rangle$ with $n = 35, \dots, 45$ and $l = 0, 1$, where $j = l \pm s$, with $s = 1/2$ the value of the electronic spin. The choice of levels imposing the use of π -polarization for the transitions, we identify 444600 possible (dipole allowed) transitions. We define the cavity frequency as $\omega = (E_3 - E_1)/2\hbar$ and the corresponding detunings according to Eq. (3).

Post-selecting on cases where the levels $|j\rangle$, $j = 1, 2, 3$ form a ladder, i.e. $E_1 > E_2 > E_3$ or $E_1 < E_2 < E_3$, cf. Fig. 1(a), and requiring further that the rotating wave approximation is well respected, $\max(|\Delta_j/\omega| < 1/10)$, as well as the far detuned limit, $\max(|g_j/\Delta_j| < 1/10)$, we are left with 104 transitions [121]. Having identified the possible candidates, we now need to evaluate the conditions (13a,13b) [here we assume that the condition (13c) can be satisfied by tuning the Rabi frequency G and the detuning δ of the external laser]. The possible transitions can be assessed according to different criteria. Here we choose to minimize the deviations from the conditions (13a,13b) as follows. We define factors $f_{a,b}$ as $|g_1|^2/\Delta_1 = f_a |g_2|^2/\Delta_2$, $|g_4|^2/\Delta_4 = -f_b |g_3|^2/\Delta_3$, so that the conditions (13) are reached for $f_a = f_b = 1$. We also note, that a value of, say, $f_a \neq 1$ requires to adjust the detuning Δ_1 by a factor of f_a or, equivalently, the detuning Δ by a factor of $1/f_a$, assuming the couplings g remain constant. For this reason we seek a figure of merit which assigns to f and $1/f$ the same distance from the ideal point $f = 1$. We thus seek to find a set of transitions which minimizes $\max(|1 - f_a|, |1 - 1/f_a|) + \max(|1 - f_b|, |1 - 1/f_b|)$. This leads us to the set of transitions $37\text{S}_{\frac{1}{2}} \leftrightarrow 37\text{P}_{\frac{3}{2}} \leftrightarrow 38\text{S}_{\frac{1}{2}} \leftrightarrow 38\text{P}_{\frac{3}{2}} \leftrightarrow 39\text{S}_{\frac{1}{2}}$ described in VII together with the relevant parameters, in particular the two-photon Rabi frequency $|\lambda| \approx 5 \text{ Hz}$.

To improve this result one can improve the search strategy by considering larger set of basis states, and, in particular, the level manipulations with external electric field \mathcal{E} through the DC Stark effect, which would allow for tuning the detunings Δ_j as stated in the main text. Here, in order to evaluate (13) one needs to compute not only the energies of the atomic levels but also the dipole elements of the allowed transitions. For $l \leq 3$ and small values of \mathcal{E} one might attempt a perturbative approach with level energies given by $E_{nlj} = -\frac{E_{\text{Ry}}}{n^{*2}} - \frac{1}{2}\alpha_0 \mathcal{E}^2$, where E_{Ry} is the Rydberg energy, $n^* = n - \delta_{nlj}$ with the quantum defect δ_{nlj} vanishing for the orbital momentum $l > 3$ [122–125], while the static polarisability $\alpha_0 = \beta_1 n^{*6} + \beta_2 n^{*7}$. Here, β_1, β_2 are coefficients which can be obtained theoretically [105] and have been found to be in good agreement with experimental values, see e.g. [126, 127] for the case of rubidium. For higher l and values of \mathcal{E} , numerical approach requiring exact diagonalization of the Hamiltonian which includes the effect of the external electric field is necessary. Such approach is very promising, but its numerical complexity goes beyond the scope of the present article.

A detailed study of this scenario as well as a systematic exploration of the coupling strengths, identification of relevant species and other possible level configurations in the case of Rydberg atoms goes however beyond the scope of the present article and we leave it for future investigations.